EXPERIMENTAL INVESTIGATION OF ROTATING WAVES AS A ROTATING STALL INCEPTION INDICATION IN COMPRESSORS

by

Vincent Hubert Garnier

Ingénieur des Arts et Manufactures,
Ecole Centrale de Paris, 1987

SUBMITTED TO THE DEPARTMENT OF AERONAUTICS AND ASTRONAUTICS
IN PARTIAL FULLFILMENT OF THE REQUIREMENTS FOR
THE DEGREE OF

MASTER OF SCIENCE IN
AERONAUTICS AND ASTRONAUTICS

at the

MASSACHUSETTS INSTITUTE OF TECHNOLOGY
May 1989

© Massachusetts Institute of Technology, 1989, All rights reserved.

Signature of Author_____
Department of Aeronautics and Astronautics
May 1989

Certified by_____
Professor Alan H. Epstein
Associate Professor of Aeronautics and Astronautics
Thesis supervisor

Approved by_____
Professor Harold Y. Wachman
Chairman, Department Graduate Committee

MASSACHUSETTS INSTITUTE OF TECHNOLOGY
JUN 07 1989
LIBRARIES

WITHDRAWN
M.I.T.
LIBRARIES

EXPERIMENTAL INVESTIGATION OF ROTATING WAVES AS A ROTATING STALL INCEPTION INDICATION IN COMPRESSORS

by

Vincent Hubert Garnier

Submitted to the Department of Aeronautics and Astronautics on May 16, 1989 in partial fulfillment of the requirements for the Degree of Master of Science in Aeronautics and Astronautics

ABSTRACT

The process of stall inception in axial compressors has been studied by using time and space resolved measurements. As predicted by an existing model, rotating stall is found to evolve from a pre-existing small amplitude travelling wave, which grows exponentially into a stall cell pattern. The stability of the compressor is equivalent to the stability of these pre-stall waves.

One three stage and one single stage low speed compressors were investigated during the study. On both, stall transients were performed at different throttle rates, with and without inlet distortion. Each time, a period of small amplitude wave propagation is observed, with a travelling speed of approximately 30% of rotor speed. This wave evolves into a stall cell without discontinuity in amplitude or angular position, showing that pre-stall travelling waves and stall cells are two stages of the same phenomenon. The wave was present through the whole single stage compressor, but was clearest immediately upstream of the inlet guide vanes. The damping of the small amplitude wave was studied as a function of flow coefficient, by fitting a first order linear model to the data. The damping was seen to decrease regularly towards the stall point, and was found to be stronger in the case of inlet distortion.

A set of data from a high-speed three stage compressor was also studied. The same pre-stall travelling wave phenomenon was clearly observed in the uniform inlet case. Travelling disturbances were also present in the distorted inlet case.

Thesis supervisor: Professor Alan H. Epstein
Title: Associate Professor of Aeronautics and Astronautics

ACKNOWLEDGEMENTS

There are many people whom I wish to thank for their contribution:

Professor Alan H. Epstein, for his help and guidance, and also for having the patience to let me make my own (experimental) mistakes in my own time; in this respect, this research was also a true learning process.

Professor Edward M. Greitzer for many passionate discussions. I think some lessons *and* some Fluid Mechanics actually sunk in, and I am grateful for both.

Dr. Gerald Guenette, for his readiness to listen, and for refreshing conversations on the Outside World (where *is* Maine, anyway?)

Dr. Choon S. Tan, for a friendly perspective on the research community.

Dr. Belgacem Jery, for allowing me to use his trusty Mac II.

Holly Rathbun and all the Administrative Staff for guiding me through the details, with friendliness and competence.

Bob Haimes and Dave Dvore for working electronic and computerese wonders in times of trouble.

Viktor Dubrowski, for keeping his machine shop the friendliest and most relaxing place in the Institute.

Jim Nash and Roy Andrews for powerful technical assistance.

Andreas Schulmeyer and Sasi Digivalli, for lending a much needed hand.

Charlie Haldeman, Reza Abhari and Yi-Lung Yang, and all my fellow RA's of GTL whom I cannot name here, for providing many enjoyable moments along the way. Your friendliness will probably be my best memory.

As for moral support (survival), I am particularly indebted to:

My friends Nicolas, Jim and Philippe, and the 28 Haskell St associates, for huge banquets or simple dinners, and helping me more than they will ever know.

All my friends in France or around the world, for sharing a part of their lives, and dragging my imagination away from M.I.T.

The MIT Fencing Team: three times a week...

My parents, for their unfailling love and support, and my brother, for somehow keeping my excitment for aeronautics alive.

Finally, to Patricia, for her love and patience (or impatience), without whom all this would have seemed quite empty.

This research was conducted under a grant from the Office of Naval Research; the support of Dr. R.J. Hanson is gratefully acknowledged. The interest of S. Koff and J. Gertz of Pratt & Whitney is also appreciated.

TABLE OF CONTENTS

LIST OF FIGURES

NOMENCLATURE

Symbols

a_k	--	Fourier coefficient of cosine decomposition
a_p	--	coefficent of time series model
A_0, A_1	--	hot wire calibration coefficients
b_k	--	Fourier coefficent of sine decomposition
B	--	stability parameter
c	--	blade chord
C_k	--	Fourier coefficent of complex exponentials decomposition
i	--	$\sqrt{-1}$
k	--	Fourier mode number
K_T	--	throttle resistance
l_c	--	total equivalent compressor length
l_e	--	lenght of compressor exit duct
l_i	--	length of compressor inlet duct
m	--	parameter for duct expansion to plenum
n	--	hot wire calibration coefficient (exponent)
N	--	number of compressor stages
	--	number of spatial measurements
p	--	order of linear model
R	--	compressor radius
R_w	--	hot wire resistance
R_2	--	anemometer bridge resistance
t	--	time
T	--	compressor time lag
T_f	--	fluid temperature
T_w	--	hot wire temperature
U	--	mean wheel speed
x	--	coordinate along compressor circumference (dimensional)

y -- coordinate along compressor axis (dimensional)

y_n -- element of time series

z_i -- eigenvalue of discrete time matrix

Δt -- sampling interval

γ -- blade stagger angle

λ -- eigenvalue of continuous time matrix

η -- coordinate along compressor axis (non-dimensional)

ξ -- time (non-dimensional)

ρ -- fluid density

τ -- compressor time lag (non-dimensional)

ϕ -- flow coefficient

φ -- velocity potential

ψ -- instantaneous total-to-static pressure rise

ψ_c -- compressor total-to-static pressure rise characteristic

σ -- damping of first order model

ω -- frequency of first order model

Operators

$\frac{d()}{dt}$ -- derivative

$\frac{\partial()}{\partial t}$ -- partial derivative

$(\bar{\ })$ -- circumferential average

$(\sim)$ -- non-axisymmetric part

CHAPTER ONE

INTRODUCTION

1-1 Introduction and background

Axial and centrifugal flow compression systems are subject to fluid mechanic instabilities, which inherently limit their flow operating range. Since these instabilities occur in a region where pressure rise and efficiency are maximum, there is great interest in trying to prevent their appearance.

The first of these instabilities (and the one encountered most often in modern jet engines) is called surge. It is a global instability in the sense that it involves the whole compression system: the compressor, but also the plenum, duct and throttle. On a compressor map, surge is characterized by a limit cycle (Fig(1-1)): the mass flow undergoes large amplitude oscillations, while the plenum (which represents the combustor in a jet engine) pressurizes and depressurizes. In deep surge, flow reversal can be observed. If kept in that mode, a jet engine will usually self-destruct quite rapidly, due to the high structural stresses present during the limit cycle described above.

The second kind of instability encountered is called rotating stall. By comparison with surge, which is a one dimensional instability along the compressor axis, rotating stall is a two dimensional phenomenon: fluid velocity varies both in the axial and in the circumferential direction. Furthermore, rotating stall is a local instability, since it is confined to the compressor blade rows; it is characterized by the presence of a stall cell, i.e. a region of the annulus where little or no through flow exists, which rotates in the direction of the rotor at 25% to 50% of rotor speed. From the point of view of the compression system, rotating stall is a steady phenomenon: the annulus averaged mass flow and pressure rise are constant in time, though both much lower than in normal pre-

stall operation. For these reasons, a jet engine cannot function with a large number of its compressor stages stalled; apart from an obvious loss of thrust, the combustor commonly goes out, or the reduced mass flow causes high turbine inlet temperatures. Stresses and heating of the compressor blades are also likely to cause terminal damage. A further complication is that stall can be a very stable operating condition: a large hysteresis makes it difficult to recover from.(Fig(1-2))

Many modern compressors have characteristics such that they enter surge directly, or after a few cycles of rotating stall. Still, rotating stall alone can be encountered in many flight conditions, such as cruise.

The point on a compressor map at which the fluid flow through the associated compression system becomes unstable is very near the maximum pressure rise and efficiency of the machine (this limit is often referred to as the "surge" or "stall" line). Operating a compressor is thus a compromise between efficiency and safety. Designers usually define a surge or stall "margin", i.e. a region near the stall line which is not entered in order to prevent any instability form developing. This margin needs to be wide enough to ensure safe operation in the presence of flow perturbations of finite amplitude (inlet distortion due to cross winds, the ingestion of shocks, wakes, hot gases from weapons firing, or a masked inlet during high angle of attack maneuvers). Obviously, designers would like to make the stall margin a small as possible to gain access to higher pressure rise regions, while retaining a sufficient degree of safety. A recent development in this domain has been to try to identify a precursor to the instability, a fluid mechanic phenomenon which would announce the coming of stall. Using this, one could safely operate closer to the stall line, and with sufficient warning, back off the compressor operating point to avoid the instability. This information could also be also be used as an input to an active control device, meant to artificially stabilize the compression system (due to the catastrophic nature of the instabilities, one definitely wants to avoid waiting for them to develop before attempting stabilization). Fig(1-3) illustrates the possible performance improvements that a stall precursor could provide. Stall control schemes have in

fact been implemented in a laboratory environment [10], but with limited success up to now.

This recent work looks more closely at the period during which the flow through the compressor transitions from stable to unstable, since a good description and a good understanding of the mechanism of stall inception is essential if we want to identify a phenomenon forewarning of stall.

1-2 Previous work on stall inception

The phenomenon of rotating stall was first identified by Emmons et al [1] in the early 1950's. They suggested a mechanism for the angular propagation of stall cells: once a group of airfoils has stalled and thus caused a sufficient flow blockage, the streamlines upstream of the compressor face are deflected by this obstacle. This raises the angle of attack of the blades at the "leading edge" of the cell, thus promoting stall there, and lowers it at the trailing edge, unstalling the blades in this region. This explanation is still widely held as accurate, although it is recognized that the boundary layers in trouble might be more those of the endwalls than of the blades. They also noted that stall can be characterized by an abrupt pressure rise drop (full-span stall), or a more progressive one (part-span stall).

Having presented this first general work on stall description, we now concentrate on a brief review of the subject of stall inception in the literature. We can broadly separate this summary into two sections: one describing theoretical work, the other describing experimental work.

1-2-1 Theoretical studies

Most studies on stall inception are based on simple two-dimensional potential flow models, describing the evolution of velocity perturbations upstream of a blade row modelled as an actuator disk. The usual assumptions used in the modelling are:

- Upstream flow field: two-dimensional inviscid flow, usually irritatingly (no reverse flow); boundary condition: disturbances vanish at upstream infinity.

- Downstream flowfield: again, two-dimensional inviscid flow, just convecting the vorticity generated by the blade row; boundary conditions are usually of two kinds:
  - constant static pressure at blade row exit
  - constant pressure at downstream infinity.

- Boundary conditions used across the blade row are usually:
  i) mass conversation
  ii) flow deflection relation
  iii) a blade row loss factor expressed as:
    - total pressure loss coefficient ([7])
    - static pressure rise coefficient ([2],[3])
    - vorticity equation with friction losses ([6])

  , all functions of the inlet flow angle.

Note that for those two last relations describing the loss factor, the unsteady behavior of the blade row has to be accounted for. For the early work in the area, quasi-steady performance was assumed: the leaving angle and the instantaneous pressure rise are functions of the instantaneous inlet flow angle (β_2) only. Later, lag parameters were included to take the fluid inertia (non-zero length of the blade passage), and thus the finite response time of the blade row into account. The general expression for the instantaneous pressure rise is:

$$\tau \frac{\partial C_p}{\partial t} = C_{pss} - C_p \qquad (1\text{-}1)$$

where τ is the lag parameter, $C_p(\beta_2,t)$ and $C_{pss}(\beta_2)$ respectively the instantaneous and steady-state pressure rise across the blade row.

Having established the equations for the fluid mechanic problem, one can investigate analytically a linearized version of these equations, assuming small perturbations around a mean quantity, or one can compute a numerical solution of the full non-linear problem. Let us first concentrate our attention on the linearized analysis. A study of this kind was performed by Stenning [2], without lag parameters in the blade row relations, also by Nenni and Ludwig [5] (with a lag parameter), and others. As was pointed out earlier, this analysis mainly aims at describing the evolution of an upstream disturbance, the amplitude of which is assumed to stay small with respect to the mean flow quantities. Since the upstream flow is potential according to the assumptions made, the disturbance has the form:

$$\tilde{\varphi}(x,\theta,t) = \sum_{|k|\neq 0} a_k(x,t)\, e^{ik\theta} \qquad (1\text{-}2)$$

(general form for the solution of Laplace's equation on a periodic domain). Substituting this expression in the equations, one obtains a first order differential equation for $a_k(t)$, which yields the following result:

$$a_k(x,t) = \lambda_k(t)\, e^{i\omega t} \qquad (1\text{-}3)$$

The solution of the linearized set of equations is thus a wave, travelling around the compressor annulus. Pressing on further, one can find conditions for those travelling waves to be neutrally stable (neither growing nor decaying), which for this model represents the limit of stable operation, and therefore the point of transition into stall (stall inception). In addition, one can obtain the disturbance travelling speed. Stenning [2], using a $C_p(\beta_2)$ function for his blade row characteristic, finds that a criterion for neutral stability is:

$$\frac{dC_p}{d\tan\beta_2} = -2\frac{(1-C_p)\cos^2\beta_2}{\tan\beta_2} \qquad (1\text{-}4)$$

This can be shown to be equivalent to the other well known condition:

$$\frac{d(P_{s2} - P_{t1})}{d\phi} = 0 \qquad (1\text{-}5)$$

where ϕ is the flow coefficient, which means that the instability develops when the total to static pressure rise reaches its peak on the compressor map. The phase speed for the instability is then:

$$V_p = \frac{\overline{W}_y(1 - C_p)}{\sin^2\beta_2} \qquad (1\text{-}6)$$

where W_y is the mean velocity in the circumferential direction ($W_y = W\sin\beta_2$). Nenni and Ludwig find relations of the same type, but in terms of the upstream and downstream relative swirl.

This class of linearized models are limited by their hypotheses; in particular, no predictions are possible concerning the behavior of the stall cells (propagation speed, number and amplitude) since the non-linear nature of their propagation is completely lost. But although somewhat simplistic, these models give good physical insight into the mechanism of stall inception: instability starts with the growth of a small amplitude wave traveling around the annulus. The stability of the compressor with respect to stall is reduced to the stability of a very simple first order differential equation.

The other approach to this problem is to solve the full non-linear set of equations numerically. This kind of studies were performed by Takata and Nagano [7], Pandolfi and Colusardo [8], Orner [9] among others. They emphasize the influence of the equation non-linearities on the development of the small amplitude disturbances (seen in the linearized version) into full-size stall cells, in particular concerning their shape and propagation speed.

1-2-2 Experimental work

A good summary of the subject of experimental studies on stall inception, and the related topic of empirical predictions, is given by McDougall [12]. As he

points out, most of this work was motivated by casing treatment evaluation; although it describes phenomena (tip leakage flows) that appear crucial in rotating stall inception, none of it describes the whole compressor upstream flow field just prior to stall. In his thesis, M^{c}Dougall gives the only work directly concerned with the understanding of stall inception. In particular, due to the short time extent of the phenomenon, most of his measurements were time-resolved.

Up to M^{c}Dougall's work, the most widely believed model for stall inception was the one suggested by Emmons [1]. This model describes stall inception as the random stall of a small group of blade passages; because of the coupling between the compressor and the upstream flow field, this stalled region first spreads circumferentially (and also radially), then starts falling behind the rotor to end up travelling at a fraction of rotor speed. To prove this experimentally, Jackson [11] measured the travelling speed of what he thought was an expanding stall cell, and indeed his results showed the wave first travelled close to rotor speed, then slowed down to roughly 40% of rotor speed.

In his thesis, M^{c}Dougall showed that Jackson's interpretation of the data was wrong. The problem comes from trying to determine the speed of an arbitrary shaped and expanding region from the speed of only a part of its boundaries (the cell leading edge in this case); this is a mathematically ill-specified problem, and practically, simple models for the stall cell's shape and expansion rates can yield vastly different estimates of the cell's rotation speed. A good definition of the cell's speed can be the speed of its geometrical center, but the determination of the center's position requires spatial information, which Jackson didn't have. M^{c}Dougall didn't have it either, so he disproved Jackson's interpretation by using hot wire velocimetry signals obtained in the rotor blade passages, near stall. On these signals, he noticed the presence of travelling disturbances (even with respect to the rotor), prior to stall. As they passed a blade passage, these disturbances modified the flowfield inside the passage (slight thickening of the endwall boundary layer), but the passage was certainly not stalled. Furthermore, from the point the disturbance could first be identified, its speed was within 20% of its final speed as a stall cell, and was in no case near rotor

speed. This experiment seemed to show that the small change in blockage due to the presence of a small amplitude disturbance was enough to cause a redistribution of the upstream flowfield, and cause the disturbance to rotate, even though it is an order of magnitude smaller than an actual stall cell. McDougall also proposed an explanation for Jackson's misinterpretation of the travelling disturbance's speed and re-plotted it, showing good agreement with his own measurements. To further disprove the mechanism of stall inception as a random blade passage stall, he examined the performance of a compressor with one blade passage strongly obstructed, or one blade removed. If Emmon's model was right, stall should always start within the artificially disturbed passage, and occur at a higher flow coefficient than normal. McDougall observed none of the above. In another experiment, using velocity measurements obtained from six probes equally spaced around the compressor annulus, McDougall was able to track the small amplitude perturbation he had observed earlier as it travelled around the annulus. When the compressor stalled, the perturbation's amplitude grew exponentially, then stabilized into a stall cell.

1-2-3 Summary

Until recently, the mechanism for stall inception has been poorly understood. Very simple actuator disk models describe the transition from stable operation into stall as the growth of an already travelling small amplitude perturbation into a full-size stall cell. Other theories see stall starting randomly as a group of stalled passages travelling with the rotor, which first expands then slows down as it starts interacting with the upstream flowfield. Measurements which seemed to validate this latter theory were shown to be misinterpreted, and experimental evidence now appears to support the small amplitude travelling wave viewpoint [13].

1-3 Scope of the present work

As was pointed out in the introduction, there is considerable interest in safely operating an axial compressor in a flow region where stall would

ordinarily be likely to occur, in order to benefit from higher pressure rise and higher efficiency. To achieve this goal, a stall "precursor" or "warning" (whatever its form) would be a great help. Given sufficient warning, it might make it possible to back off the compressor operating point in time to prevent the instability from developing, or it could be used as an input to some fluid mechanic device to actively control the flow. The present effort is an attempt to find such a "precursor", and if one exists, describe its characteristics. Looking for a precursor implies understanding the stalling process, and both classes of models described above and their supporting experimental evidence suggest that this process could be well described (at least in its early stages) by a first order differential equation. This equation links the stability of the compressor to the stability of a small amplitude disturbance travelling around the compressor annulus prior to stall, which grows into a stall cell as the machine turns unstable. Orienting our search for a "precursor" towards this promising phenomenon, we ask the following questions:

- Do these predicted pre-stall small-amplitude travelling waves exist, as McDougall's measurements seem to show ?

- Are those waves always present prior to stall, does stall always evolve from them, or can it happen without their presence? In other words, are these waves a necessary condition for stall to occur ?

- If this phenomenon is to be used as a stall precursor, how well does it react to typical situations like inlet distortions, or rapid mass flow variations?

- If these waves exist, can the growth or decay rate of their amplitude, and their propagation speed be measured ? If so, what can those parameters tell us about the stability of the compressor, and can they be used for stall prediction ?

- Last but not least, and since the present models cannot predict the compressible case, are high speed machines (such as typically found in modern jet engines) subject to the same phenomenon ?

CHAPTER TWO

LINEARIZATION OF THE MOORE-GREITZER MODEL

2-1 Introduction

The Moore-Greitzer model for the description of rotating stall transients is given in great detail in two companion papers, [4] and [5]. In this chapter, we first summarize the derivation of the full set of equations. The equation which models the evolution of the non-axisymmetric component of the velocity potential will then be linearized for the case of small amplitude disturbances. Finally, predictions are given for the behavior of this small amplitude mode.

2-2 Summary of the Moore-Greitzer model

This section summarizes the major assumptions and results found in the Moore-Greitzer model for rotating stall transients. A description of the compression system is first given, with definitions of the variables used. The momentum balance is then built section by section, to finally obtain the equations for the system.

The compression system is represented on Fig(2-1). It is composed of an inlet duct of length l_i, followed by the compressor blade rows, then by an exit duct of length l_e, a plenum and finally a throttle. The quantities used to non-dimensionalize all variables are the mean blade speed U, and the mean radius R. The non-dimensionalized variables are the following:

circumferential coordinate: θ

axial coordinate: $\eta = y/R$

time: $\xi = Ut/R$

compressor inertial time lag: $T = 2UN\tau/R$, $\Omega = 1/T$, $\tau = cr/U\cos\gamma$

where c is the blade chord, γ the stagger angle, N the number of compressor stages, and r a parameter included to take the blade row spacing and the viscous effects into account.

We now evaluate the total-to static pressure rise across the whole system by adding the total-to-static pressure difference at the inlet, the static-to-static pressure rise across the compressor blade rows, and the static-to-static pressure difference between the exit plane and far downstream.

Upstream flow region

The flow coefficient in the upstream flow region will be denoted ϕ. It can be decomposed into a circumferential average $\bar{\phi}$ and a non-axisymmetric part $\tilde{\phi}$, as defined by:

$$\phi(\xi,\theta,\eta) = \bar{\phi}(\xi) + \tilde{\phi}(\xi,\theta,\eta) \tag{2-1}$$

Besides, the flow in this region is potential, and according to the distinction made above, we can also separate the velocity potential into a circumferential average and a non-axisymmetric part:

$$\varphi(\xi,\theta,\eta) = \bar{\varphi}(\xi,\theta) + \tilde{\varphi}(\xi,\theta,\varphi) \tag{2-2}$$

$$\bar{\phi} = \frac{\partial \bar{\varphi}}{\partial \eta} \tag{2-3}$$

$$\tilde{\phi} = \frac{\partial \tilde{\varphi}}{\partial \eta} \tag{2-4}$$

so that, in particular (taking $\varphi(-l_i)=0$):

$$\bar{\varphi}(\xi,\theta) = \left[\eta + l_i\right] \bar{\phi}(\xi) \tag{2-5}$$

Now, φ has to satisfy the Laplace equation with periodic boundary conditions; therefore, we have:

$$\tilde{\varphi} = \sum_{|k|\neq 0} a_k(\xi)\, e^{|k|\eta}\, e^{ik\theta} \tag{2-6}$$

Compressor face

The total-to-static pressure difference in the upstream flow region is:

$$\frac{P_{t0}-P_{s0}}{\rho U^2} = \frac{1}{2}\left[u^2+v^2\right] + \left[\frac{\partial\varphi}{\partial\xi}\right]_{\eta=0} \tag{2-7}$$

where u and v are the axial and circumferential non-dimensional velocities at the compressor face; we have:

$$u = \phi_0 = \phi(\eta=0) \tag{2-8}$$

$$v = \left[\frac{\partial\tilde{\varphi}}{\partial\theta}\right]_{\eta=0} \tag{2-9}$$

so that:

$$\frac{P_{t0}-P_{s0}}{\rho U^2} = \frac{1}{2}\left[\phi_0^2+\left[\frac{\partial\tilde{\varphi}}{\partial\theta}\right]_{\eta=0}^2\right] + \frac{d\bar{\phi}}{d\xi} I_i + \left[\frac{\partial\tilde{\varphi}}{\partial\xi}\right]_{\eta=0} \tag{2-10}$$

Across the compressor

We have (including IGV and EGV inertial lag, and IGV loss):

$$\frac{P_{se}-P_{s0}}{\rho U^2} = \Psi_c(\phi_0) + \frac{1}{2}\phi_0^2 - \left(\frac{1}{\Omega}+\frac{1}{\Omega_{gv}}\right)\frac{\partial\phi_0}{\partial\xi} - \frac{1}{2\Omega}\frac{\partial\phi_0}{\partial\theta} + \frac{K_I}{2}\left[\frac{\partial\tilde{\varphi}}{\partial\theta}\right]^2 \qquad (2\text{-}11)$$

where Ψ_c is the compressor axisymmetric total-to-static pressure rise characteristic, and K_I the IGV loss coefficient.

Downstream flow region

The flow in this region is assumed to obey an approximation of the kind $\nabla^2 P=0$, and we assume constant pressure far downstream, at l_e. Using continuity across the compressor, we link the downstream exit static pressure to the upstream velocity potential:

$$\frac{P_{s\infty}-P_{se}}{\rho U^2} = -l_e\frac{d\bar{\phi}}{d\xi} - (m-1)\left[\frac{\partial\tilde{\varphi}}{\partial\xi}\right]_{\eta=0} \qquad (2\text{-}12)$$

where m=2 corresponds to a long exit duct, m=1 to a sudden expansion to the plenum.

Total-to-static pressure rise across the compression system

Summing all the components computed above, we obtain the total-to-static pressure rise across the compression system. We note this quantity the following way:

$$\frac{P_{s\infty}-P_{t0}}{\rho U^2} = \Psi(\xi) \qquad (2\text{-}13)$$

If we take into account that:

$$\frac{\partial \phi_0}{\partial \xi} = \frac{d\bar{\phi}}{d\xi} + \left[\frac{\partial^2 \tilde{\varphi}}{\partial \eta \partial \xi}\right]_{\eta=0} \tag{2-14}$$

$$\frac{\partial \phi_0}{\partial \theta} = \left[\frac{\partial^2 \tilde{\varphi}}{\partial \eta \partial \xi}\right]_{\eta=0} \tag{2-15}$$

we obtain:

$$\Psi(\xi) = \Psi_c(\phi_0) - (l_i + l_e + \frac{1}{\Omega} + \frac{1}{\Omega_{gv}})\frac{d\bar{\phi}}{d\xi} - (\frac{1}{\Omega} + \frac{1}{\Omega_{gv}})\left[\frac{\partial^2 \tilde{\varphi}}{\partial \eta \partial \xi}\right]_{\eta=0} \tag{2-16}$$
$$- \frac{1}{2\Omega}\left[\frac{\partial^2 \tilde{\varphi}}{\partial \eta \partial \theta}\right]_{\eta=0} - m\left[\frac{\partial \tilde{\varphi}}{\partial \xi}\right]_{\eta=0} + \frac{1}{2}(K_l - 1)\left[\frac{\partial \tilde{\varphi}}{\partial \theta}\right]^2_{\eta=0}$$

Let us make the following definitions:

$$l_c = l_i + l_e + \frac{1}{\Omega} + \frac{1}{\Omega_{gv}} \tag{2-17}$$

$$\frac{1}{\Omega_{eq}} = \frac{1}{\Omega} + \frac{1}{\Omega_{gv}} \tag{2-18}$$

We now decompose the pressure into an axisymmetric and a non-axisymmetric part:

$$\Psi_c(\phi) = \bar{\Psi}_c(\bar{\phi}) + \tilde{\Psi}_c(\xi,\theta) \tag{2-19}$$

and similarly:

$$\left[\frac{\partial \tilde{\varphi}}{\partial \theta}\right]^2_{\eta=0} = \bar{G}(\xi) + \tilde{G}(\theta,\xi) \tag{2-20}$$

we finally obtain:

$$\bar{\Psi}(\xi) = \bar{\Psi}_d(\xi) - l_c \frac{d\bar{\phi}}{d\xi} + \frac{1}{2}(K_l - 1)\,\bar{G}(\xi) \tag{2-21}$$

$$\begin{aligned} 0 = \tilde{\Psi}_d(\xi,\theta) &- \frac{1}{\Omega_{eq}}\left[\frac{\partial^2 \tilde{\varphi}}{\partial\eta\partial\xi}\right]_{\eta=0} - \frac{1}{2\Omega}\left[\frac{\partial^2 \tilde{\varphi}}{\partial\eta\partial\theta}\right]_{\eta=0} \\ &- m\left[\frac{\partial\tilde{\varphi}}{\partial\xi}\right]_{\eta=0} + \frac{1}{2}(K_l - 1)\,\tilde{G}(\xi,\theta) \end{aligned} \tag{2-22}$$

The behavior of the system is completely determined by including the throttle equation:

$$\frac{d\bar{\phi}}{d\xi} = \frac{1}{4B^2 l_c}\left[\bar{\phi}(\xi) - \sqrt{\frac{2\Psi(\xi)}{K_T}}\right] \tag{2-23}$$

where K_T is the throttle resistance, and B the stability parameter, defined by Greitzer [14] .

Equations (2-21) and (2-23) concern the circumferential average mode. Equation (2-22) describes the behavior of non-axisymmetric modes; this is the equation we wish to study in more detail, for it is the one which small amplitude perturbations will obey.

2-3 Linearization

The assumption of small amplitude perturbations allows us to:

- neglect the pressure loss due to the circumferential velocity

$$\left[\frac{\partial \tilde{\varphi}}{\partial \theta}\right]^2_{\eta=0} << \left[\frac{\partial^2 \tilde{\varphi}}{\partial \theta \partial \eta}\right]_{\eta=0} \tag{2-24}$$

- linearize circumferential variations of the compressor pressure rise around the mean flow coefficient:

$$\tilde{\Psi}_c(\xi,\theta) = \frac{d\bar{\Psi}_c}{d\bar{\phi}} \left[\frac{\partial \tilde{\varphi}}{\partial \eta}\right]_{\eta=0} (\xi,\theta) \tag{2-25}$$

Remembering the expression for :

$$\tilde{\varphi} = \sum_{|k|\neq 0} a_k(\xi)\, e^{|k|\eta}\, e^{ik\theta} \tag{2-26}$$

we have:

$$\left[\frac{\partial \tilde{\varphi}}{\partial \eta}\right]_{\eta=0} = \sum_{|k|\neq 0} |k|\, a_k(\xi)\, e^{ik\theta} \tag{2-27}$$

$$\left[\frac{\partial^2 \tilde{\varphi}}{\partial \eta \partial \xi}\right]_{\eta=0} = \sum_{|k|\neq 0} |k|\, \dot{a}_k(\xi)\, e^{ik\theta} \tag{2-28}$$

$$\left[\frac{\partial \tilde{\varphi}}{\partial \xi}\right]_{\eta=0} = \sum_{|k|\neq 0} \dot{a}_k(\xi)\, e^{ik\theta} \tag{2-29}$$

$$\left[\frac{\partial^2 \tilde{\varphi}}{\partial \theta \partial \xi}\right]_{\eta=0} = \sum_{|k|\neq 0} ik\,|k|\, a_k(\xi)\, e^{ik\theta} \tag{2-30}$$

Plugging these values into equation (2-22), and decomposing along Fourier modes, we get:

$$\left[m + \frac{|k|}{\Omega_{eq}}\right]\dot{a}_k(\xi) = |k|\left[\frac{d\bar{\Psi}_c}{d\bar{\phi}} - \frac{ik}{2\Omega}\right]a_k(\xi) \qquad (2\text{–}31)$$

Let us make the following definitions:

$$\sigma_k = \frac{d\bar{\psi}_c}{d\bar{\phi}} \frac{|k|}{m + \frac{|k|}{\Omega_{eq}}} \qquad (2\text{-}32)$$

$$\omega_k = \frac{k}{2\Omega} \frac{|k|}{m + \frac{|k|}{\Omega_{eq}}} \qquad (2\text{-}33)$$

Equation (2-31) is a first order differential equation. Its solution is:

$$a_k(\xi) = \lambda_k e^{(\sigma_k - i\omega_k)\xi} \qquad (2\text{-}34)$$

We note that for φ to be real, we must have

$$a_k(\xi) = \bar{a}_{-k}(\xi) \qquad (2\text{-}35)$$

The exponential in equation (2-34) is already such that this is true; therefore:

$$\lambda_{-k} = \bar{\lambda}_k \qquad (2\text{-}36)$$

Finally:

$$\tilde{\varphi} = \sum_{|k|\neq 0} \lambda_k e^{(|k|\eta + \sigma_k \xi)} \; e^{i(k\theta - \omega_k \xi)} \qquad (2\text{-}37)$$

We see that each Fourier mode is the product of a damping term and a travelling wave term. $e^{(|k|\eta + \sigma_k \xi)}$ is the damping term, which is a function of axial

position (η), and time (ξ). $e^{i(k\theta-\omega_k \xi)}$ is the travelling wave term, function of circumferential position (θ), and time.

2-4 Predictions and discussion

We can make the following predictions concerning the characteristics of a small amplitude disturbance in the travelling upstream flowfield of the compressor:

- exponential decay with distance from the compressor face. Furthermore, the decay rate is proportional to the Fourier mode number, so that higher number modes will be attenuated more strongly.

- Exponential decay or growth with time, at a rate proportional to the local slope of the total-to-static pressure rise characteristic. In particular, the neutral stability point, which corresponds to stall inception, is predicted to occur when the slope of the characteristic becomes zero. This is a well-known criteria (already seen in chapter one), which has had mixed success: many compressors are known to stall with a strongly negative slope. Thus, the zero slope criteria should be taken as a lower limit beyond which the compressor must stall. We retain the qualitative idea that the damping of the small amplitude travelling wave, σ_k, should tend to zero at stall (whether it is linked to the slope of the characteristic or not).

We note that, in this model, the mechanism by which the small amplitude wave travels is only due to the compressor time lag, and not to a redistribution of the upstream flowfield, as McDougall's or Emmons' models predict. In the present model, the wave can propagate with circumferentially uniform boundary layers in the blade passages (any boundary layer modification would be a second order effect, neglected in the linearization).

CHAPTER THREE

EXPERIMENTAL APPARATUS AND TECHNIQUE

3-1 Introduction

As we have seen from the two previous chapters, our goal is to investigate the flowfield of the compressor immediately prior to and during the machine's transition from stable operation to rotating stall. We hope to identify small amplitude perturbations travelling around the annulus prior to stall, which grow into full-size stall cells as the compressor goes unstable. This chapter gives a description of the facilities used for this study. Also described are the pressure and velocity measurement instrumentation with comments on calibration procedures and error analyses. The chapter is closed by a section on data acquisition and data processing techniques.

3-2 Description of the facilities

3-2-1 Introduction

The Gas Turbine Laboratory at MIT has two low speed compressor facilities, one is a three stage machine, the other a single stage machine. Both were used during this study. This section gives a short description of these facilities, only emphasizing the aspects important to the problem at hand, and references more complete sources of information.

3-2-2 Three stage compressor

This facility was built by Pratt & Whitney as a research facility for the JT9D program. Its installation and subsequent modifications are extensively described in Gamache [15] and Lavrich [16]. A schematic of the rig is given in Fig (3-1). The

work done to date on this machine includes the mapping of the characteristic of three different builds, including the reverse flow region ([15], [16]). It was also used to perform detailed time-resolved measurements of the flow field in the compressor during operation in rotating stall [16].

The build used during all the runs performed on this rig is referenced as build #2, or low reaction build, in [16]. Table 3-1 gives the design specifications and blading parameters for this build. A speedline taken at 2225 RPM is given in Fig (3-2). Some minor precisions about the conditions in which the experiments were performed: the 15 inch orifice plate [16] was used for mass flow measurements; the industrial roof blower was never turned on, and its impeller was held fixed to avoid disturbances, making it a purely resistive part of the circuit. A crucial element for our experiments was the variable speed throttle, the position of which could be recorded via an LVDT.

3-2-3 Single stage compressor

This rig was built as a research compressor in the 1950's, and has only one stage: inlet guide vanes, rotor and stator. Its arrangement is extensively described in Johnson [17], and Lee [18]. Past research on this compressor includes a study of hub casing treatment for stall margin improvement ([18]). A schematic of the facility is shown in Fig (3-3). The rotor and stator blade stagger angles used for all experiments were set by Schulmeyer [19] to obtain a high rotor loading, and thus promote stall there (a D factor of 0.6 was chosen). All precisions can be found in [19]. Table (3-2) gives the blading parameters used. A speedline taken at 2700 RPM is given in Fig(3-4). The existing throttle didn't permit fine control of the compressor mass flow: the drive motor didn't have variable speed, and asymmetric thrust made the throttle wobble as it closed. A new variable speed drive system (motor and transmission) was therefore installed, to ensure a smoother motion and allow precise positioning of the throttle. The system consists of two ball bearing screws (for the linear motion), driven by a variable speed electric motor, via a chain. The motor speed can vary continuously from 0 to 60 RPM. At maximum speed, the throttle translation speed is 0.5 cm/s. This corresponds to a

mass flow derivative of 2.5 m/s^2, or 8. 10^{-4} flow coefficient points per rotor revolution at 2700 RPM. Here again, throttle position is monitored using an LVDT.

3-3 Pressure measurements

It soon became necessary to perform the study of the compressor stalling process in relation to steady-state compressor parameters such as mass flow and pressure rise (the total-to-static pressure rise characteristic of the compressor plays a key role in the theory exposed in chapter two). Steady state pressure measurements are also needed to study the characteristics of inlet distortions. This section describes or references the layout of pressure instrumentation in both compressors.

For the three-stage compressor, this layout is described by Lavrich [16], and a schematic is given in Fig (3-5). Note that all mass flow measurements were obtained from the 15 inch orifice plate, in particular to overcome the problem of estimating mass flow with an inlet distortion. All pressure measurements were made using a very high accuracy MKS baratron unit. The differential pressure head has a total range of 14000 Pa, and can be read with a precision of 1 Pa. Measurement range was roughly 1500 Pa. Typical error was due to unsteadiness, and was less than 1%.

The single stage pressure instrumentation was set in place by Schulmeyer, and is described in detail in [19]. A schematic of this instrumentation is given in Fig (3-6). It consists of 30 static pressure taps (20 upstream of the blade rows, 10 downstream), and 30 total pressure probes (20 upstream, 10 downstream). For reasons of speed of acquisition, and also to avoid the wakes of the inlet struts, only 20 total and static pressure probes were used upstream (cf Fig (3-6)). The mass flow was obtained from a circumferential average of the velocities given by the total-to-static pressure difference at each station. All pressure measurements were obtained through a 48 port Scanivalve, regularly calibrated against the Baratron. Total range was about 8000 Pa, and precision is limited by the Analog-digital converter count to about 15 Pa. Measurement range was around 1300 Pa, and typical error was about 40 Pa, i.e. 3.1%.

3-4 Velocity measurements

3-4-1 Introduction

The goal of the experiment is to investigate the flowfield upstream of the compressor face, in order to test the hypothesis that small amplitude waves travel around the annulus just prior to stall. This section presents the choice of instrumentation for these measurements, then describes the requirements that the expected characteristics of the phenomenon place on the number and location of the measurement probes. Finally, calibration procedures and error analyses are presented.

3-4-2 Choice of velocity instrumentation

The only things clear from the start about the phenomenon we wish to study are the following:

- It is unsteady (since the disturbance is supposed to travel at 30% of rotor speed, and if we want to resolve two harmonics of the wave, an upper limit for the bandwidth is not more than twice the rotor frequency, about 100 Hz).
- It is of small amplitude (we expect an amplitude of 1% of the mean axial velocity).

Only high frequency response pressure sensors and hot-wire anemometry have the necessary frequency response. But pressure transducers do not have a sufficient sensitivity over the flow range we are interested in, contrary to the hot wire instrumentation. Despite its fragility and strong tendency to drift, the latter system was therefore chosen. Eight DANTEC 56C17 anemometers were usually used, sometimes in conjunction with TSI model 1250 anemometers.

3-4-3 Number and location of probes

From previous experimental efforts on the subject, we expect a pre-stall travelling disturbance to vary in time and space in rather complicated ways: its shape might vary, its travelling speed might depend on time and/or space. We

therefore need to have good spatial information on the disturbance, at all instants in time. This kind of resolution is quite stringent, but is necessary to obtain a faithful picture of the phenomenon, and avoid misinterpretations due to lack of information. More precisely, since the perturbation is periodic in the circumferential direction, it can be decomposed as a Fourier series, i.e. as a linear combination of sine and cosine waves of increasing wave numbers. A good measure of the accuracy which N spatial measurements provide in describing a wave shape is the number of Fourier series coefficient one can compute with them; a well-known rule of Fourier analysis states that in order to compute N Fourier coefficients in a series, at least 2N+1 measurements are needed. "Complicated" shapes or shapes with sharp edges, which have a high number of coefficients in their series decomposition, will require a large number of measurements to be accurately described. Another aspect of the problem is that any Fourier component of the signal higher than the ones which can be resolved will not only be lost, but will contaminate the lower Fourier coefficients; this phenomenon is called aliasing. Therefore, one should make sure that the unresolved Fourier coefficients are small enough (ideally zero) with respect to the computable ones, so that no information on the wave shape is lost, and that the available information is not distorted.

In the experiments we are to perform, we expect the disturbance amplitude to decay exponentially with distance from the compressor face; we also expect the Fourier components of the disturbance to decay at a rate proportional to their wave number. In other words, the upstream flowfield is supposed to act as a fluid mechanic filter, rounding off the disturbance's sharp edges as we go further upstream. It becomes apparent that there exists a trade-off between (i) the number of probes to use in order to get an accurate picture of the disturbance's shape, and (ii) the distance from the compressor face at which they are placed. Close to the blade row, the disturbance will have a larger amplitude (easier to detect), but with a more complicated shape (greater spatial sampling needed to describe it). Further upstream, the disturbance amplitude will be smaller, but it can be resolved spatially with fewer probes. In the experiments performed, different combination of number of probes and distance from the compressor

face were used, often after trial and error. It turns out that spatial aliasing is rarely a problem, and that a good starting point is to place 8 probes half a compressor radius upstream of the first blade row.

3-4-4 Calibration

As many as 12 hot wire probes were used simultaneously, which ruled out the possibility of calibrating each wire independently, since that would be much too time consuming. The hot wire probes were therefore calibrated in place, by running the compressor at different mass flows. The calibration relation used was the classic generalized King's law [21]:

$$\frac{E^2 R_w}{R_w + R_2} = \left[A_0 + A_1 \rho V^n\right](T_w - T_f) \qquad (3\text{-}1)$$

where R_W is the hot wire resistance, R_2 the resistance of the anemometer in series with the hot wire, E the voltage across the anemometer bridge, T_W and Tf respectively the wire and fluid temperatures, V the fluid velocity, and ρ the fluid density. A_0, A_1 , and n are the calibration coefficients. The exponent, n, is usually close to 0.5.

This relation provides an adequate curve fit for a wide velocity range. Nevertheless, since the velocity range of interest was roughly $\pm$ 2 m/s around a known mean value, calibration points were taken in this region only. A reference voltage was taken at zero flow, in order for the calibration curve to keep an acceptable shape outside of the region of interest. No corrections were made for fluid temperature difference between calibration and experiment, since both were performed in the same conditions; see also the error analysis on this subject. Fig(3-7) gives a typical calibration curve.

3-4-5 Error analysis

The sources of error are so numerous in hot wire anemometry that it is difficult not to forget one. The main ones are:

- Drift, an all-time headache. The flow environment in a compressor is extremely tough for a fragile sensor like a hot-wire. A substantial amount of dust and fibers gets ingested carried by the air flow, and ends up burned on or entangled around the wire. This slowly or abruptly modifies the heat transfer properties of the sensor, and changes the relation between flow velocity and voltage output from the anemometer bridge. In the two hours a typical run would last, the slope of this voltage-velocity relation could change by as much as 5%. To keep this error down, a calibration was performed immediately before and after each run.

- Flow temperature change. The flow temperature was constantly monitored during runs. In all the experiments, the compressor was run for some time before calibrations or measurements were actually made, so that thermal equilibrium could be reached in the room. The maximum temperature change recorded was 3 °F. For a mean temperature difference from wire to fluid of 400 °F (typical), this gives a relative temperature error of 0.8%. From the form of King's law, we see that that relative error in temperature gives twice as much relative error in velocity, so that our error due to temperature change is 1.5%.

- Directional sensitivity of the probe. A typical error in angular position of the probe was 10 degrees. Since the probe was calibrated in place, this had supposedly no effect in the case (most common) where the measurements were performed at the same station as the calibration. In other cases though, the velocity error goes like the cosine of the angle error, so that a 3% error in velocity is expected from angular positioning inaccuracies.

- Inlet flow non-uniformities. Since the probes were calibrated in place using an annulus averaged velocity obtained from total and static pressure measurements, the calibration doesn't "see" any inlet non-uniformities. A study of the non-uniformity level revealed that the maximum error in assuming uniform flow was 2%.

Assuming they are uncorrelated, these errors can be combined (RMS added), and this yields the overall figure of 3.2% error in velocity measurements.

3-5 Data Acquisition and Processing

3-5-1 Introduction

Once a measurement was taken, it had to be recorded in the computer memory; high speed acquisition of velocity data, in particular, had to be performed that way. This section presents the measurement's journey through the digital world. We first describe its conversion from analog to digital, and all the precautions this implies. Digital processing of the high-speed data is then described. A schematic of the data acquisition and data processing chain is given on Fig(3-8).

3-5-2 Analog to digital conversion

Anti-aliasing filters were used in all experiments to low-pass filter the analog signal before digitizing it. Those filters are 4 pole Bessel filters. The travelling waves we are to study are supposed to travel at 30 to 50% of rotor speed, and we want to resolve the first two spatial harmonics of that wave (for example). The frequency range of interest for the study is thus from 0 Hz to rotor frequency plus 20 % (say), typically not more than 55 Hz. The lowest cut-off frequency the anti-aliasing filters could be set at was 100 Hz, so this was chosen. Taking the filters' cut-off rate and Shannon's sampling theorem into account, we set the sampling frequency of the analog-digital converter to 625 Hz per channel, i.e. 10 kHz for the total of the 16 A/D channels. The A/D input range was 0-10 volts, coded on 12 bits, which means a voltage of 2.44 mV per count. A typical noise level at the A/D input was about 5 mV, i.e. two A/D counts, which indicates that the A/D resolution was sufficient (still, it can be noted that 2.5 mV represent a speed variation of 0.25 m/s at a mean value of 40 m/s, see Fig(3-7)). The analog-digital converter was calibrated, and it was found that the calibration constants depended rather heavily on the data acquisition rate. In consequence, the same sampling rate was used in the calibration routines and the data logging routines.

3-5-3 Digital processing

After the signal has been converted back to engineering units by passing through the A/D and the hot wire calibrations, one can try to enhance some of its properties by filtering it with digital techniques. For our experiments, it was rapidly discovered that the actual mean level of velocity indicated by a probe was neither important nor really precise (drift etc.). More important was the variations of the velocity around this mean level, since this would really be what indicated the presence of a disturbance. All signals were thus high-pass filtered at 4 Hz to get rid of their DC component. Also, no relevant information was found to exist above rotor frequency plus 20%, so the signal was low-pass filtered at that frequency. Obtaining this rule of thumb for the cut-off frequency certainly took trial and error: although one wishes to enhance the signal to noise ratio by removing as much noise as possible, too narrow a filter can "invent" some very misleading information. The digital filter used belonged to the finite impulse response category, for their desirable property of introducing only linear phase shift in the frequency domain, i.e. a pure time lag in the time domain. In our case, the filter was implemented acausaly, which means it used information from before and after a point to filter it; this eliminated the time lag mentioned above.

The last operation performed on the velocity data was to discrete Fourier transform the measurements in space. At each point in time, one has (say) 8 velocity measurements taken around the compressor annulus; from these, 8 complex valued Fourier coefficients can be obtained using the following formula:

$$C_k = \frac{1}{8}\sum_{n=0}^{7} V_n \exp\left[\frac{-2ik\Pi}{8}\right] \qquad (3\text{-}2)$$

where V_n is the velocity at angular position n; k varies from -3 to +4 in our case, and the C_k's are periodic with period 8. Furthermore, since V_n is real, C_k and C_{-k} are complex conjugates. Fourier analysis says that C_{-k} has the phase and half the amplitude of the wave, so that by studying these C_{-k}'s we have all the required information about the wave position and amplitude as a function of time.

Note that since the A/D scans all channels consecutively, the 8 velocity measurements are not taken precisely at the same time, but with a maximum of

half a sampling period between them. This was dealt with by linearly interpolating the values of the channels between two clock cycles, but no difference was noticed when no interpolation was performed.

CHAPTER FOUR

LOW SPEED EXPERIMENTS

4-1 Introduction

This chapter describes the experiments performed on MIT/GTL's low speed compressors to test the hypothesis that small amplitude waves travel around the compressor annulus before stall. A typical experiment for the identification of these pre-stall waves is first described and discussed, some questions are raised, and a framework for the study of this phenomenon is defined. Next, we discuss the statistical aspect of the stalling process from the point of view of small amplitude travelling waves. The reaction of the stalling process to typical engine operating conditions like mass flow transients and inlet distortion is then studied. Finally, a section covers the influence of the axial position of sensors for best pre-stall wave detection. The chapter is closed by a summary of the experimental evidence exposed.

4-2 Identification and description of small amplitude travelling waves: one typical experiment

4-2-1 Introduction

The experiment presented in this section is typical of almost all others referred to later in the chapter. Our purpose is to explain with this example some general characteristics of the experiment and its results, and how these characteristics influenced our investigation method: what information is found to be important and how this information is plotted.

4-2-2 Presentation of the experiment

The experiment presented here was conducted on the three stage compressor described in chapter three. The spatial arrangement of the hot-wire probes was the following: eight probes were placed around the compressor annulus, equally spaced, 13.5 cm (or 0.47 radii) upstream of the inlet guide vanes. The compressor RPM was 2225. The experiment was performed in the following way: the compressor was first brought "very close" to stall. In practice, this means the closest one could get while being reasonably sure not to stall from some larger than usual disturbance being swallowed by the machine. Typically, it was within 0.005 flow coefficient points from the stall point on the compressor map, see Fig (3-2). Using the fine control variable speed throttle, the mass flow was then reduced as slowly as possible, while hot wire data was recorded for a fixed period of 25 seconds. With a bit of practice, the closeness to stall and the slowness of the throttle motion could be balanced in such a way that the whole sequence fit within the time data was taken. This was mainly a trial and error business: no automatic logging routine was available which could continuously rewrite a memory section and keep only (say) the last 10 seconds before stall. Globally, one out of two trials led to a "good" result, i.e. in which stall occurred in the last 15 seconds of the data logging interval. The compressor was then quickly unstalled.

4-2-3 Results

Fig (4-1) gives the time traces of the eight filtered velocity signals obtained. As described in the last chapter, these signals were first discrete Fourier transformed in space to obtain the coefficient C_{-k} of each spatial harmonic. The C_{-k}'s (C_0 to C_{-3}) give the amplitude and phase of each harmonic, and are thus complex valued functions of time. A question of plotting method comes up, since such functions can be represented in many different ways:

- on a three-dimensional graph, representing amplitude and circumferential position vs time,
- on two ordinary graphs, plotting amplitude vs time and circumferential position (phase angle) vs time,
- on two graphs showing real and imaginary part vs time.

This third method has less physical significance than the first two, since the real and imaginary part of the Fourier coefficient represent the projection of the wave onto two axes which are perfectly equivalent. This plotting method will therefore not be used.

Fig(4-2) gives the amplitude of the first Fourier harmonic during the 140 rotor revolutions preceding the stall point, which is referenced as t=0 on the plot. We can see clearly a stretch of finite amplitude (always > 0.1m/s) starting at t=-90 revs, finally growing exponentially into a stall cell. During the same time interval, the phase angle of C_{-1}, plotted on Fig(4-3), shows a very regular propagation. For a better estimation of the phase speed, the phase can be "unwrapped", and this method is used on Fig(4-4) to display the angular propagation of the first and second Fourier harmonics. The phase of C_{-1} is seen to travel at around 13 Hz during the small amplitude stage of the wave, and this turns to 14 Hz for the stall cell. The phase of C_{-2} shows no clear propagation, which indicates that the small amplitude wave does not have a C_{-2} component; any C_{-2} present in the data is really due to noise. This is confirmed by Fig(4-5), which shows that the amplitude of C_{-2} is always nearly zero, in any case much smaller than that of C_{-1}. From this point on, we will consider that all relevant information concerning the small amplitude wave position and amplitude is contained in its first Fourier harmonic (this proved to be true for the single stage compressor as well). The amount of noise reduction that this simplification provides is illustrated by Fig(4-6), which gives three-dimensional representations of the velocity data and of the first Fourier harmonic during the last 20 rotor revolutions before stall. The wave propagation is much more obvious in the Fourier harmonic than in the raw velocity data. We also note that quantitative analysis is difficult using three dimensional plots, and therefore only two dimensional plots will be used in the rest of this study.

4-2-4 Discussion

The results exposed above indicate very clearly the presence of a small amplitude travelling wave prior to stall. We note the following characteristics:

- There is no phase or amplitude discontinuity as the wave finally grows into a full-size stall cell; this seems to show that small amplitude travelling waves and stall cells are two stages of the same physical phenomenon. From the time it is first identified, the wave is travelling at a phase speed of 13 Hz, which turns to 14 Hz for the stall cell; at no time is it near rotor speed. Also, the wave amplitude can remain "small" (typically less than 5% of the stall cell amplitude) for a considerable time (90 rotor revolutions). These observations are not in accordance with Emmon's view of stall inception as groups of blades stalling randomly, then slowing down to stall cell speed. On the other hand, the Moore-Greitzer theory predicts this behavior very well.

During this last period of uninterrupted propagation, the wave amplitude seems to vary almost randomly around a mean value. An explanation would be that disturbances are convected in and tend to reinforce or diminish the already existing wave according to their relative angular positions (in phase or out of phase). This observation raises the question of the nature of the disturbances which excite the system, and this is addressed in the next section.

4-3 Statistical aspect of the stall inception process

4-3-1 Introduction

The experimental results presented in the previous section qualitatively conform to the following ordinary differential equation

$$\dot{C}_k(t) = (\sigma_k - i\,\omega_k)\, C_k(t) \qquad (4\text{-}1)$$

which was established by the Moore-Greitzer linearized theory in chapter two. According to this model, any disturbance swallowed, or generated inside the compressor (structural, fluid mechanical) ought to act as an excitation for the compressor-flowfield system, or another way of seeing it, as an initial condition for the ordinary differential equation. It would seem therefore that the compressor environment (disturbances convected to the blade row, or structural modes) is an important factor in determining the amplitude and time extent of

pre-stall travelling waves. In particular, the intermittency and amplitude of these excitations are crucial parameters. If perturbations appear too rarely or too weakly to excite even a barely stable system, no travelling disturbance will exist for any appreciable length of time before the compressors turns unstable (in which case the smallest disturbance will grow exponentially).

A problem encountered if one tries to answer the question of the nature of the driving disturbances is that one cannot really separate inputs or excitations from the system's reaction to them. We can try to distinguish between the two by the fact that a disturbance convected in will not be travelling circumferentially, before it actually reaches the weakly stable blade row and excites the system. Unfortunately, the time during which a disturbance is being convected is too short to permit a good estimation of its angular travelling speed. In practice then, inputs and outputs of the system are indistinguishable.

4-3-2 Experiments

A question one wishes to answer, though, is wether the statistical characteristics of the disturbances exciting the system are such (amplitude, intermittency, randomness) that a small amplitude travelling wave will be present for any length of time every time we try an experiment such as described above. More basically, we wish to know if the stalling process always starts as a small amplitude travelling wave, or if its nature is sometimes different.

The experiment described above was repeated a number of times over a large period of time (6 months). The inlet conditions (and thus probably the level of disturbances) were similar except for changes in the sound absorbing material placed on the muffler. Two experiments were performed at 1075 RPM, seven others at 2225 RPM. The length of time of the last uninterrupted propagation of small amplitude wave before stall is plotted for each experiment on Fig(4-7). We see that:

- Even in terms of rotor revolutions (which is the natural time scale for the phenomenon, according to theory), the waves may subsist longer at 1075 RPM than at 2225 RPM. More statistical evidence is certainly necessary before drawing a definite conclusion.

- In all cases, a small amplitude wave exists prior to stall, travelling at 35% of rotor speed for more than 30 rotor revolutions before turning into a stall cell. This seems to establish that in the three stage compressor, used in these operating conditions, the stalling process always starts as an already travelling small amplitude phenomenon.

4-4 Effects of mass flow transients and inlet distortion on the stalling process

4-4-1 Introduction

In this section, we wish to find out if typical engine operating conditions like inlet distortion or quick throttle transients modify the nature of the stall inception process we observed before, in cases of quasi zero $\left[\frac{d\phi}{dt}\right]_{stall}$. As discussed in the last section, the characteristics of pre-stall travelling waves could depend somewhat on the nature and rate of excitation from external disturbances; does this mean that in non-optimal situations, these waves do not exist? If they still exist, are their characteristics modified?

4-4-2 Presentation of the experiments

Experiments with a non-zero throttle rate at stall were performed on both the three stage and the single stage machines, both with a clean inlet and with distortion. This section describes the experimental set-ups used, and the way data was obtained and processed.

4-4-2-1 Three stage experiments

Three different ranges of throttle closing rates were used on the three stage compressor, the lowest being quasi-zero (as described in the previous section), the highest corresponding roughly to a flow coefficient rate of change of 0.1 flow coefficient points per 100 rotor revolutions. Data was simply recorded during the transient, up to and after stall; the hot wire probes were placed at the same position as before: 0.47 radii upstream of the IGVs. The compressor rotation speed was 2225 RPM.

In all experiments, a time resolved mass flow through the compressor was estimated by an average of the eight velocity measurements taken around the compressor circumference. Due to sensor drift, those measurements were only precise to within 5%; low frequency oscillations further compromised the value of the flow coefficient estimate, despite heavy low-pass filtering. The time derivative of the flow coefficient at stall was obtained by least-squares fitting a line to the last second of data before stall, with a typical standard deviation of 5%.

The inlet distortion was obtained by placing a plastic sheet on the FOD screen, covering 180 deg of the bellmouth. The characteristic of the distortion at a flow coefficient near stall (ϕ=0.488) is given on Fig(4-8).

4-4-2-2 Single stage experiments

Five different throttle transient rates were used on the single stage compressor, the highest corresponding to 0.08 flow coefficient points per 100 rotor revolutions, the smallest being 10 times slower. 2700 RPM was the rotation speed for all experiments. Again, data was recorded during the transients by eight hot wires placed 0.43 radii upstream of the rotor, i.e. immediately upstream of the IGVs.

The time resolved mass flow and mass flow derivatives at stall were estimated by the same procedure as for the three stage experiments. In this case however, the hot wires were re-calibrated before each run, giving an accuracy of 0.005 flow coefficient points (see the compressor map on Fig (3-4)). Another estimate of the mass flow was obtained by monitoring the throttle position, and calibrating this position vs flow coefficient before and after each run. Both estimates were within 0.005 points of one another, over the calibration range of the throttle (i.e. up to the stall point).

Inlet distortion was obtained with a three sector screen giving a gradual blockage over 180 deg of the compressor circumference. The screen was placed immediately downstream of the inlet bellmouth contraction. Fig(4-9) illustrates the distortion obtained at ϕ=0.350, just before stall.

4-4-3 Definition of the stall point and of travelling wave existence

On all plots in this chapter, the stall point is chosen as time reference. This implies to have a precise time-resolved definition of a stall point. After having tried many different definitions, the following was adopted: the stall point is the time at which the amplitude of the pre-stall wave reaches half of the stall cell's amplitude. This definition does not bear more physical relevance than any other; in particular, it does not correspond to the neutral stability point, which would be somewhat earlier, even before the start of the wave exponential growth. The actual start of the instability proved very difficult to identify with precision, especially on the single stage compressor, and this is why the definition given above was adopted.

To determine the length of the last unbroken stretch of small amplitude travelling wave, it was tracked backwards from the stall point until either its amplitude went below a certain level, or the phase speed exceeded a certain range (a sign the wave is not travelling uniformly any more). The limit levels for the amplitude and phase speed were determined by mean values obtained far away from stall, where no wave exists. Both criteria yielded the same values most of the time. When they didn't, the more "pessimistic" (i.e. the smaller) estimation was kept. Besides, the values obtained proved very insensitive to the limit levels chosen. Table 4-1 gives the limit levels used for the experiments.

Fig(4-10) illustrates the use of the definitions given above on one typical experiment.

4-4-4 Results and discussion

This paragraph describes the results of the experiments presented above, and discusses the effect of throttle transients and inlet distortion on the stalling process.

4-4-4-1 General characteristics

The phase plots of the first Fourier harmonic for all experiments are given in Fig(4-11), (4-12), (4-13) and (4-14), regrouped by machine and without or with inlet distortion. We see that, in all cases, the stall point is preceded by a stretch of straight phase, indicating the propagation of a small amplitude disturbance, at

10Hz for the single stage compressor, 13 Hz for the three stage. This is the main point to come out of this series of experiments: in both machines studied, regardless of the mass flow transient rate or the inlet conditions, the stalling process always starts as a small amplitude travelling wave, which eventually grows into a stall cell. This shows that whatever the conditions, stall does not occur without the prior presence of a small amplitude wave from which it can develop. In essence, the stability of the compressor with respect to stall is equivalent to the stability of this small amplitude travelling phenomenon, the evolution of which is set by a first order linear differential equation. This is an important simplification for the study of the compressor stability.

4-4-4-2 Effects of mass flow transients

For the rate of change of mass flow we have been using, the compressor behavior is quasi steady. From the linearized Moore-Greitzer model, we expect the damping of small amplitude waves to decrease as we get closer to the stall point, turning to zero there. Very crudely then, and for explanatory purposes, we can consider that there exists a flow coefficient region over which compressor damping is weak enough that small travelling waves can "survive" there, given sufficient excitation. Pre-stall wave existence time should therefore be roughly inversely proportional to $\left[\frac{d\phi}{dt}\right]_{stall}$. This can be shown by plotting the time extent of the last uninterrupted stretch of wave propagation leading to stall (a rough measure of the overall wave existence), vs $\left[\frac{d\phi}{dt}\right]_{stall}$. Fig(4-15) gives this for the three stage compressor, Fig(4-16) for the single stage compressor. As expected, we see a $1/\phi$ dependence in both plots, with an offset: whatever the throttle closing rate, wave existence seems to be longer than a certain limit. This is due to our definition of the stall point as the time when mid stall cell amplitude is reached; the duration of the exponential growth to mid amplitude is approximately constant, whatever $\left[\frac{d\phi}{dt}\right]_{stall}$. In fact, for the fastest transient cases, the small amplitude wave rises exponentially almost as soon as it is identified. Still, the expected dependence is observed.

4-4-4-3 Effects of inlet distortion

The effect of inlet distortion on the stalling process can be seen most clearly by comparing the first harmonic phase plots of the clean and distorted inlet runs (Fig(4-11) and (4-12)) on the three stage compressor. On the plots corresponding to the clean inlet, we see that before the last stretch of unbroken travelling wave leading to stall, some other, smaller stretches exist which die out because of stronger compressor damping at that point than immediately before stall. The presence of smaller stretches of travelling waves manifests itself by a global (though less regular) angular propagation of the phase. This propagation however, is much less present in the case of inlet distortion, which indicates that small amplitude waves have more difficulties travelling through a distorted upstream flowfield.

This observation is confirmed by the fact that the time of the last unbroken propagation of the wave leading to stall is generally smaller with inlet distortion than without, as seen on Fig(4-15) and especially on Fig(4-16). In fact, let us consider more closely the first experiment performed with inlet distortion on the three stage compressor, at quasi-zero throttle closing rate. It shows an unusually short propagation time of the small amplitude wave before stall develops, in what should be an "easier" case than faster transients. This illustrates the fact that even with slow mass flow transients, the nature of the system excitation is such that we cannot be 100% sure of having a period of pre-stall travelling wave longer than a certain limit before it grows into stall. Stall always starts as a small amplitude travelling wave, but the small amplitude stage can be short, especially in the case of inlet distortion.

The greater abruptness of the stalling process in case of inlet distortion is further illustrated by Fig(4-17). This shows a comparison between the first Fourier harmonic amplitudes of two transients on the single stage compressor, one with a uniform inlet, the other with inlet distortion. We see that the growth of the instability is very gradual in the clean inlet case, but much more rapid in the distorted case. Fig(4-18) shows the flow coefficients at which the final stretch of small amplitude wave leading to stall is first identified, for the uniform inlet and the distorted inlet transients. We see that for the clean inlet case, the last period of

wave propagation always starts at a higher flow coefficient than the steady-state stall point. The contrary is true for the distorted runs. We note that our estimation of the mass flow in the case of inlet distortion may be wrong, since we obtain a lower flow coefficient at stall with distortion than without. Nevertheless, the mass flow measurements are consistent within a group (distorted or undistorted).

4-4-4-4 Discussion of the effects of inlet distortion

The fact that wave propagation is more difficult in an upstream flowfield can be explained by the following arguments. In McDougall's model, a disturbance is caused to rotate by the slight blockage increase and the redistribution of the upstream flowfield it induces; we see that the mechanism will work better in the obstructed region (low flow, blades more loaded), but not as well in the clean region (higher flow than average). In the Moore-Greitzer model, the propagation mechanism is a just a function of the compressor lag in responding to local fluid acceleration caused by the passage of a disturbance. On the other hand, the wave damping depends on the local slope of the total-to-static pressure rise characteristic. If we regard a compressor with inlet distortion as two parallel compressors each operating at a different flow coefficient, it is clear that the distorted one is nearer to stall than, and might even be artificially stabilized by, the clean inlet compressor; small amplitude perturbations travel easily through the distorted (unstable) region, but are dampened out as soon as they reach the clean (stable) region. The extension of the Moore-Greitzer model to the inlet distorted case is discussed in detail in [20].

Another aspect of the problem is that a distortion is a continuous source of disturbances (unsteadiness, turbulence) to excite the system; but since this excitation is biased spatially (much more present in one region than the other), it may actually be a hindrance to a travelling wave.

The transition to stall is more sudden in the case of inlet distortion, and we propose two explanations for this. The first is that on the time scale of a stall event, the excitation responsible for the wave start may be random, but not white i.e. not equiprobable in time or in space, especially for the inlet distortion case. This argument is particularly true for mass flow transients: a few, if not one,

convected perturbations would determine the immediate behavior of the system. For this reason, it is felt that the same abrupt stall would occur much less often with a uniform inlet flow. A second explanation, is that (as was mentioned before) the wave may be so hindered by its interaction with the distorted region that it does not grow immediately, even though the compressor is potentially unstable. When it finally grows, it does so more suddenly.

Besides, we note that the greater abruptness of the stalling process in the case of inlet distortion may be an artifact of the way we look at the phenomenon. In particular, the higher Fourier harmonics (which we have decided to neglect) are more present in the case of inlet distortion, and may play an important role. This is illustrated by Fig (4-19), which shows that, in one inlet distortion experiment at least, the second Fourier harmonic went unstable before the first.

4-5 Influence of the axial position of sensors on wave detection

4-5-1 Introduction

Our hypothesis to explain the existence of pre-stall small amplitude travelling waves is the following: disturbances are swallowed by the compressor and convected until they encounter a weakly stable blade row. There, they are "caught" and start to rotate, while decaying or growing slowly. From equation (2-37), we expect the magnitude of the travelling disturbance to decrease exponentially upstream of the compressor face, but nothing is known about the flowfield inside the compressor. It is therefore not clear where along the compressor axis is the best location for wave identification, and this is the question that this section addresses.

4-5-2 Experiments and results

The experiments were performed on the single stage compressor, for reasons of ease of implementation. Fig(4-20) shows the different stations used along the compressor axis, and table 4-2 gives the axial location of the blades and of the hot wire stations. The rotor being the reference point, we have: station 1 0.94 compressor radii upstream, station 2 0.43 radii upstream (just upstream of the

IGVs), station 3 0.12 radii upstream (between IGVs and rotor), station 4 0.17 radii downstream (between rotor and stator), station 5 0.43 radii downstream (immediately downstream of the stator), and station 6 0.75 radii downstream. The compressor mean radius is 26 cm.

In the first series of experiments, eight hot-wire probes were placed in turn at station 2 to station 6 (station 1 had four hot-wire probes to monitor mass flow). Each time, the compressor was throttled to obtain the slowest $\left[\frac{d\phi}{dt}\right]_{stall}$ possible. As we have seen before, the small amplitude travelling wave phenomenon seems to have a statistical dimension, which really means that it is not exactly repeatable. Therefore, these experiments cannot be quantitatively compared, in particular in terms of wave amplitude and time extent; only qualitative comparisons can be made. Fig(4-21) shows the phases of ten such experiments, performed at stations 2 to 6. Again, in all cases, a small amplitude travelling wave is present before stall occurs. Actually, some of these waves are there uninterrupted since before data was started to be recorded. On the whole, no major differences can be seen between the different stations. Wave propagation seems to be more difficult a station 4, and also (to a lesser extent) at station 5, than elsewhere. The other stations appear more or less equivalent. This is all the information that can be inferred from this series of experiments.

In another series of experiments, four hot-wire probes were left at station 1, while two other groups of four wires were placed at different stations along the compressor axis. This way the amplitude of the rotating wave at each station could be referenced to the amplitude at station 1, so that different experiments could be quantitatively compared to each other. Again, the compressor was throttled as slowly as possible. The amplitude of first Fourier harmonic during the last 220 rotor revolutions before stall is given in Fig(4-24), (4-25), (4-26), (4-25) for five different experiments, which allows comparison of the amplitude at different stations. For stations 2 to 6, the ratio of the amplitude at that station to the amplitude at station 1 was computed at each instant, then averaged over 6 seconds to yield just one number. These ratios are plotted on Fig (4-26), along with the theoretical prediction (again with reference to station 1) for the upstream

flowfield, which is given by the following equation (which follows from equation (2-37)):

$$\frac{A(n)}{A(1)} = e^{\frac{x(n)-x(1)}{R}} \qquad (4\text{-}2)$$

where A(n) is the amplitude at station n, and R is the compressor radius. We see that amplitude at station 2 is actually larger than expected; amplitude at station 3 is lower than it should be, but the theory may not extend to this station placed between IGVs and rotor. The large oscillations (17 Hz) seen in the wave amplitude at this station (Fig(4-22)) may bias the averaging process by which the final ratio was obtained. For reasons as yet unclear, the amplitudes at stations 4, 5, and 6 rise according to the distance along the compressor. We note that for these stations, the hot-wires were oriented so as to monitor the velocity at the expected leaving angle from the blades, which may not be the best direction to choose. An approximation of the axial amplitude of the wave can be obtained by multiplying the wave amplitude by the cosine of the angle of the hot-wires with the compressor axis.

What is probably more important for control purposes is how "clean" the signal is (i.e. free from noise not relevant to the travelling phenomenon), and how well it reflects the actual wave characteristics: position and amplitude. In other words, we would like to reason in terms of signal to noise ratio. The sources of noise are the following:

- Turbulence: constant upstream, grows as we go through the compressor.
- blade row interaction, wakes: none upstream, increasing as we go through the compressor.

The magnitude of the signal of interest grows exponentially as we get closer to the unstable blade row, steps down as we go through the IGVs, then rises again (Fig(4-26)). On the other hand, we see from Fig(4-22) - Fig(4-25) that the noise increases dramatically as we enter the compressor blade rows, and decreases only far downstream of the stator. A rough measure of the signal to noise ratio at a given station can be to compute the standard deviation of the amplitude at that

station relative to the amplitude at station 1, and divide this number by the mean of this relative amplitude (as computed in the last paragraph). This is plotted on Fig(4-27), and we see that the signal to noise ratio indeed drops sharply as we go through the compressor blade rows, to rise only far downstream of the stator. We conclude that for best signal to noise ratio in the active control implementation, the probes will want to be installed around station 2, immediately upstream of the IGVs.

4-6 Conclusions

In this chapter, we addressed the question of the nature of the stall inception mechanism. Two low speed axial compressors were experimentally investigated for the experiments. First, a typical experiment was presented. Its results clearly showed the existence of a small amplitude wave, travelling at 35% of rotor speed for 90 rotor revolutions before stall occurred. Furthermore, the stall cell evolved directly from the exponential growth of this wave, without any discontinuity in amplitude or angular position. Qualitatively, this phenomenon is well described by the linearized Moore-Greitzer model. The results also established a framework for the future study of the phenomenon, in particular the choice of data representation. A section then described the possible statistical nature of the travelling wave process, and gave supporting experimental evidence: 9 out of 9 experiments, showed that stall evolved from small amplitude travelling waves. In all 9 cases, the time extent of the last uninterrupted stretch of travelling wave was longer than 30 rotor revolutions. Next, we studied the reaction of the compressor-upstream flowfield system to typical causes of compressor stall in jet engines: throttle transients and inlet distortion. All cases showed the same behavior for stall inception as observed before, and this established the universality of this stalling process. Side consequences of throttle transients are a reduced existence time of the small amplitude stage of wave propagation, inversely proportionally to the mass flow derivative at stall. Inlet distortion seems to make the travelling wave propagation more difficult, and the stalling process more abrupt. Finally, the question of the best axial station for wave detection was addressed; a station

just upstream of the IGVs was found to have the best characteristics, mainly the large amplitude and the cleanness of the signal obtained there.

CHAPTER FIVE

STUDY OF THE COMPRESSOR-FLOWFIELD SYSTEM STABILITY USING SMALL AMPLITUDE TRAVELLING WAVES

5-1 Introduction

The linearized Moore-Greitzer theory derived in chapter two predicts that any small amplitude perturbations in the compressor upstream flowfield should travel according to the following wave equation:

$$\tilde{\varphi} = \sum_{|k|\neq 0} \lambda_k e^{(|k|\eta+\sigma_k\xi)} \; e^{i(k\theta-\omega_k\xi)} \qquad (5\text{-}1)$$

From the first term of the right hand side, we expect exponential attenuation with distance from the compressor face, and exponential growth or damping in time according to the local slope of the total-to-static pressure rise characteristic of the compressor. The attenuation with distance has been partially dealt with in the previous chapter, showing reasonable agreement with the theory. In this chapter, we address the question of the damping or growth in time. First, we introduce different analytical tools for time series analysis, which will allow us to retrieve the dynamics of our system from the noise and other unmodelled dynamics present in the data. Using these techniques, we obtain a measure of the system's time damping as a function of the compressor flow coefficient, and discuss the consequences. The chapter is closed by a section on the possible engineering use of the small amplitude travelling wave phenomenon as a stall announcer.

5-2 Presentation of the tools and techniques

5-2-1 Introduction

In this section, we present some tools for the analysis of time series. These techniques fall into two strongly interrelated categories: power spectral density, and system identification techniques.

5-2-2 Power spectral density analysis

Spectral analysis consists in determining the distribution of the power of a signal over its different frequency components. In our case for example, we wish to identify the frequencies present before stall in the first spatial harmonic of the velocity data. The travelling wave we are interested in should manifest itself by a peak at around 10 Hz for the single stage compressor, since this is the approximate travelling speed of the phenomenon in this machine. The height of the spectral peak represents roughly the power of the wave, concentrated around the frequency of the peak. We see that PSD analysis (as it is often called) is a quick and efficient way of knowing if travelling waves actually exist, just by looking for a peak in a narrow frequency range. It is also a more systematic way of investigating the wave presence than just studying the phase of the first Fourier harmonic. The phase, in fact, is driven by the strongest frequency component present in the data; if the travelling wave is not the strongest spectral component, it will not appear in the phase propagation, but it will still appear as a peak in the PSD. As an example of the PSD's capacity to distinguish hidden spectral features, let us consider Fig(5-1). We see that the rotor frequency (in this case) is perfectly apparent in the PSD, even though the phase doesn't show it. Another important feature of PSD analysis is that even if the wave is present only intermittently because of strong system damping, a peak will still exist in the spectrum.

As was discussed in chapter four, the intermittency of the system excitation is responsible for the intermittency of the wave appearance. In addition, the amplitude of the excitation (the initial condition of the ODE) conditions the length of time during which the wave exists, for a given system damping. With these two characteristics (intermittency and amplitude), the excitation will act directly on the power of the wave, and influence the PSD peak. On the other hand, the wave

power is also a function of the system damping; thus, if the intermittency and the amplitude of the driving disturbances are independent of the compressor operating point, the height of the spectral peak corresponding to the travelling wave will be a function of the system's damping alone. But we know that environments like inlet distortion may modify the characteristics of the excitation, and thus change considerably the height of the spectral peak, even for a constant system damping. We therefore predict a problem in trying to use the PSD as a universal tool for system stability prediction.

PSD analysis is usually based on a procedure employing the Fast Fourier Transform (FFT). This approach is popular because it is computationaly efficient, and produces acceptable results for a wide range of signals. However, it suffers from two important limitations: first, its frequency resolution is roughly inversely proportional to the time interval available for analysis. Secondly, the absence of information for the data outside the time interval causes energy leakage from peaks into "sidelobes", distorting the spectral response. These limitations are of course particularly troublesome in the case of short data records, or for data with time varying spectral content. Alternative methods have recently been developed to alleviate this problem, and those are the ones which will be used in this study. A wide body of theory exists on these methods, and we will not attempt to describe them here; a very good summary is given in Kay and Marple [22]. The basic principle is to fit a linear model to the data, using the same procedure as system identification (which we will describe later), but without any consideration for the physical relevance of the model chosen. The main advantage of these methods is their ability to resolve sharp spectral features, even with short data records. For short data records though, the heights of the spectral peaks obtained have little physical meaning, and suffer from high variance.

5-2-3 System Identification

A discrete time series y_n can always be modelled as the solution of a difference equation:

$$y_n = a_1 y_{n-1} + \ldots + a_p y_{n-p} + v_n \qquad (5\text{-}2)$$

where v_n is a noise term with unknown characteristics, which acts as the excitation of the system (turbulence, or any convected disturbances in our model). Choosing the "right" number of parameters and estimating the parameters a_i themselves is the subject of system identification.

Equation (5-2) has an equivalent state representation as a first order linear difference system of dimension p:

$$Y_n = F Y_{n-1} + V_n \qquad (5\text{-}3)$$

$$Y_n = \begin{bmatrix} y_{n-p+1} \\ . \\ . \\ y_n \end{bmatrix}, \quad F = \begin{bmatrix} 0 & 1 & . & 0 \\ . & . & . & . \\ 0 & . & 0 & 1 \\ a_p & . & . & a_1 \end{bmatrix}$$

Both the p^{th} order difference equation (5-2) and the linear difference system (5-3) have continuous time equivalents, respectively as a p^{th} order linear differential equation, and as a linear differential system of dimension p. If A is the matrix of this latter system, we have:

$$F = e^{A\Delta t} \qquad (5\text{-}4)$$

where Δt is the sampling frequency of the time series.

The characteristic polynomial of equation (5-2) is also the determinant of zI_d-F, where I_d is the identity matrix. The zeros z_i of this polynomial are the eigenvalues of matrix F, and correspond to the eigenvalues λ_i of matrix A. Furthermore, we have:

$$z_i = e^{\lambda_i \Delta t} \qquad (5\text{-}5)$$

We see that estimating the p coefficients a_i of equation (5-2) really consists in fitting a p^{th} order linear model to the data. This linear fitting makes good sense in practice providing a model already exists, which spares us the much more delicate task of choosing the model order; only the parameters themselves are left to be estimated. The results that this technique can yield are also enhanced if unmodelled dynamics and correlated noise present in the data are taken out by adequate filtering. Unmodelled dynamics can be identified by looking at a PSD of the data. If filtering cannot eliminate them, they should at least be accounted for by using a higher order model. Correlated noise can also be modelled: if only white excitation noise is present, we have a pure AR (AutoRegressive) model; correlated noises or additive measurement noises can be dealt with by ARMA (AutoRegressive-Moving Average) models. Reference [23] can be consulted for more details.

The fitting of the model to the data can be performed in two different ways:

- in the time domain
- in the frequency domain, fitting the transfer function of the model to the PSD of the data.

The time domain fitting is the only one we will use, since it is well suited to real time implementation. The fitting is done by least squares techniques, either recursively (on-line), by updating the estimates of the model parameter for each new data point taken [24] [25], or by processing the whole data sequence as a batch (off-line) [26]. Recursive methods are particularly interesting because they do not use the assumption that the signal is wide sense stationary (w.s.s). Consequently, they do not restrict the eigenvalues of the model to the left half-plane, and this allows to track unstable poles (which off-line methods cannot do, since they assume a wide sense stationary signal, and set forward and backward prediction errors equal [23]). In addition, recursive methods can be made to follow time varying parameters, by using a "forgetting" factor to gradually discard old data. This forgetting factor is denoted q, and $0<q\leq 1$ ([23]-[25]). Each past data point is weighted by q^k, (where $k\Delta t$ is the time between the past data point in question and the most recent data point taken), so that points further in the past are weighted by a lower weight factor. $q=1$ corresponds to no forgetting at all, and the

faster the time variations in the parameters to be identified, the lower q should be set. A common choice is to take q=0.99.

The amount of computations required by the Recursive Least Squares algorithm is proportional to p^2, (where p is the model order), but faster algorithms are now available with only linear dependence in p [27]. Off-line least squares algorithm such as Marple's [26] also have a computational time proportional to p.

In conclusion, we see that the parameter identification approach is potentially very interesting, considering the amount of information it can yield. Nevertheless, many side aspects of the method such as noise dynamics, and the related problem of choosing the "right" number of coefficients (i.e. the model order) make the parameter identification problem heavier and more delicate in practice than the power spectral density methods described in the previous section. Therefore, both methods will be used, PSD analysis for a first study of the problem, and system identification techniques when more precise information is required.

5-3 Experiments and results

5-3-1 Introduction

Let us first summarize what we know or suspect about the stalling process, and its relation to the small amplitude travelling wave phenomenon. Up to very recently, the notion of the stability of a compressor with respect to stall was purely empirical: if a normally operating compressor went into stall after a finite time, it was called unstable, stable otherwise. Equation (5-1) gives an a priori different meaning to the notion of "compressor-upstream flowfield stability", that of a linear system: if the damping term (σ_k) in this equation is negative, hypothetical small amplitude travelling waves will decay, and the system is called "stable". Otherwise, the waves amplitude will grow exponentially, and the system is "unstable" (the non-linear extension of equation (5-1) reconciles the theory with the empirical definition given above by predicting the exponentially

growing waves to level off into a stall cell). Now, in the previous chapter, we have verified experimentally that:

- small amplitude travelling waves do exist,
- the stability of those small amplitude waves is equivalent to the global stability of the compressor with respect to stall. In fact, both notions describe the same physical phenomenon although at different stages, and stall will always occur from, but only from, the exponential growth of small amplitude travelling disturbances.

The small amplitude wave aspect is just a more time resolved look at the global phenomenon of stall. Also, this approach brings a new dimension to qualify the system stability. The traditional view of stall was very much a binary, stable/unstable viewpoint, in occasions linked (with little success) to a zero slope of the total-to-static compressor characteristic. Now, we have observed an experimentally phenomenon which seems to reflect a degree of stability of the system. More precisely, we know that travelling disturbances are dependent not only upon the system damping but also upon the excitation (which was not studied here), and until now we haven't been able to tell them apart. This section is an attempt to distinguish one from the other, to average out the apparently random contribution of the excitation to the travelling wave, and study directly the compressor damping (σ_k), which is the quantity of interest since it really determines the system behavior. It could indicate how stable the compressor is, how close it is to stall, and thus be used as a stall anticipator. The goal of this section is thus to use the small amplitude travelling wave phenomenon as a indicator of stability, by applying the data analysis techniques presented in section 5-2. We want to know in what flow coefficient range can stretches of travelling waves be identified, and if the system's damping can be obtained from this analysis. We will then study the variation of the system damping with flow coefficient, and it dependence upon the compressor environment.

5-3-2 Experiments and result

The experiments performed were simple: the single stage compressor was just run at a steady operating point, while 12.3 seconds of velocity data was

recorded. By varying the flow coefficient at which these points were taken, a complete map of the compressor's behavior was obtained. For all the experiments, the compressor rotation speed was 2700 RPM.

As we pointed out in section 5-2, we have two basic tools at our disposition to study the dynamics of the system: PSD analysis and system identification techniques. A PSD may yield less quantitative information, but it is more straightforward to use. Before attempting system identification and its subtleties, we would like to establish that travelling waves are actually identifiable over a reasonable range of flow coefficient away from stall.

5-3-2-1 PSD analysis

Let us study the variation of the height of the spectral peak corresponding to the small amplitude travelling phenomenon with respect to the flow coefficient. This is plotted on Fig(5-2), for both the uniform and the distorted inlet flow cases. For both cases, the curves show a nice sensitive growth of the PSD peak as we decrease the flow coefficient towards stall. Note that at the highest flow coefficient represented on the plot for the distorted case (ϕ=0.405), the spectrum is almost flat (Fig (5-3)): nothing but a slight hump can be seen around 10 Hz, which indicates that any wave travelling in the compressor has a power density barely greater than that of the background noise; the signal to noise ratio is effectively down to 0 dB at that point. As was noted in chapter four, the flow coefficient at stall is lower in the distorted case than in the uniform case (see the speedlines of on Fig(5-4)). Whether this is actually an error or not, we can still qualitatively compare the two cases. In particular, we see that the PSD peak curve is much flatter with distortion than without, and the level near stall is much lower. This reflects the increased difficulty the wave encounters when it travels in a distorted environment, which is a conclusion we had already drawn from the experiments described in chapter four. But since PSD analysis cannot separate the respective contributions of the damping and of the excitation on the wave power, we cannot conclude if inlet distortion affects the system damping or not.

PSD analysis has enabled us to identify a range of flow coefficient over which travelling waves can exist. Nevertheless, it doesn't allow us to study the

system damping, for it is also sensitive to the level of disturbances driving the system. We will now resort to system identification techniques for more information.

5-3-2-2 System identification

Our model for the small amplitude phenomenon is the following ODE

$$\dot{C}_{-1}(t) = (\sigma_c - i\,\omega_c)\, C_{-1}(t) + V(t) \qquad (5\text{-}6)$$

with a corresponding discrete time model:

$$C_{-1}(n) = a_1\, C_{-1}(n-1) + V(n) \qquad (5\text{-}7)$$

$$a_1 = e^{(\sigma_c - i\omega_c)\,\Delta t} \qquad (5\text{-}8)$$

where C-1 is the first harmonic data, and V the driving noise; σ_c and ω_c are respectively the damping and the frequency of the travelling wave, and are the parameters to be estimated.

As described in section 5-2, we want to remove from the data all the dynamics not relevant to this equation. Let us consider for example a PSD taken at ϕ=0.377 with uniform inlet, which is given in Fig(5-5). It shows a peak at 30 Hz which is unmodelled (and unexplained), and a peak at 0 Hz which corresponds to the DC shift of the sensors; this latter peak can be smoothed out, but the 30 Hz peak is more difficult to deal with elegantly: we will simply low-pass filter the data from -25 Hz to 25 Hz (brute force). This also enables us to bring the sampling period down to 12 times the one we used to take take the data. This tends to "whiten" the driving noise present in the data, which is a good feature for our parameter identification.

Having adequately processed the data, we can perform the parameter identification itself. This can be done off-line (batch processing), or on-line (recursively). Fig(5-6) illustrates the quadratic convergence of the recursive algorithm on a high signal-to-noise ratio case: uniform inlet flow at ϕ=0.361. In

this case, 150 rotor revolutions are sufficient for convergence. Fig(5-7) however, shows that the convergence can be much slower for low signal-to-noise ratio situations (inlet distortion, ϕ=0.398); more than 300 rotor revolutions are necessary in this case. The data intervals we took are 12.3s long, which represents 540 rotor revolutions, so we can be sure that convergence is obtained in each case.

Fig(5-8) shows a comparison between the PSD of uniform inlet data at ϕ=0.361 and the fitted first order model. Fig(5-9) shows a similar plot for the inlet distortion case, at ϕ=0.356. We see very good agreement between the data and the fitted model, which justifies both the method and the model used, for both clean and distorted cases. Further away from stall, damping is stronger and the signal is weaker, so that measurement noise can be a problem. To alleviate this, two estimates of the damping were computed, one with an AR(1) model (first order system driven by white noise), the second a (1,1) ARMA model [23] (first order system driven by white noise, with additive measurement noise). Both estimates were usually close, except in cases of very low signal to noise ratio, as Fig (5-10) illustrates at ϕ=0.382 with inlet distortion: the pure AR model can be "fooled" by the spectral floor of noise, and tend to overestimate the damping; the ARMA model, on the other hand, takes this noise into account.

A complication occurred in the inlet distorted case, near stall: a peak appeared at -11 Hz, i.e. the frequency opposite that of the travelling wave; of course, this peak cannot be filtered out without filtering the wave itself, so it had to be accounted for by taking a model of order two. The procedure is illustrated on Fig(5-11), at a flow coefficient of 0.353.

Fig(5-12) shows the damping ratios computed by the AR(1) and the ARMA(1,1) methods vs the flow coefficient, for both the uniform inlet and the distorted inlet case. The two curves rise nicely to near zero damping close to stall, but our main observation is that the rise to instability is much sharper in the case of inlet distortion. Away from stall, the system with inlet distortion is more strongly damped than the uniform inlet case: for a given excitation, travelling waves die out more quickly in the distorted environment. As we mentioned in chapter four, the distorted system can be thought of as two parallel systems with

different degrees of stability, causing a propagating wave to travel in turn through a stable and an unstable region. This might partly explain our observation, but reality is certainly more complex. Besides, the model developed in chapter two may not be strictly valid here , especially at the interface between both regions (no vorticity hypothesis); a discussion is given in [20].

We should link the above observation with the one we made earlier (Fig(5-11): near stall, a peak appears in the PSD at -11HZ, which is the frequency opposite to the travelling wave frequency. It seems that when the wave reaches a certain amplitude, it starts to interact very strongly with the distortion, and this creates a standing wave in the annulus. The PSD interprets this phenomenon as the interaction between the wave travelling at 11 Hz, and another smaller wave travelling at the same speed, but in the other direction (at -11 Hz). This interaction translates as a "leakage" of power from the travelling wave peak to the negative frequency peak. This leakage probably accounts for the slight drop-off of the PSD and damping curves very near stall, which would indicate a sort of artificial stabilization near stall. It may also explain the abrupt transitions to stall observed in chapter four. But the main point we draw from this observation is that an additional phenomenon occurs near stall in the inlet distorted case, which is not contained in the linear model developed in chapter two. It is therefore not properly analyzed by our system identification technique, even though an additional pole was introduced to take it into account.

5-4 Engineering use of pre-stall travelling waves as stall precursors

5-4-1 introduction

This section tries to address the difficult subject of an evaluation of pre-stall travelling waves as a stall precursor. We can broadly separate possible applications into two groups: the applications in which time for analysis is unlimited, and the others.

5-4-2Steady applications

As we have seen in the previous section, the compressor damping can be very well estimated if a sufficient time (say more than 300 rotor revolutions) of Fourier harmonic data is available. The compressor damping is the most consistent precursor, in the sense that it gives a direct measure of the system's stability. What it doesn't give, on the other hand, is how far an operating point is from the stall point, in terms of flow coefficient, since the rise to instability is different for each compressor. In the single stage compressor, for example, this rise takes place over 0.06 flow coefficient points, whereas on the three stage compressor the same region is 0.02 points. In addition, we have seen that for a given compressor, inlet distortion can modify the damping at a constant flow coefficient. Therefore, a priori knowledge of the damping vs ϕ curve doesn't help if the inlet flow conditions are not known.

5-4-3 Real time (unsteady) applications

This section concerns stall warning schemes suitable for use on engines undergoing transients. This is of course a much more challenging application than the steady applications described in the last paragraph, since these transients typically take between 40 and 400 revolutions from the operating line to the stall line. Furthermore, only part of the region from the operating line to the stall line may be favorable to the propagation of travelling waves. As the operating point crosses this region, the wave damping will vary from strong (say -40) to zero, which is an additional complication. Consequently, one shouldn't expect to obtain a very consistent estimate of the compressor damping during stall transients.

To follow time varying parameters, the identification algorithm used in section 5-3-2-2 can be run with a forgetting factor, to gradually discard old data; this factor can be set very close to one (slow response and lag, but small variance in the estimate), or closer to 0.9 which will make the estimate less consistent but quicker to react. Fig(5-13) shows the on-line estimation of the compressor damping for the five throttle transients on the single stage compressor, with a clean inlet (section 4-4-4-1). For all five cases, the forgetting factor was set at 0.99. Also reproduced on this graph are the steady-state points of Fig(5-12). By

comparing the throttle transient curves with the steady-state one, we see that the first two transients are slow enough as to be quasi steady for the algorithm: instability is well predicted, and even anticipated. On the other hand, the algorithm is too slow for the last three transients: the forgetting factor is too high in these cases to ensure a fast enough response, and follow the system parameters. The response can be ameliorated somewhat by turning down the forgetting factor, but at the expense of consistency. This is illustrated by Fig(5-14), which shows on-line estimations during the fastest throttle transient, using three different forgetting factors: 0.99, 0.94, and 0.89. We see that the consistency of the estimate is degraded, but that instability is approached sooner.

In a general sense, changing the forgetting factor from 1 to 0.9 corresponds to shifting our aim from trying to estimate the compressor stability (which requires a lot of information and therefore takes time), to merely spotting the start of the small amplitude wave which will turn into stall (which is much less ambitious, but is ultimately all the useable warning we are likely to get). In other words, as the throttle transients get faster, we expect to obtain a proportionally reduced amount of information before stall, and our algorithm should be parameterized to take that into account. For example, the forgetting factor can be lowered if transients are expected.

Inlet distortion also promises to be a challenge: we know it dampens rotating waves more strongly, thereby reducing the amount of information available. Furthermore, in this case, the linear model doesn't describe the wave behavior correctly near stall, which makes system identification more delicate. For this reason, no on-line estimation was performed during transients with inlet distortion.

5-5 Conclusions

This chapter has been concerned with the use of the pre-stall travelling wave as a reflection of the system's stability, to estimate the damping of the compressor. The first order ODE predicted by the Moore-Greitzer theory was fitted to the data with excellent agreement for both clean and inlet distorted cases. The

damping ratios estimated were found to be dependent upon the flow coefficient, but also upon the compressor environment (inlet distortion). Finally, recommendations concerning the use of pre-stall travelling waves as a stall precursor were given.

CHAPTER SIX

HIGH SPEED EXPERIMENTS

6-1 Introduction

The Moore-Greitzer theory and its linearized version use the assumption of incompressible flow through the compressor, and in the upstream and downstream flow regions. This is a key element in the derivation of the equations, and the extension of the model to the compressible case (the only relevant one for high speed machines) is still to be performed. Nevertheless, it is felt that the mechanism for stall inception in high and low speed machines should be qualitatively quite similar. Since it has been found that in low speed compressors the stall inception mechanism is the growth of small amplitude waves, it is worth looking for the same phenomenon in high speed machines, since only high-speed machines are of practical interest.

6-2 Three stage high-speed experiments

6-2-1 Description of the rig, instrumentation and technique

The experiments described in this section were performed by Pratt & Whitney Government Engines Business, West Palm Beach, Florida, on a three stage high-speed machine. Three groups of eight Kulite high response pressure transducers formed the instrumentation. These transducers measured static pressure at the compressor casing, and each group was placed at the leading edge of one of the three stators. Station 4 designates the first stator, station 5 the second, and station 6 the third. Within these groups, the taps were distributed around the compressor circumference as uniformly as possible, but the angular spacing between two neighboring taps could not be made constant because of

already existing instrumentation conflicting with the desired placement. Table 6-1 gives the circumferential location of the pressure transducers for the three axial stations used. This unequal spacing is not a problem from a theoretical point of view: the spatial Fourier transform can be performed just as well. Its derivation is given in appendix A. The only practical consequence is that the error on the measurements is amplified when calculating the Fourier coefficient. This amplification is small in our case, since the probes are nearly evenly spaced.

The signals processed were in volts, i.e. not converted to engineering units. Nevertheless, the output voltage of a pressure transducer is roughly proportional to the pressure level. As for the low speed experiments, the signals were band-pass filtered to remove the DC level and high frequency noise from the data. According to our rule of thumb from chapter three, we first band-pass filtered from 5% to 120% of rotor frequency. All interesting information was found never to exceed 75% of rotor frequency, so the data was subsequently low-pass filtered at that frequency. Before the processing, the DC level and the RMS level of some of the signals were very different from the others at the same axial position. Even with a distorted inlet, this can only be attributed to sensitivity variation from sensor to sensor (remember that we are processing voltages not actual pressure). The RMS level of the "bad" sensor was therefore adjusted to the level of the neighboring sensor, and generally yielded good information.

All the experiments presented in this section were performed in much the same manner as the low-speed experiments described in chapter four: the flow coefficient was reduced by closing the throttle valve while data was being recorded. As soon as surge was sensed, bleed valves were opened to stop the instability.

6-2-2 Very slow throttle transients, uniform inlet case

This section presents results from two experiments performed with a uniform inlet, each with a different vane stagger (IGV and stators). The transient was as slow as the throttle would allow. Both sets of data were similar in many respects, and we present some characteristics common to both.

- Fig(6-1) shows eight pressure traces taken at station 4. We note that the RMS level of the signals are quite different. On this graph, the RMS level of channel 4 (which was obviously low), has been adjusted to that of channel 5.

- The data from station 4 (Fig(6-2) and Fig(6-3)) clearly indicates the propagation of small amplitude disturbances before the occurrence of stall/surge. Furthermore, we note that both the first and the second Fourier harmonics are rich in information (which is a situation that had not been observed in the low-speed experiments of chapter four). Actually, the second harmonic has a higher amplitude than the first most of the time, as is illustrated by Fig(6-2), and both amplitudes seem to vary independently. The phases of the first and second harmonic are shown on Fig(6-3), and we see that the propagation of the second harmonic is more regular than that of the first. The last unbroken stretch of second harmonic existence lasts for more than 100 rotor revolutions, which is an enormous time scale. Within the same time period, the first harmonic "disappears" a couple of times; nonetheless, it is present for stretches of up to 60 rotor revolutions. The third harmonic, however, is virtually non-existent.

- The leading edge of the first stator is the location where the signal is the strongest. This is seen by comparing the amplitude (Fig(6-4)) and phase (Fig(6-5)) of the second harmonic at different stations. The difference between stations is more pronounced here than in the case of the single stage compressor studied in chapter four.

- The PSD of C_{-1} and of C_{-2} for the whole data sequence up to stall/surge is given in Fig(6-6), and shows clearly the peaks corresponding to the first and second harmonics respectively at 18.5% of rotor frequency for the first and 37% for the second. This seems to indicate that both modes are actually travelling together, which is confirmed on Fig(6-7), showing the wrapped phases of both harmonics. The ratio of the travelling speed of the first harmonic to rotor speed is an important parameter for wave identification as performed in chapter five. In this case, it is only 0.18, compared to 0.28 and 0.22 respectively for the three stage and the single stage compressors investigated in chapter four: there are fewer wave revolutions for a constant number of rotor revolutions.

As we mentioned at the beginning of the section, two experiments were performed, each with a different vane setting. All the plots given above correspond to a "nominal" setting. The experiment conducted with the other setting also showed clear pre-stall wave propagation, for period of up to 50 rotor revolutions. This is less than for the experiment we analyzed above, which may indicate that the vane stagger angles are important parameters for the propagation of small amplitude waves. In any case, 50 revolutions is more than enough for stall warning.

In conclusion, these experiments are very encouraging: they prove the existence of pre-stall small amplitude rotating waves in high-speed machines, for a considerable length of time (50 rotor revolutions) before the occurrence of stall.

6-2-3 Very slow throttle transient, distorted inlet case

One stall transient was performed with a 180 deg inlet distortion, again by closing the throttle as slowly as possible. The phases of the first, second, and third Fourier coefficients are plotted on Fig(6-8). The second harmonic has what can be considered as a noisy slope, which may or may not indicate some overall disturbance propagation. On the other hand, a small stretch of well defined slope exists between -120 and -100 rotor revolutions, which suggest that a disturbance does in fact travel during that time. This is evident if one looks at Fig(6-9) which displays the eight pressure traces taken at station 4. Channel 0 shows some sizeable disturbances, which appear at a well defined frequency: 6% of rotor frequency (shedding from the inlet distortion?). These disturbances, for example the one starting at t=-135 revs, are strongly attenuated by the time they reach probe 1; probe 2 barely sees them at all. But the disturbance starting at t=-120 revs travels for 15 rotor revolutions, at 13% of rotor speed. This is not the same frequency as observed in the uniform inlet case (18.5%). We also note that when the compressor finally turns unstable, large disturbances start travelling at yet another frequency: 8% of rotor speed.

The PSD of the second harmonic for the whole sequence up to surge/stall is given on Fig(6-10), and shows a complicated picture. The two peaks at -6% and 6%

are due to the disturbances seen on channel 0. The small peak at 13% shows the propagation of the disturbance between -120 and -100 revs. The other peaks, at 26% and 50%, are unexplained.

It would appear from Fig(6-9) that disturbances are being created inside a well defined region (around probes 7 and 0) and get strongly attenuated once they travel out of the region. As we mentioned in chapters four and five, we may think of the system as two parallel compressors operating at two different flow coefficients, and therefore with different degrees of stability. Travelling waves propagate easily through the unstable region, only to be damped as they travel out of it. This phenomenon may be troublesome if we want to use the small amplitude travelling wave as a stall precursor. A solution can be to look for travelling disturbances on a more local scale, i.e. in part of the annulus only. To do so, we can for example cross-correlate the outputs from two neighboring transducers, according to the following formula:

$$R_{xy}(p,N) = \frac{1}{40} \sum_{n=N-39}^{N} x(n)\, y(n-p) \qquad (6\text{-}1)$$

$R_{xy}(p,N)$ is the cross-correlation of signals x and y, with a lag p, and taken at time N. The number 40 is arbitrary; here, for example, it was chosen such that $40\Delta t$ equals one period of a wave travelling at 13% of rotor frequency (as the disturbance observed above seemed to). The lag can be expressed as a period of rotation, by dividing it by the angle (in deg) between the two transducers in question, and multiplying by 360 deg. As an example, let us consider Fig(6-11), which shows the cross-correlation between channels 0 and 1, at t=-110 revs. The cross-correlation has a maximum at a lag of 8.1 rotor revolutions, which indicates that , at t=-110 revs, a wave is travelling between channels 0 and 1 at $1/8.2 \approx 13\%$ of rotor speed. This can be verified by looking at Fig(6-9). Now, we can calculate what that maximum cross-correlation is at each instant in time, and keep only the maxima that have a lag between 7% and 70% of rotor speed (see Fig(6-11)). This is plotted on Fig(6-12) (again for the cross-correlation between channels 0 and 1). This figure can be compared to Fig(6-9) to show that indeed, the peaks of the max

cross-correlation correspond to the disturbances travelling from channel 0 to channel 1, for example at times t=-170 revs, t=-150 revs, but also just before stall, at t=-30 revs, and t=-15 revs. Let us now calculate the max cross-correlation for each pair of neighboring sensors, and compare them. This is done on Fig(6-13). The cross-correlation of channels 0 and 1 shows some travelling disturbances in this region as soon as t=-180 revs, 60 rotor revolutions before any disturbance manages to travel around the annulus. On the other hand, nothing travels between channels 4 and 5 before t=-115 revs. This simple analysis shows that looking for travelling disturbances on a more local scale can be an answer to the problem posed by inlet distortion.

6-2-4 Fast throttle transient case

The throttle transient studied took 450 rotor revolutions from the operating line to the stall line. The phase of the first harmonic at station 4, 5, and 6 are given on Fig(6-14), while the second harmonic phase is plotted on Fig(6-15). We note the following points:

- The phase of the first harmonic travels in the direction of the rotor at station 4, but in the opposite direction at station 5 and 6.

- The same observation holds for the second harmonic, except that in this case it is the phase at station 5 which travels in the direction of the rotor, while the phase at station 4 travels in the opposite direction.

We thus have the following situation: at a given station (4 or 5), the first and the second harmonic travel in opposite directions; in parallel, a given harmonic travels in opposite directions at station 4 and station 5. This characteristic is difficult to reconcile with the idea of a fluid mechanic disturbance travelling around the annulus, since all phases would then be travelling in the same direction (preferably in the rotor direction). Another intriguing feature of the phase traces is that they travel right from the beginning of the data, and they continue to propagate after the stall event, when the compressor has been brought back to stability (Fig(6-14)). Again, this is not in accordance with the idea that the small amplitude travelling wave is only present when the compressor is weakly stable, immediately before stall. Let us

now consider the amplitude of the first and second harmonic at station 4, which is given on Fig(6-16). We see no time during which these amplitudes are measurably above zero, as would be the case if a travelling wave such as we have observed until now were present in the data.

All these points lead us to believe that the phase propagation observed here may not be due to the presence of a travelling wave, at least not a phenomenon of the kind we have seen until now.

6-3 Conclusion

The small amplitude travelling wave phenomenon has been observed in a high-speed three stage machine, during two very slow throttle transients with uniform inlet flow. Its characteristics were very similar to those of the waves observed in low-speed machines in chapter four and five: small but finite amplitude, along with regular phase propagation were observed before the instability developed, for periods of up to 100 rotor revolutions.

A distorted inlet flow case was also studied, and travelling disturbances were clearly observed, but for a reduced period of time (15 rotor revolutions). The compressor seemed divided into two zones: one generating strong disturbances, the other damping them, which is a problem for stall precursor applications. Looking for travelling disturbances on a more local scale (a part of the annulus only) can be a solution.

Finally, a throttle transient was analyzed. Travelling information was strongly present in this case, but its characteristics were not in accordance with the small amplitude travelling wave behavior observed until to then: propagation in the direction opposite to the rotor, different propagation directions at two different stations.

CHAPTER SEVEN

CONCLUSIONS AND RECOMMENDATIONS FOR FUTURE WORK

7-1 Introduction

This chapter presents the main conclusions of the present work, divided along the following sections: existence and method of study of pre-stall small amplitude travelling waves; reaction of the stalling process to mass flow transients and inlet distortion; use of the pre-stall waves for compressor stability estimation and as a stall announcer; study of some high-speed data. The chapter is closed by some recommendations for future work on the pre-stall small amplitude travelling wave phenomenon, both for the insight it brings into the stalling process and for stall warning applications.

7-2 Existence and method of study of pre-stall travelling waves

In a typical experiment, during which the stall inception process was studied in the upstream flowfield of the three stage compressor, we have observed that:

- Small amplitude waves exist prior to stall, travelling for more than 90 rotor revolutions, with an amplitude less than 5% of the stall cell amplitude, and a constant phase speed of 35% of rotor speed as soon as it is identified.

- The small amplitude wave grows exponentially into a stall cell, without any discontinuity in phase or amplitude. During this transition, the phase speed changes from the wave's speed of 13 Hz to the stall cell speed of 14 Hz.

- This behavior is in agreement with the linearized Moore-Greitzer model for stall transients.

- For the three-stage compressor, all interesting information on the wave angular position and amplitude is found to be contained in the first Fourier harmonic. Thereafter, only this quantity is studied for quantitative analysis, and is represented by its amplitude and phase angle.

The experiment performed was repeated nine times, at two different rotation speeds of the machine. Each time, the same stall inception process was observed: a finite stretch of small amplitude wave travelled for more than 30 revolutions before growing into stall cell. In view of the very irregular amplitude of the wave, the excitation which provides its initial conditions may be thought to be random; but the experiments described above proved that the nature of the stalling process is not affected by this possible stochastic characteristics of the excitation.

7-3 Reaction of the stalling process to throttle transients and inlet distortion

Stall transients were performed with both uniform and distorted inlet flow on the three stage and the single stage compressor. The following points were noted:

- The compressor environment (inlet distortion) or operating conditions (mass flow transients) do not change the nature of the stalling process: in all experiments performed, stall evolved from an already travelling small amplitude perturbation, with no observed phase speed variations during the small amplitude stage.

These experiments establish that:

- small amplitude travelling waves and stall cells are two stages of the same physical phenomenon

- small amplitude waves are a prerequisite for stall to occur; a stall cell can only develop from an exponentially growing travelling wave, and will always result from it.

In addition, we note the following side effects of mass flow transients and inlet distortion:

- The throttle closing rates used were slow enough for the compressor operation to be quasi steady, and the only effect expected was observed: the last stretch of uninterrupted wave propagation leading to stall was found to be roughly inversely proportional to d(phi)/dt at stall. This simply indicates that the compressor spends less time in the flow coefficient region favorable to the propagation of small amplitude waves.

- Inlet distortion effects were more subtle to analyze, for they seemingly influence both the compressor stability and the wave excitation. Roughly, inlet distortion hinders wave propagation, and can cause abrupt stall inception even during very slow throttle transients.

7-4 Use of the pre-stall travelling wave phenomenon for compressor stability estimation and stall warning

A map of the single stage compressor was obtained by taking long periods (600 rotor revolutions) of data at different flow coefficients, up to stall. After proper conditioning, a first model linear model was fitted to the first Fourier harmonic of the data. The following results were obtained:

- The fit of the model to the data was excellent at all flow coefficients, and for uniform or distorted inlet flow (except maybe very near stall for the distorted case). This proves that the first order model describes adequately the compressor-upstream flowfield interaction and the travelling wave behavior, and that the system parameters (damping and frequency) can be accurately estimated, given enough data for analysis to average out the contribution of the excitation.

- The estimated damping of the first order system was plotted vs the flow coefficient, and was seen to decrease towards zero as the compressor neared stall. The damping was found to be stronger in case of inlet distortion, explaining the greater difficulty encountered by travelling waves in a distorted environment.

- Very near stall, in the case of inlet distortion, strong wave interaction with the distorted region causes the wave power to decrease. This effect is non-

linear, and is not included in our model. It may produce an artificial stabilization by delaying the wave development into a stall cell, and thus be responsible for the abruptness of the stalling process in some cases of inlet distortion.

The use of the small amplitude travelling wave as a stall precursor was discussed, and the following points outlined:

- For steady applications (test rigs), the compressor damping can be very well estimated, but this does not indicate how close the stall point is without a priori knowledge of the compressor, since the damping curve can vary arbitrarily from compressor to compressor.

- For real-time applications, such as stall transients on engines, the parameter identification algorithm used for damping estimation can be set to track time varying parameters, but at the expense of the estimate accuracy.

- In the case of inlet distortion, looking at more local information (cross-correlation between two neighboring measurements) can indicate wave propagation in a reduced region only.

7-5 High-speed experiments

Sets of data from stall transients on a three stage high-speed machine were examined, and the following conclusions reached:

- The stall inception process appears qualitatively similar in compressible and incompressible machines. Very clear wave propagation could be seen during two stall transient with a uniform inlet. Travelling disturbances were also present during a distorted inlet experiment, but strongly damped in the "clean" region, and continuously excited in the other.

- For this compressor, the second Fourier harmonic contained at least as much information as the first one, which is an important information for future experiments.

7-6 Recommendations for future work

This work has provided a more time and space resolved view of the stalling process as seen by the upstream flowfield, but has not brought more insight into the fluid mechanic phenomenon which causes the compressor-upstream flowfield system to turn unstable. In particular, the cases of compressors stalling with a negative slope of the characteristic are still unexplained, and suggest that an important factor as been omitted in the analysis. The transition mechanism remains the only unknown of the stalling process, and a detailed study of the flowfield immediately close to or inside the rotor passages can bring an answer to this question.

Further investigation is needed to identify clearly the nature of the initial condition, or the excitation, of the small amplitude wave phenomenon. Are they convected in or generated within the machine (or both), and should they be considered as a noise (white or colored), or as a deterministic quantity.

The mechanism of the interaction between small amplitude travelling waves and the inlet distortion is not well understood at the end of this work. A more detailed study may yield useful information on the specificity of the stalling process in the case of inlet distortion, an important source of compressor stalls in aeronautic applications.

The Moore-Greitzer theory has to be extended to the compressible case, in order to obtain predictions of the wave characteristics in high-speed machines.

The linearized Moore-Greitzer theory can give quantitative predictions for the wave damping and travelling speed, although empirical factors have been kept to account for viscous effects. Using data from different compressors, a parametric study can be performed to investigate the effect of the Reynolds number (and perhaps other non-dimensional parameters) on the wave characteristics.

Finally, but not least, a large amount of analysis and tests remains to be performed to validate a range of applications for the small amplitude wave phenomenon as a stall precursor.

REFERENCES

1. Emmons, H.W. , Pearson, C.E., and Grant, H.P. "Compressor Surge and Stall Propagation", ASME Transactions, Vol. 79 pp 455-469, April 1955.

2. Stenning, A.H., "Rotating Stall and Surge", ASME Journal of Fluids Engineering, Vol 102, March 1980.

3. Dunham, J., "Non-Axisymmetric Flows in Axial Compressors", Mechanical Engineering Science, Monograph No. 3, Institution of Mechanical Engineers, October 1965.

4. Moore, F.K., and Greitzer, E.M., "A Theory of Post-Stall Transients in Axial Compressors: Part I - Development of the Equations", ASME Journal of Engineering for Gas Turbine and Power, Vol 108, pp 68-76, January 1986.

5 Greitzer, E.M., and Moore, F.K., "A Theory of Post-Stall Transients in Axial Compressors: Part II - Applications", ASME Journal of Engineering for Gas Turbine and Power, Vol 108, pp 231-239, January 1986.

6. Nenni, J.P., and Ludwig, G.R., " A Theory To Predict the Inception of Rotating Stall in Axial Flow Compressors", AIAA Paper No. 74-528, June 1974.

7. Takata, H., and Nagano, S., "Nonlinear Analysis of Rotating Stall", ASME Paper No. 72-GT-3, March 1972.

8. Pandolfi, M., and Colusardo, G., "Numerical Investigations on the Generation and Development of Rotating Stalls", ASME Paper No. 78-WA/GT-5, December 1978.

9. Orner, N., "Rotating Stall in Axial Flow Compressors", VKI Lecture Series 3: "Unsteady Flow in Turbomachines", 1979.

10. Ludwig, G.R., and Nenni, J.P., " A Rotating Stall Control System for Turbojet Engines" ASME Paper No. 78-GT-115, April 1978.

11. Jackson, A.D., " Stall Cell Development in an Axial Compressor", ASME Paper No. 86-GT-249, June 1986.

12. M^{c}Dougall, N.M., "Stall Inception in Axial Compressors", PhD Thesis, Cambridge University, 1988.

13. M^{c}Dougall, N.M., Cumpsty, N.A., and Hynes, T.P., "Stall Inception in Axial Compressors", Submitted to 1989 ASME Gas Turbine Conference.

14. Greitzer, E.M., "Surge and Rotating Stall in Axial Compressors, Part I: Theoretical Compression System Model", and "Part II: Experimental Results and Comparison with Theory", ASME Journal of Engineering for Power, April 1976.

15. Gamache, R.N. "Axial Compressor Reversed Flow Performance", PhD Thesis, MIT Dept. of Aeronautics and Astronautics, May 1985.

16. Lavrich, P.L., "Time Resolved Measurements of Rotating Stall in Axial Flow Compressors", PhD Thesis, MIT Dept. of Aeronautics and Astronautics, January 1988.

17. Johnson, M.C., "The Effect of Hub Treatment on Compressor Endwall Flowfield", M.S. Thesis, MIT Dept. of Aeronautics and Astronautics, January 1985.

18. Lee, N.K.W., "Effects of Compressor Endwall Suction and Blowing on Stability Enhancement", M.S. Thesis, MIT Dept. of Aeronautics and Astronautics, September 1987.

19. Schulmeyer, A., "Enhanced Compressor Distortion Tolerance Using Asymmetric Inlet Guide Vane Control", M.S. Thesis, MIT Dept. of Aeronautics and Astronautics, August 1989.

20. Hynes, T.P., and Greitzer, E.M., "A Method for Assessing Effects of Circumferential Flow Distortion on Compressor Stability", Journal of Turbomachinery, Vol. 109, pp 371-379, July 1987.

21. Goldstein, R.J., editor, "Thermal Anemometers", Chapter IV, Fluid Mechanics Measurements, Hemisphere Publishing Corporation, New York, 1983.

22. Kay, S.M., and Marple, L.S,, "Spectrum Analysis - A Modern Perspective", IEEE Proceedings, Vol. 69, No. 11, pp1380-1419, November 1981.

23. Graupe, D., Time Series Analysis, Identification and Adaptive Filtering, Robert E. Krieger Publishing Company, Malabar, Florida, 1984.

24. Goodwin, G.C., and Sin, K.S., Adaptive Filtering, Prediction and Control, Prentice Hall, 1984.

25. Friedlander, B., "The Overdetermined Recursive Instrumental Variable Method", IEEE Transactions on Automatic Control, Vol. AC-29, No. 4, pp 353-356, April 1984.

26. Marple, L.S., "A New Autoregressive Spectrum Analysis Algorithm", IEEE Transactions on Acoustics, Speech, and Signal Processing, Vol. ASSP-28, No. 4, pp 441-454, August 1980.

27. Ljung, L., Morf, M., and Falconer, D., "Fast Calculations of Gain Matrices for Recursive Estimation Schemes", International Journal of Control, Vol. 27, No. 19, pp 1-19, 1978.

Three Stage Compressor Design Specifications and Blading Design

Number of Stages	3
Tip Diameter (mm)	610
Hub-to-Tip Radius Ratio	0.88
Design Average Reaction	0.75
Design Flow Coefficient	0.59
Total Pressure Rise Coefficient (measured)	2.05
Efficiency at Design Conditions (measured)	83.5

	No. of Blades	Chord (mm)	Camber (Deg)	Stagger Angle (Deg)
Inlet Guide Vanes	124	20.1	11.0	8.1
Rotor 1	54	45.2	17.0	42.8
Stator 1	85	31.4	27.0	11.0
Rotor 2	55	44.8	18.0	43.5
Stator 2	88	31.3	25.0	12.0
Rotor 3	49	50.7	20.0	44.6
Stator 3	90	31.4	53.0	5.5

Table (3-1)

Single Stage Compressor Design Specifications and Blading Design

Number of Stages	1
Tip Diameter (mm)	597
Hub-to-Tip Radius Ratio	0.75
Total Pressure Rise Coefficient (measured)	0.41

	No. of Blades	Chord (mm)	Camber (Deg)	Stagger Angle (Deg)
Inlet Guide Vanes	46	40.0	10.0	15.0
Rotor	44	38.0	25.1	37.9
Stator	45	39.0	25.5	45.0

Table (3-2)

Limit Levels for Determination of Small Amplitude Wave Start

	Lower Limit for Amplitude (m/s)	Lower Limit Phase Derivative (rad/s)	Higher Limit Phase Derivative (rad/s)
Three Stage Comp. Uniform inlet	0.04	-40	200
Three Stage Comp. Distorted Inlet	0.1	-40	200
Single Stage Comp. Uniform Inlet	0.04	-70	230
Single Stage Comp. Distorted Inlet	0.05	-70	230

Table (4-1)

Axial Position of Blades and Hot Wire Stations in the Single Stage Compressor

Axial positions are given with respect to the rotor plane, and the axis is in the direction of the flow (upstream stations have negative coordinates, downstream stations positive ones).

	Axial Position (mm)	Axial Position (in Comp. Radii)
Inlet Guide Vanes	-80	-0.307
Rotor	0	0
Stator	73	0.280
Station 1	-245	-0.941
Station 2	-113	-0.434
Station 3	-32	-0.123
Station 4	44	0.169
Station 5	112	0.430
Station 6	194	0.745

Table (4-2)

Pressure Transducer Location in High-Speed Compressor

Compressor Axial Location	Channel No.	Circumferential Position (Same Direction as Rotor)
Stator 1 Leading Edge	0	31.9
	1	73.4
	2	115.0
	3	163.4
	4	205.0
	5	246.5
	6	281.2
	7	329.6
Stator 2 Leading Edge	0	31.8
	1	71.8
	2	106.8
	3	161.8
	4	206.8
	5	241.8
	6	281.8
	7	326.8
Stator 3 Leading Edge	0	10.0
	1	50.9
	2	104.1
	3	140.9
	4	193.1
	5	230.9
	6	280.0
	7	320.9

Table (6-1)

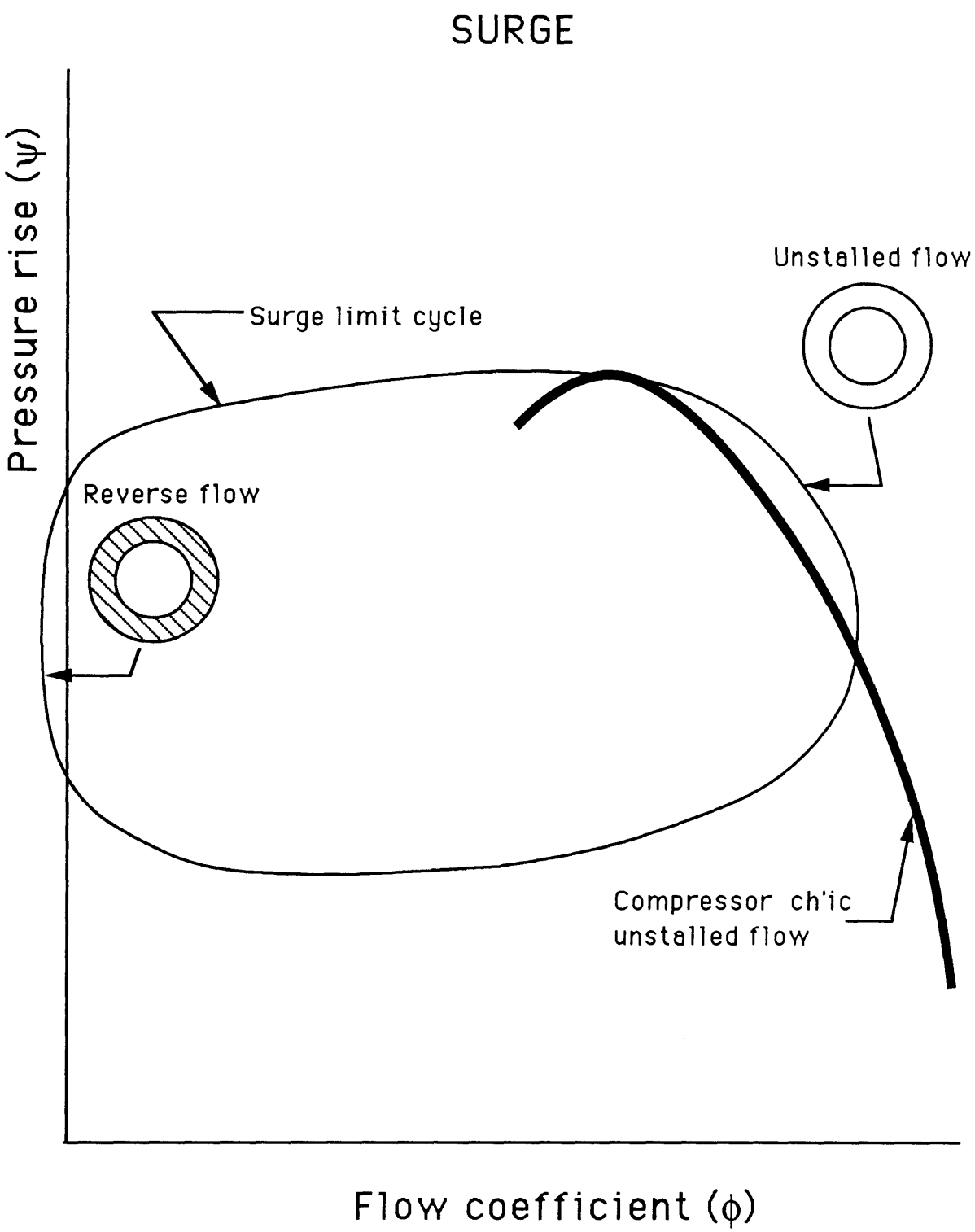

Figure (1-1) Surge Limit Cycle

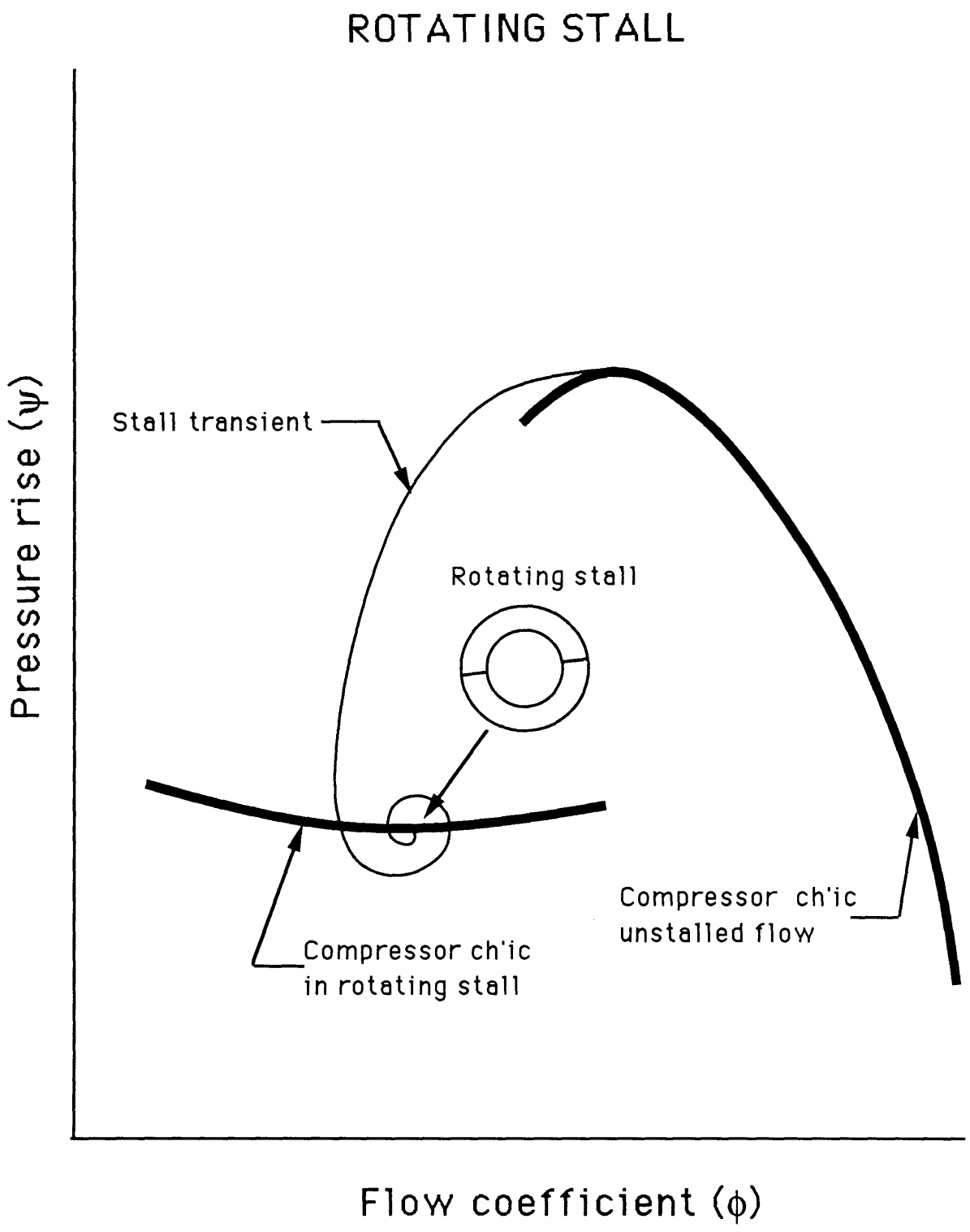

Figure (1-2) Rotating Stall

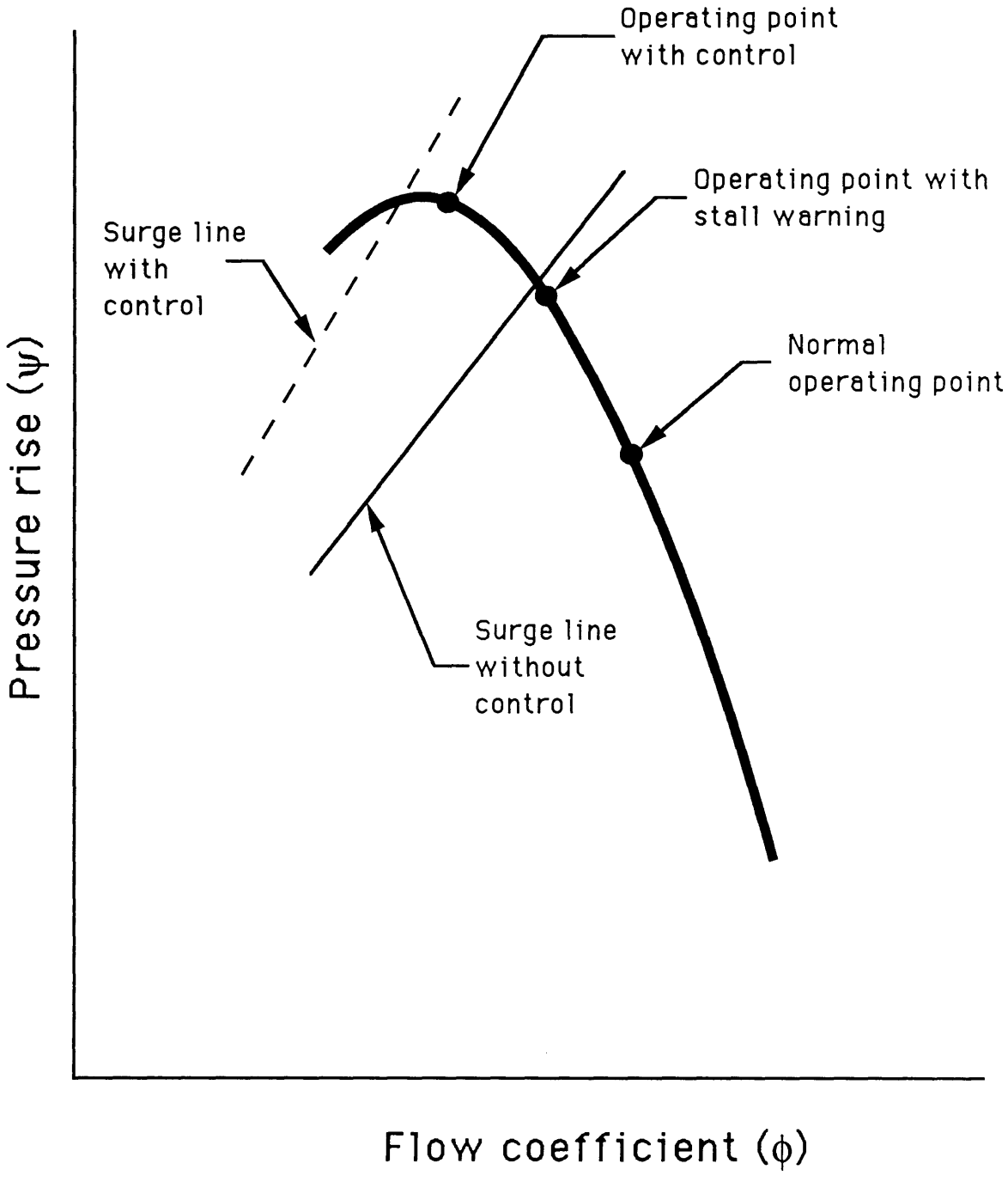

Figure (1-3) Performance Improvements Expected From a Stall Precursor: Active Control, and Stall Warning

COMPRESSION SYSTEM

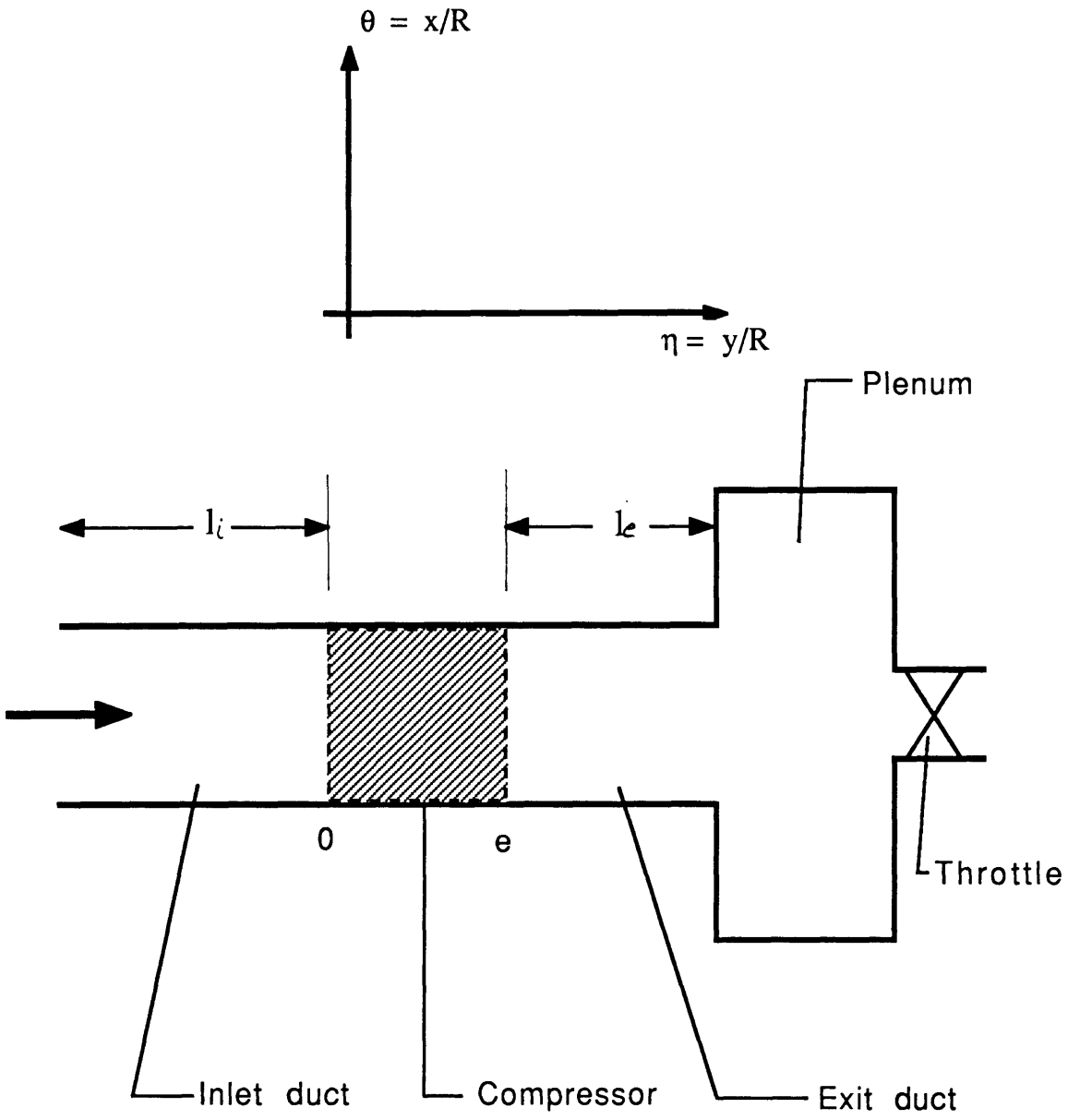

Figure (2-1) Schematic of a Compression System

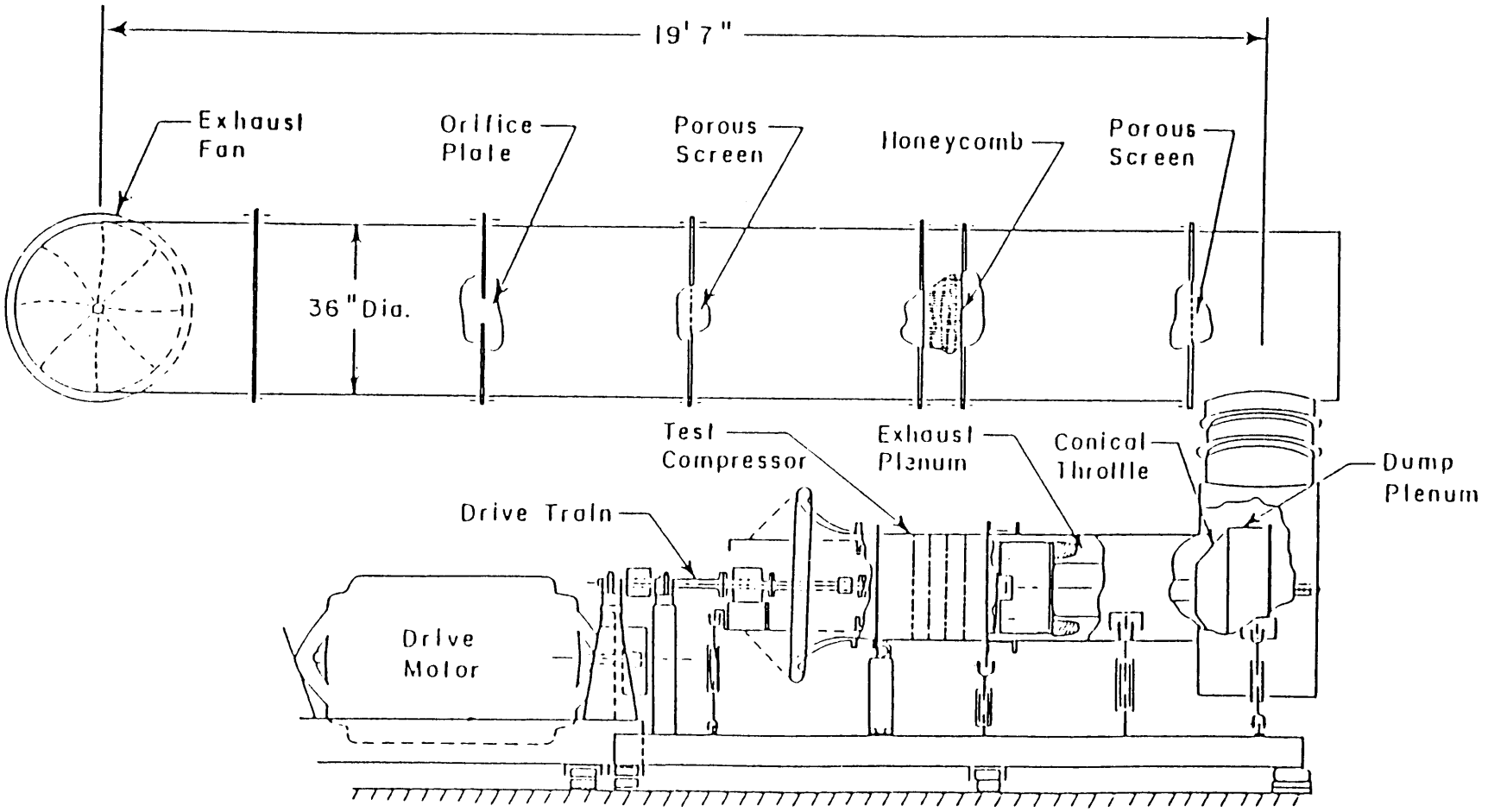

Figure (3-1) Three Stage Low-Speed Compressor Rig Schematic (from [16])

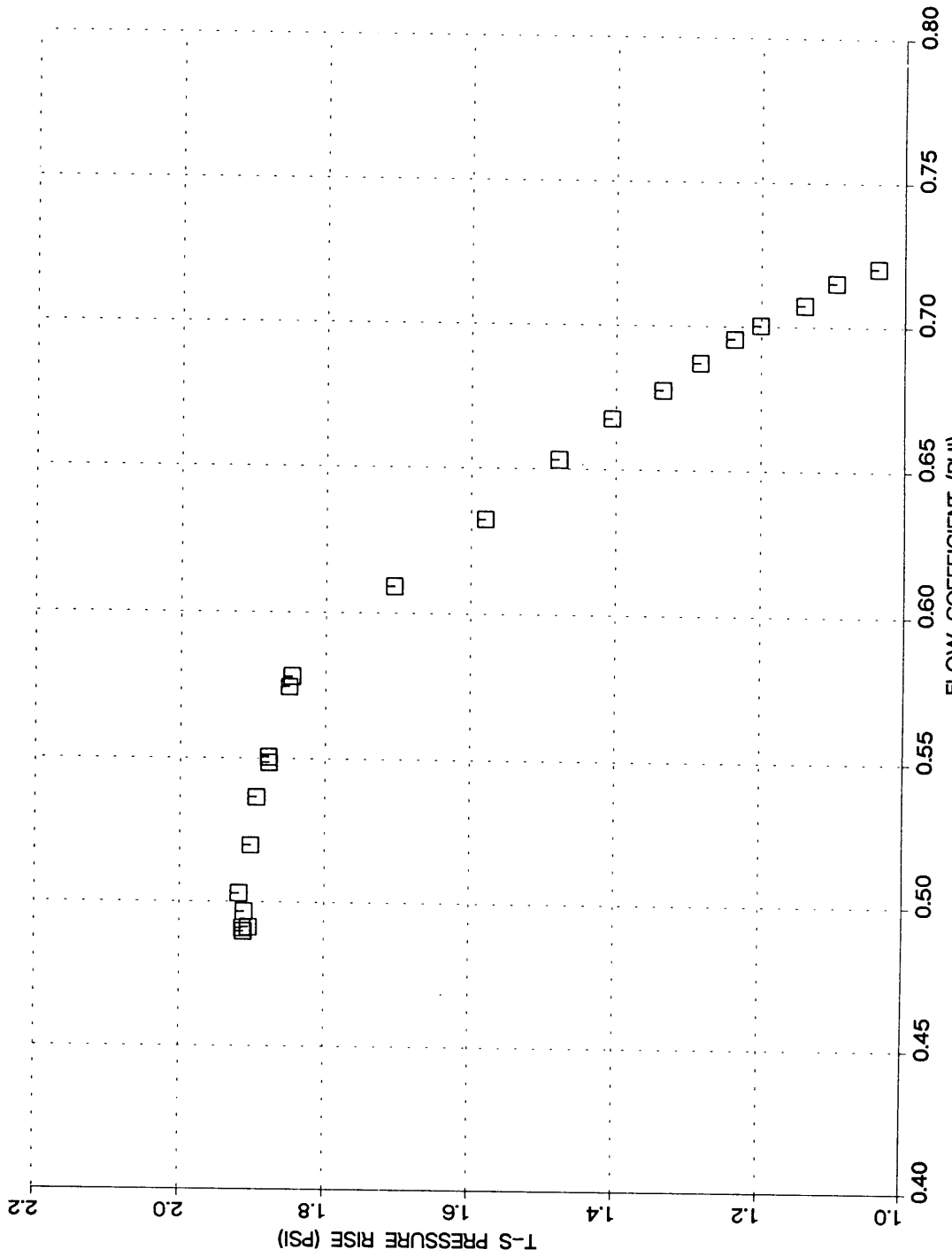

Figure (3-2) Three Stage Low-Speed Compressor Speedline (2225 RPM)

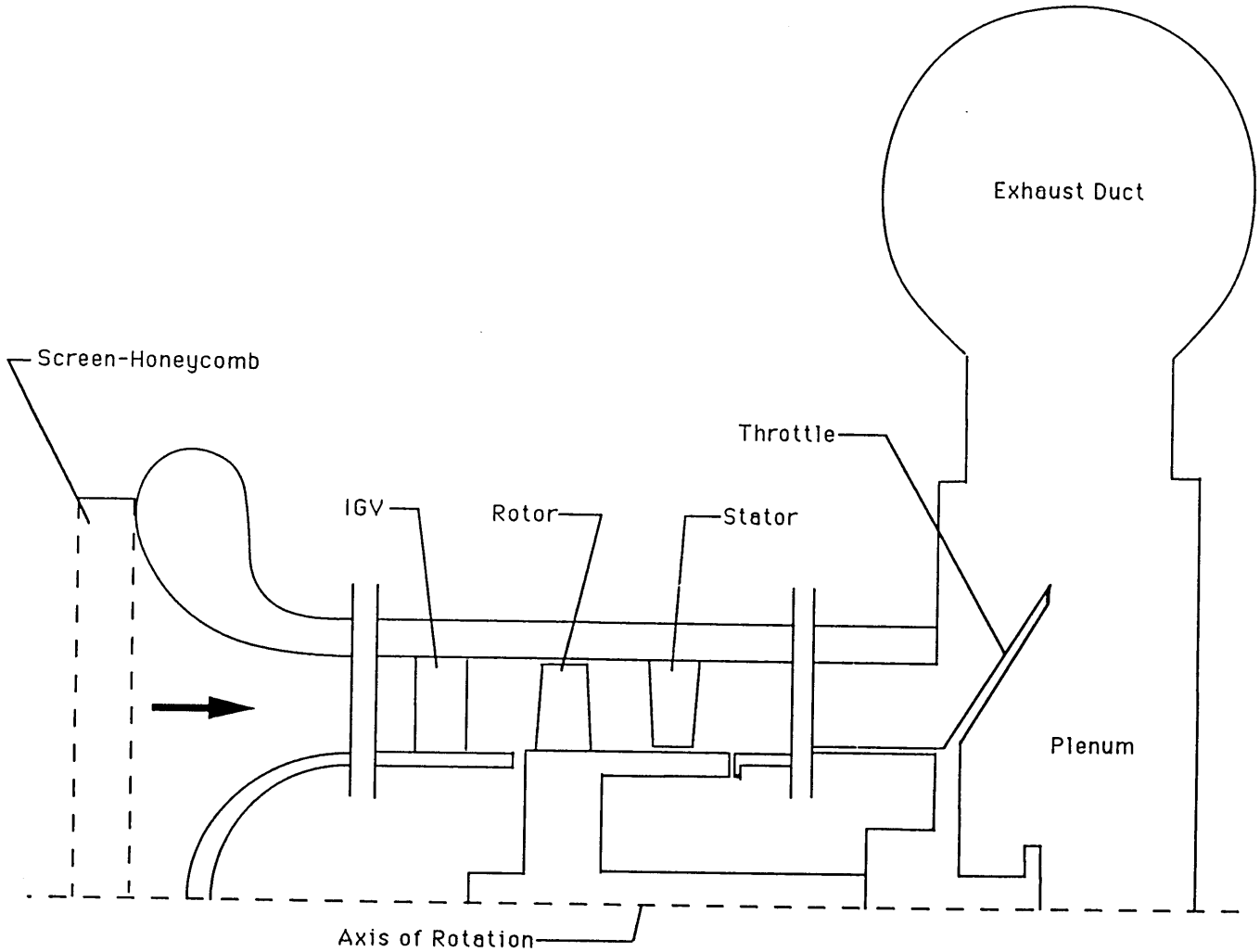

Figure (3-3) Single Stage Low-Speed Compressor Rig Schematic

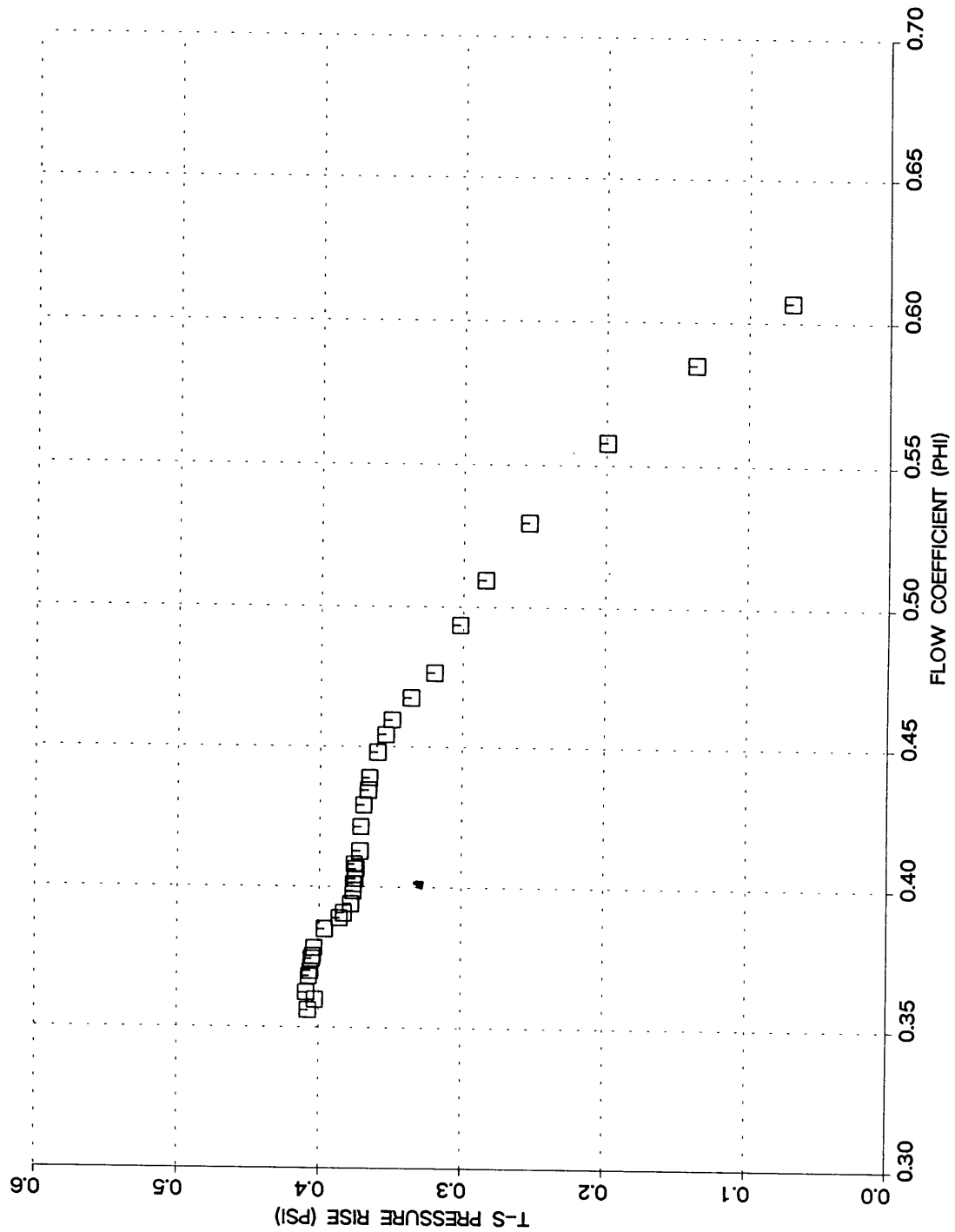

Figure (3-4) Single Stage Low-Speed Compressor Speedline (2700 RPM)

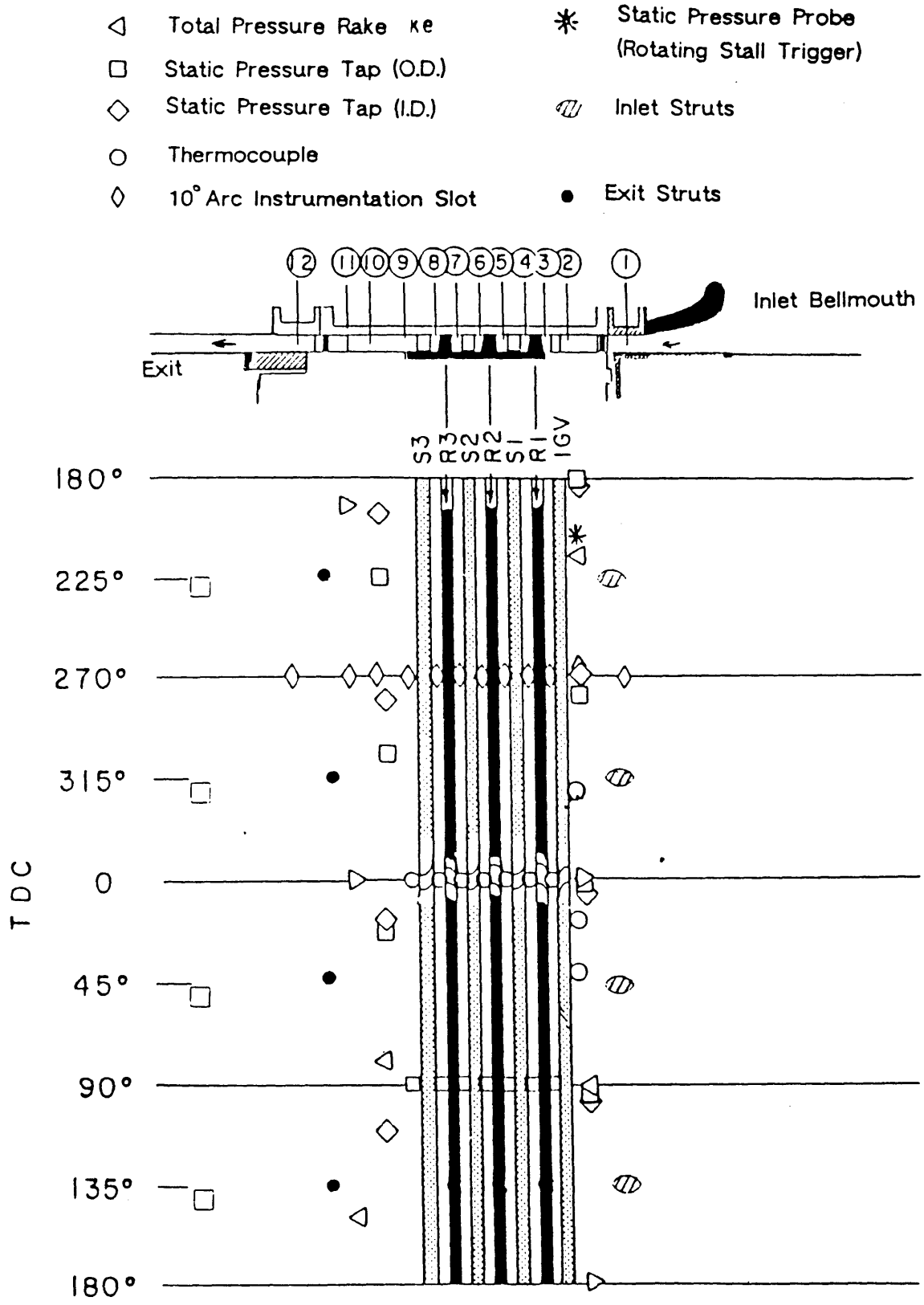

Figure (3-5) Three Stage Compressor Steady State Instrumentation Layout (from [16])

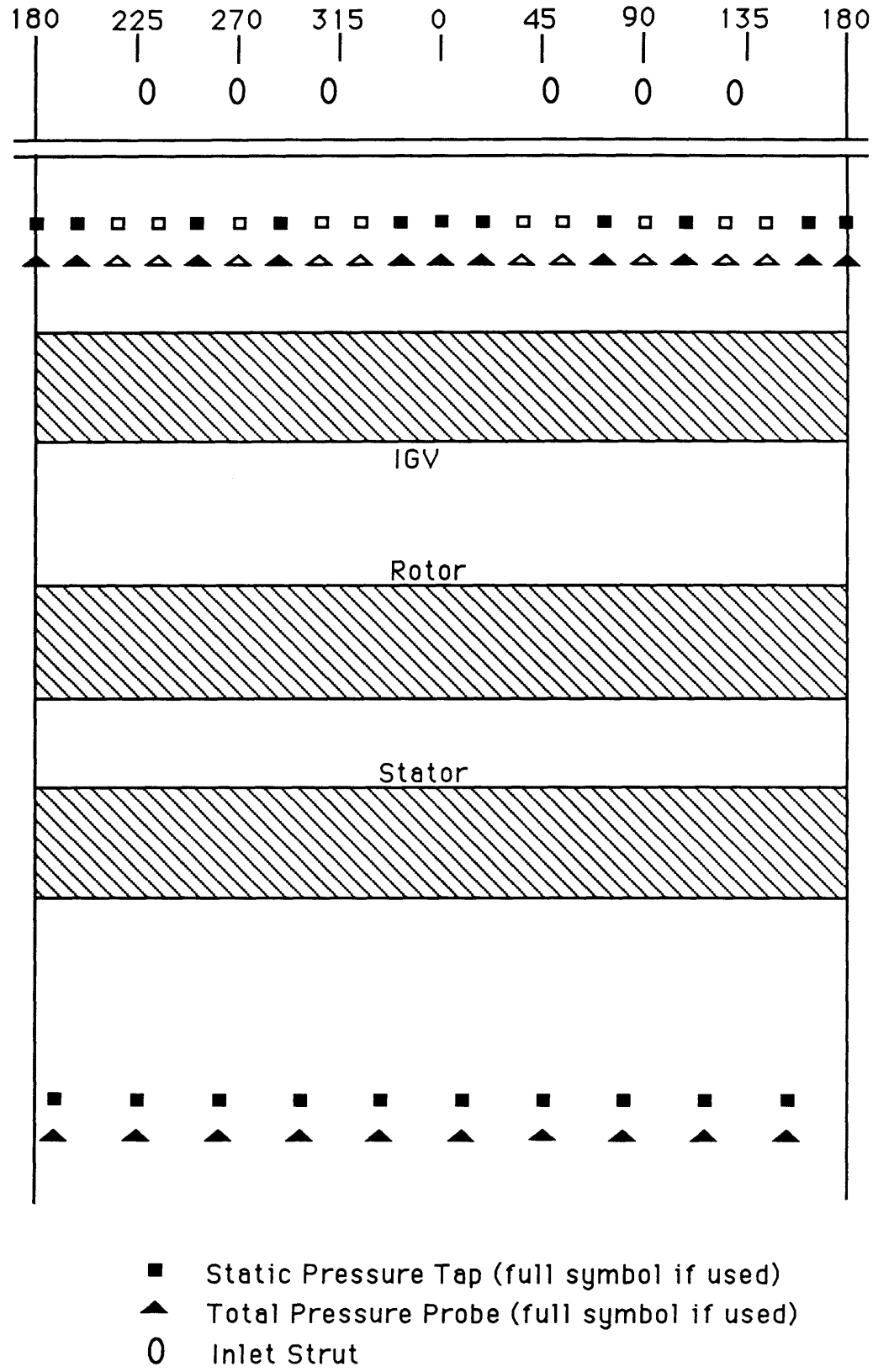

Figure (3-6) Single Stage Compressor Steady State Instrumentation Layout

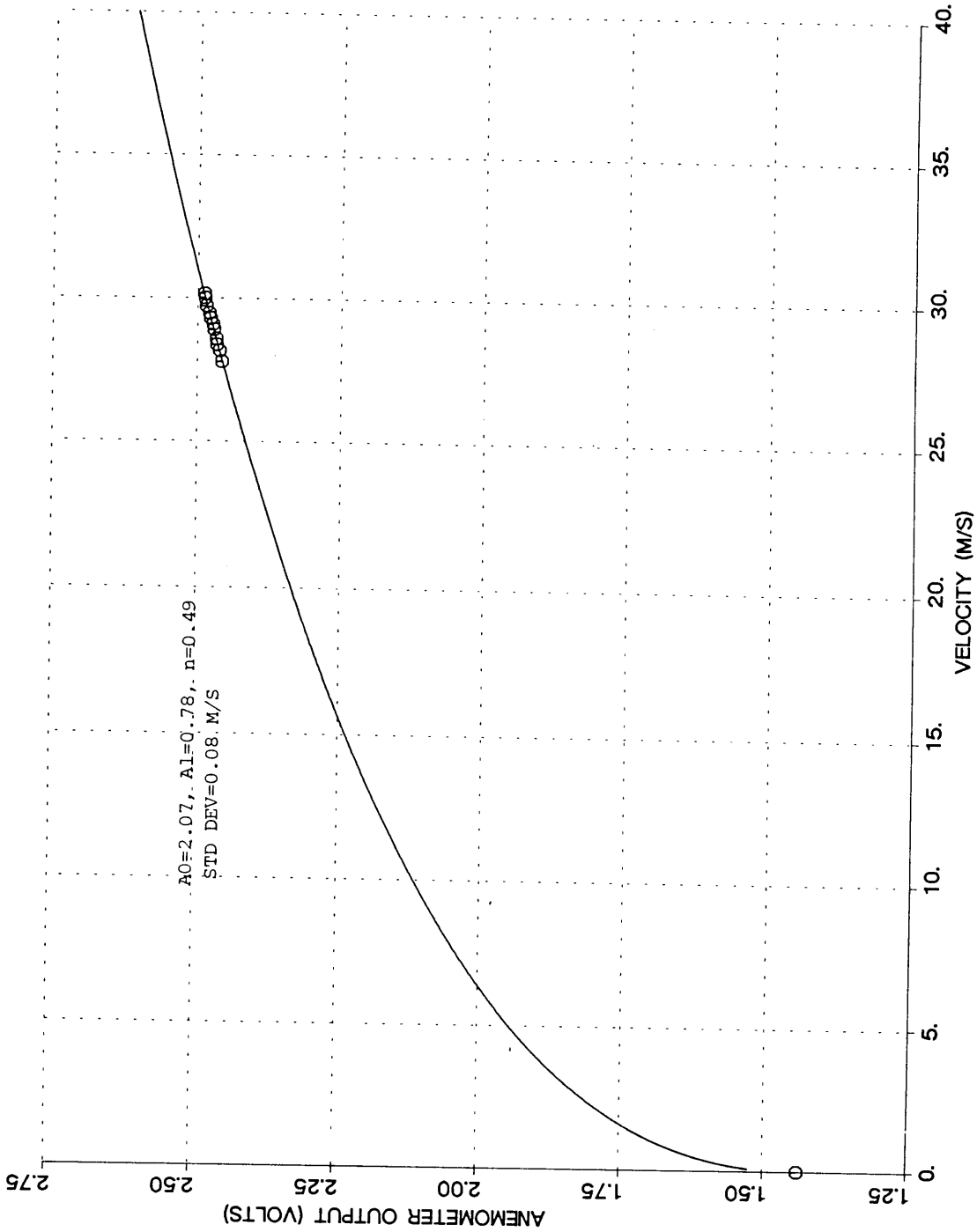

Figure (3-7a) Typical Hot Wire Calibration Curve

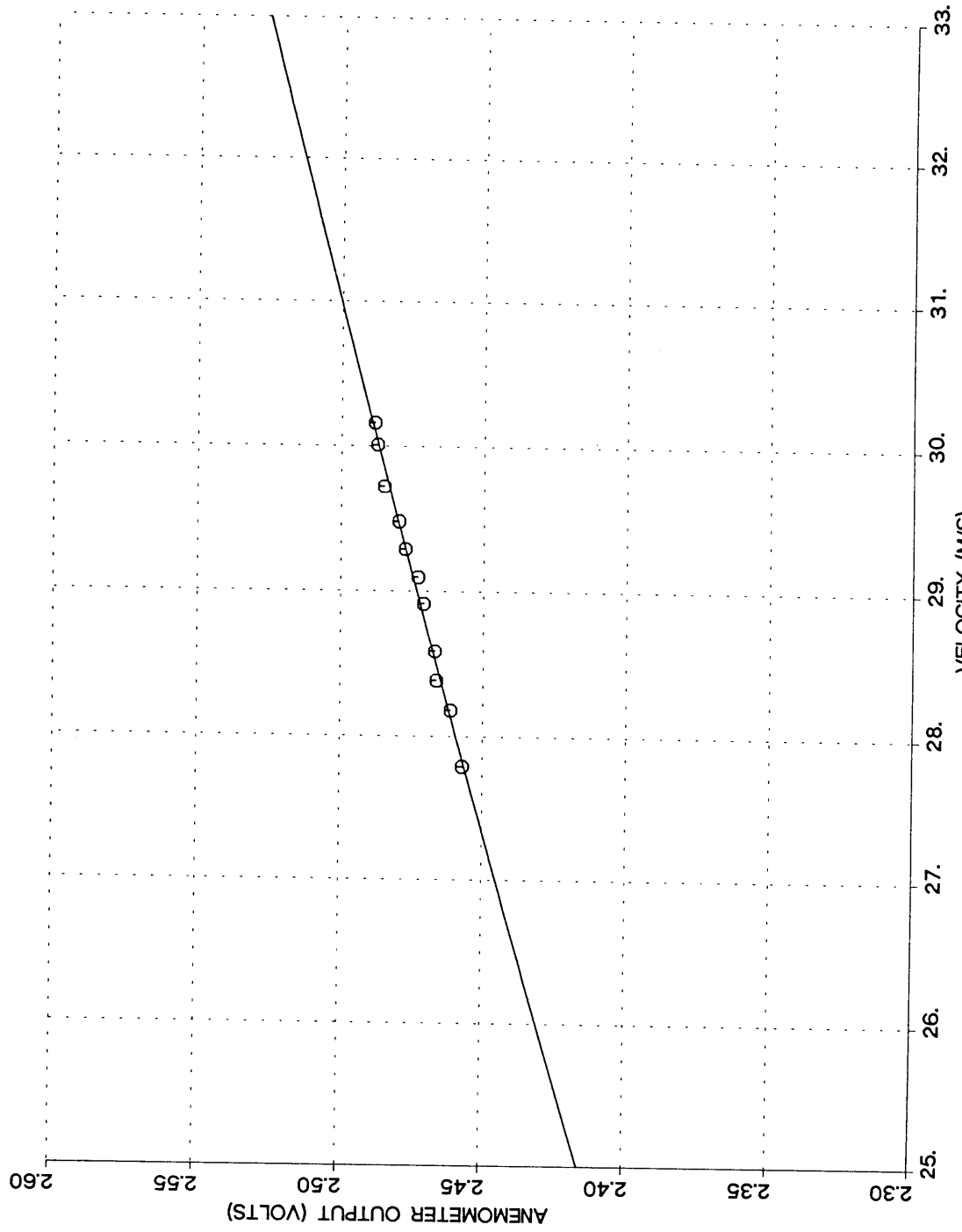

Figure (3-7b) Typical Hot Wire Calibration Curve (Blown-Up)

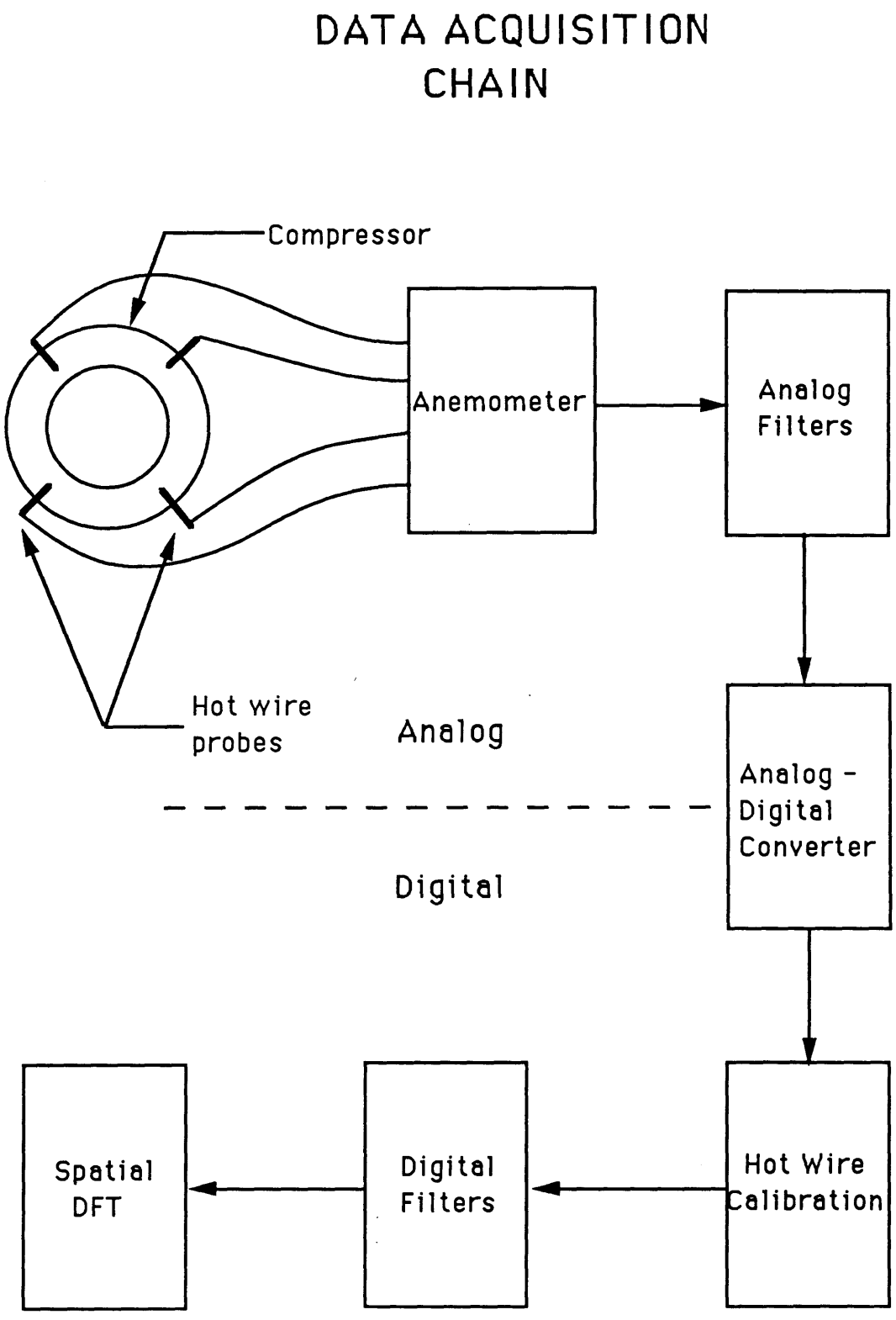

Figure (3-8) Data Acquisistion and Data Processing Chain

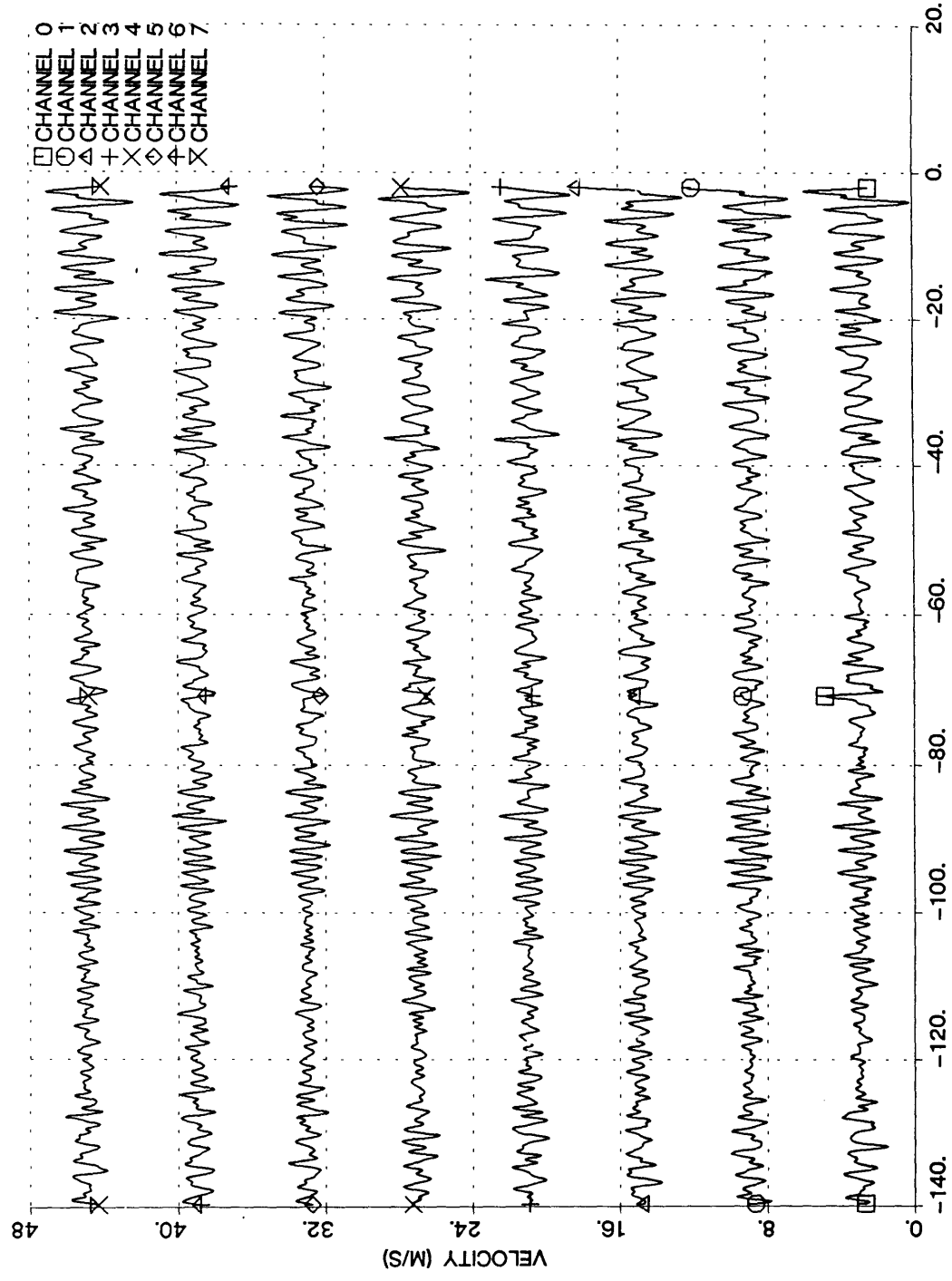

Figure (4-1) Typical Experiment: Velocity Traces From Eight Probes Equally Spaced Around the Compressor Circumference, 0.44 Radii Upstream of the IGVs

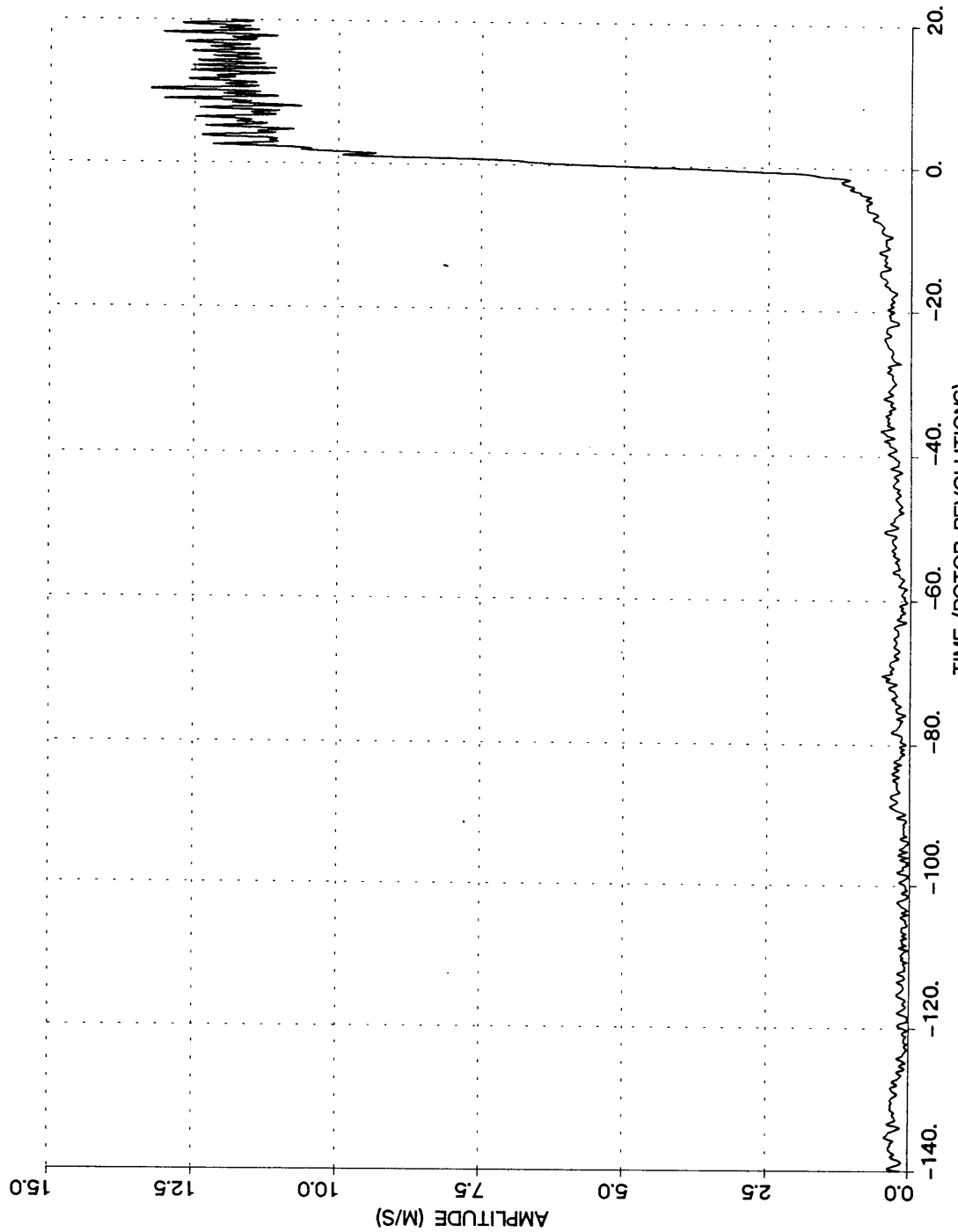

Figure (4-2) Typical Experiment: Amplitude of First Fourier Harmonic

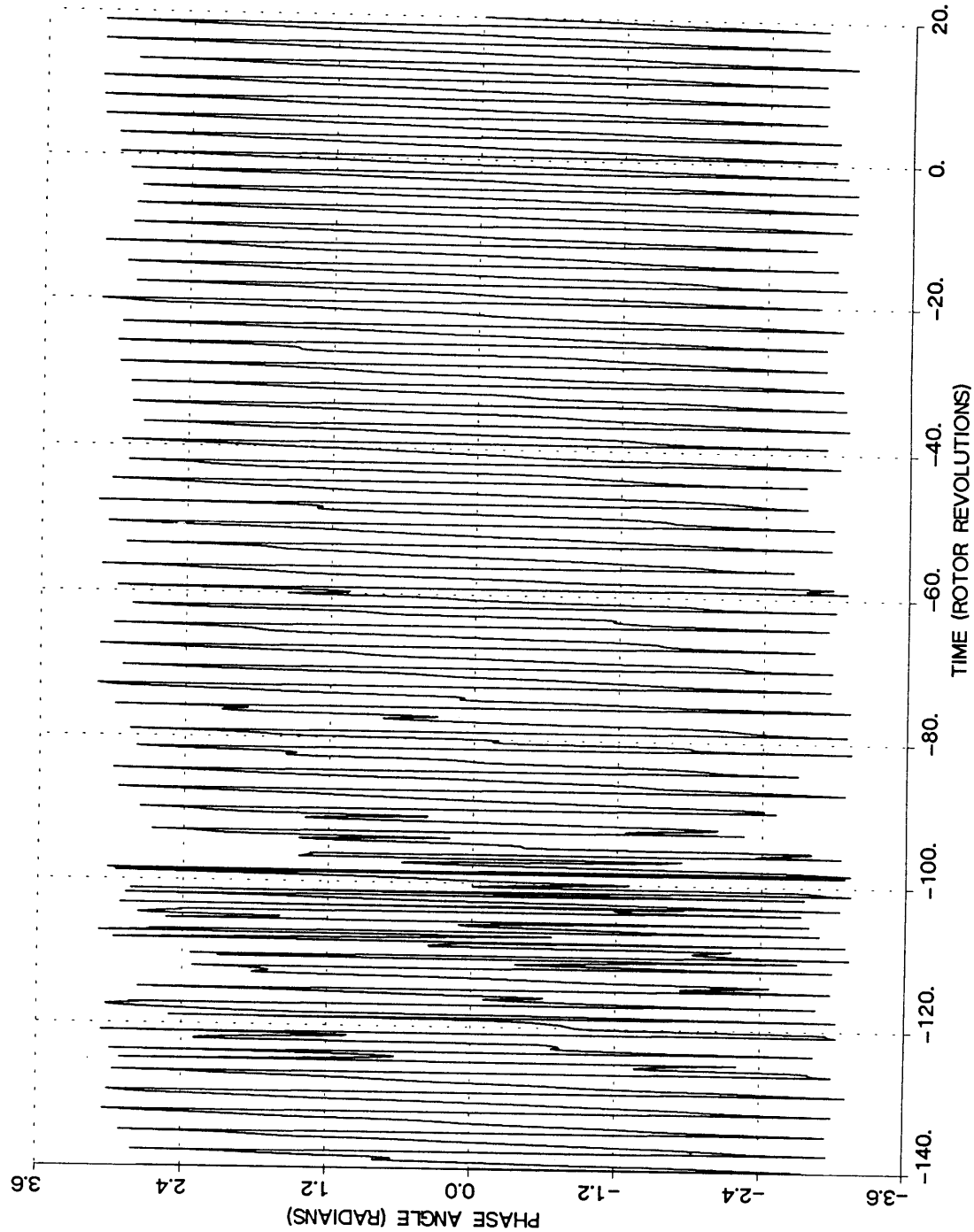

Figure (4-3) Typical Experiment: Phase of First Fourier Harmonic (Wrapped)

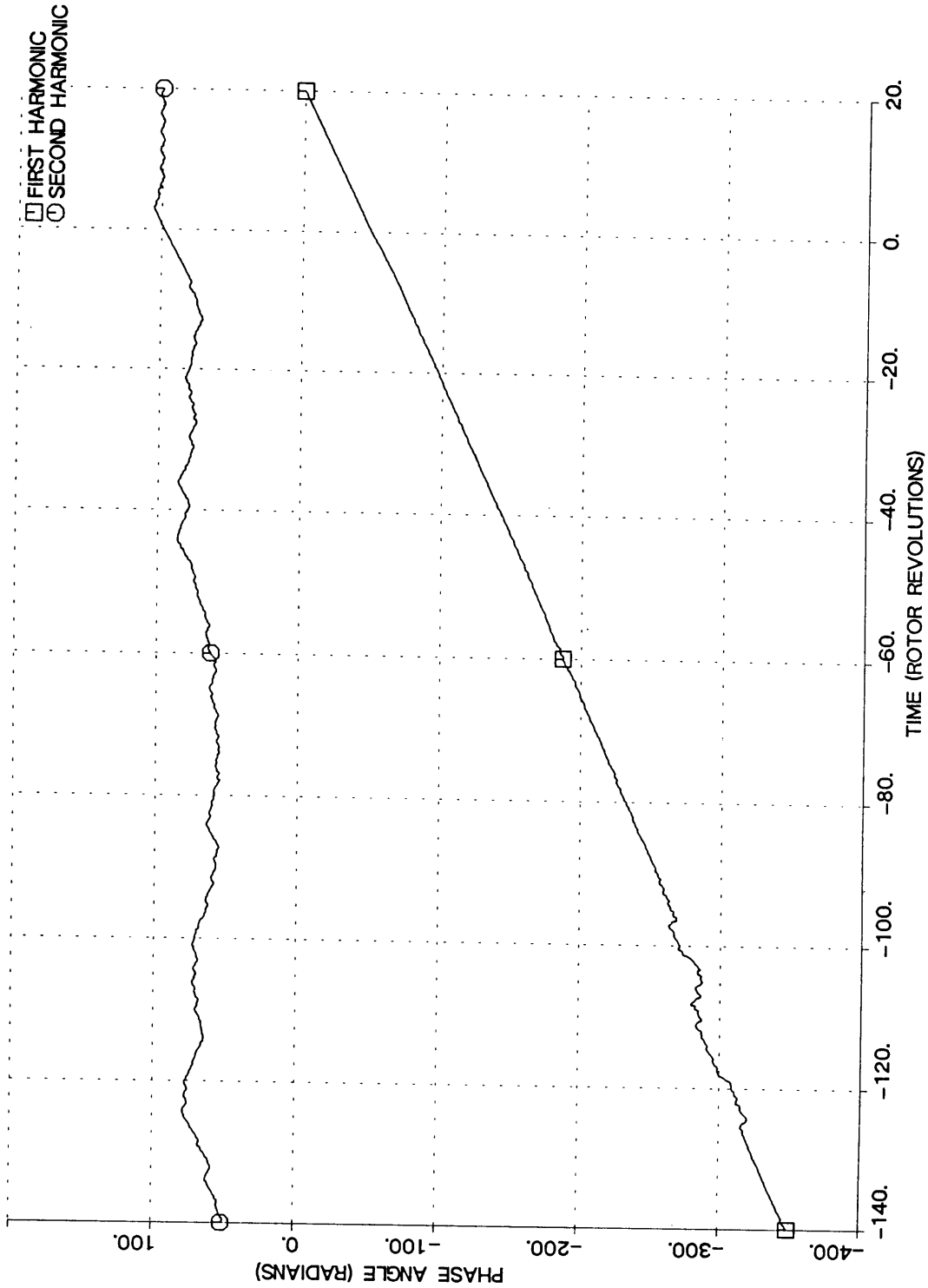

Figure (4-4) Typical Experiment: Phases of First and Second Harmonic (Unwrapped)

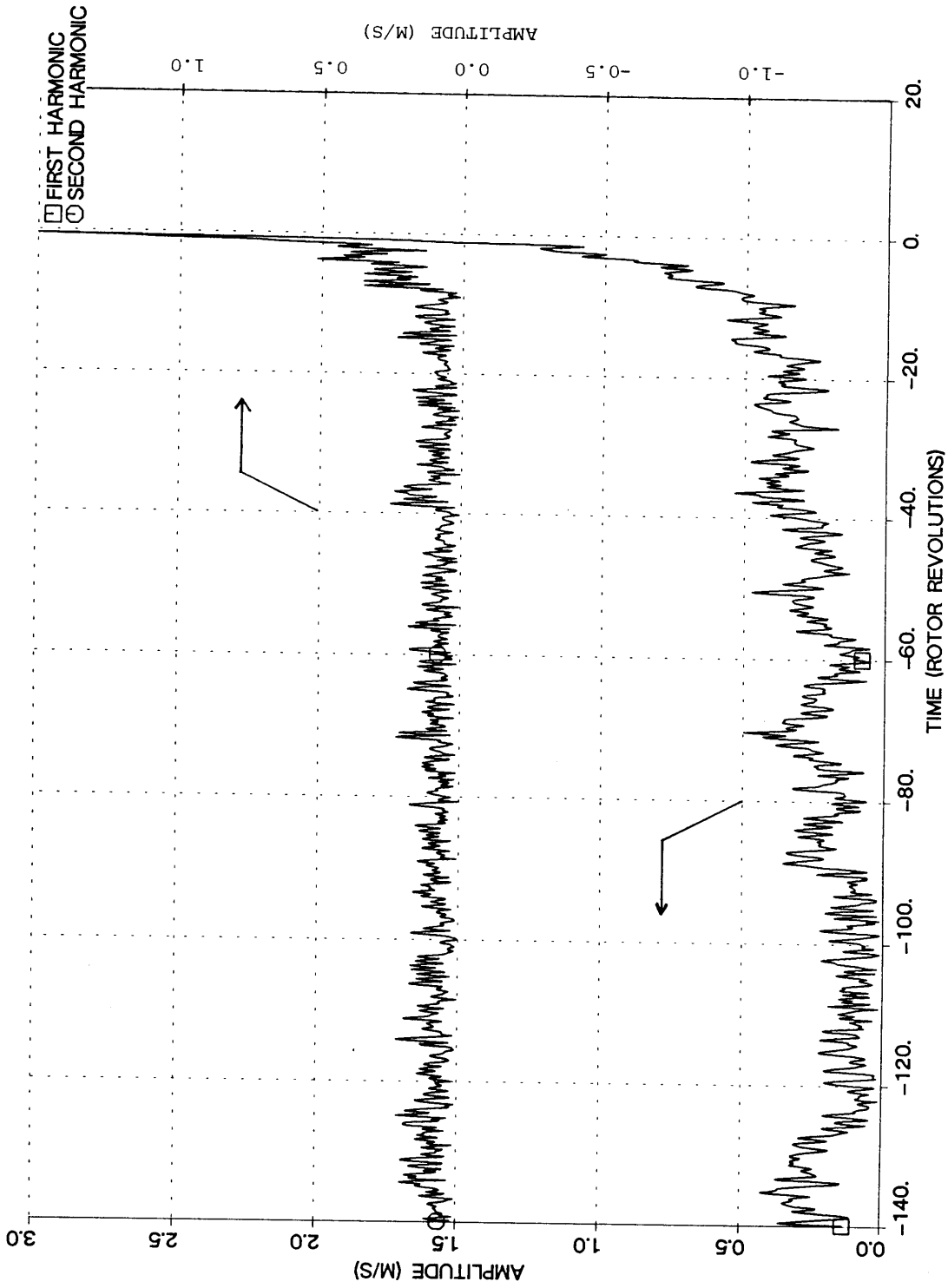

Figure (4-5) Typical Experiment: First and Second Harmonic Amplitude

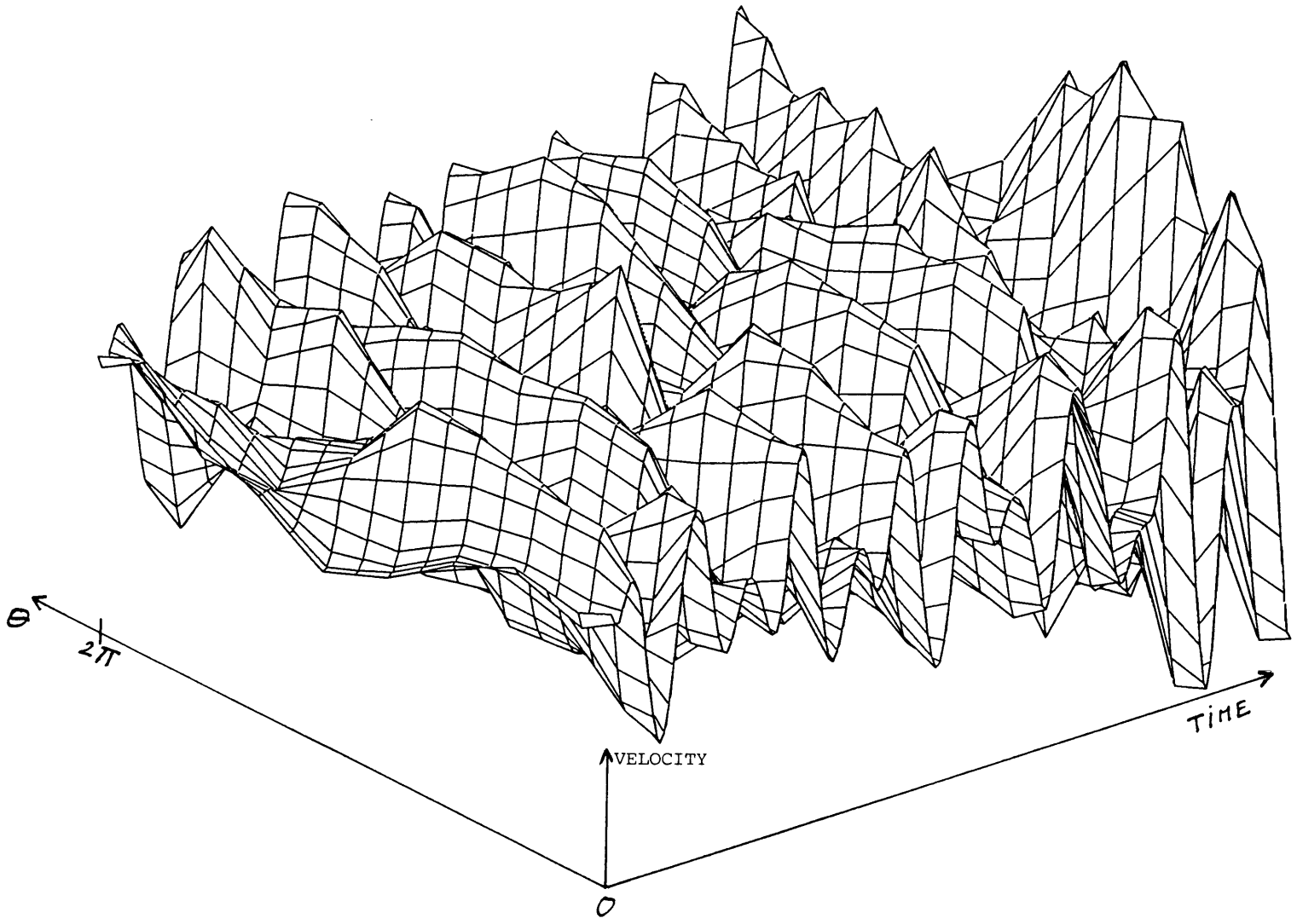

Figure (4-6a) Three Dimensional Representation of Velocity Data

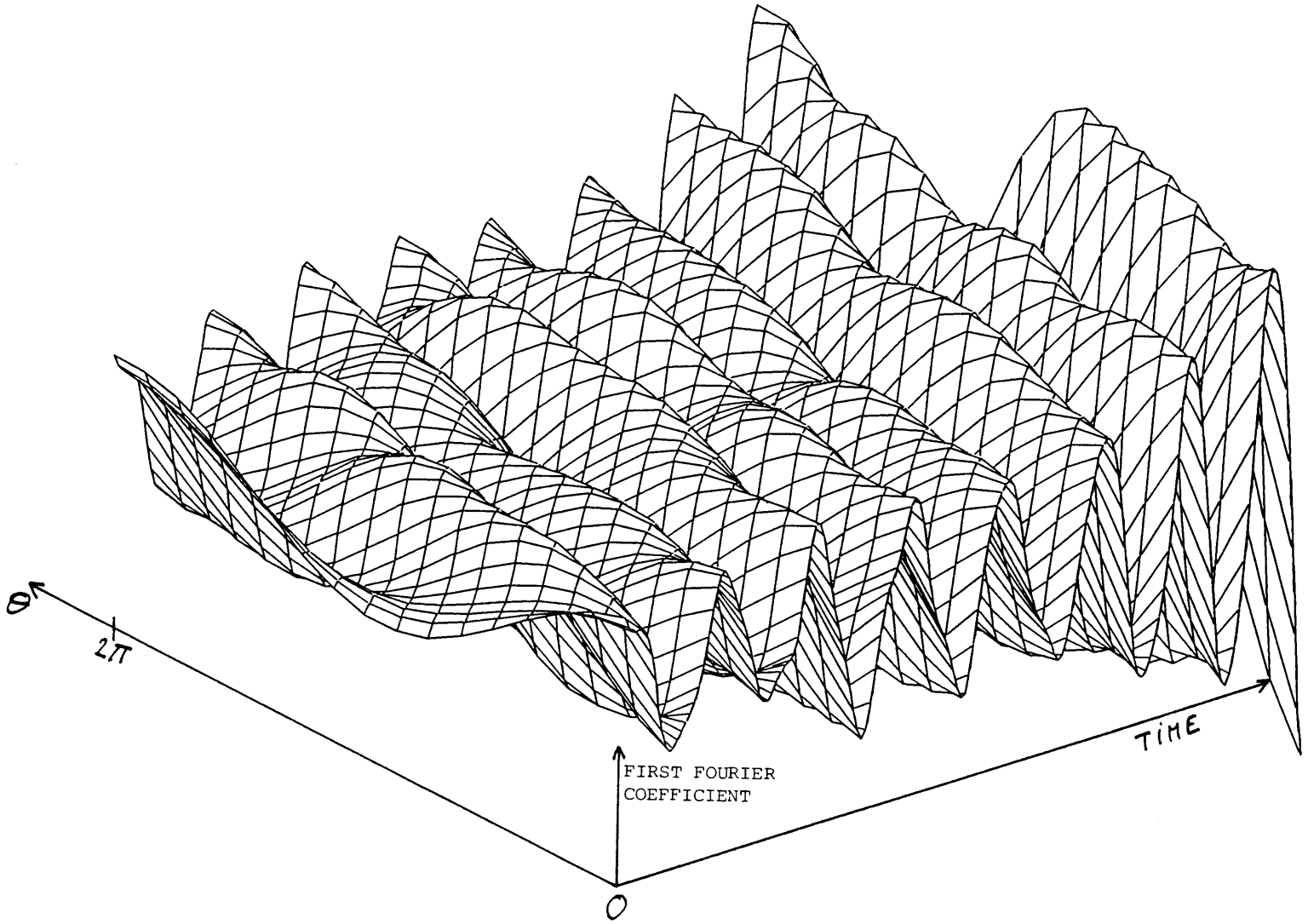

Figure (4-6b) Three Dimensional Representation of First Harmonic

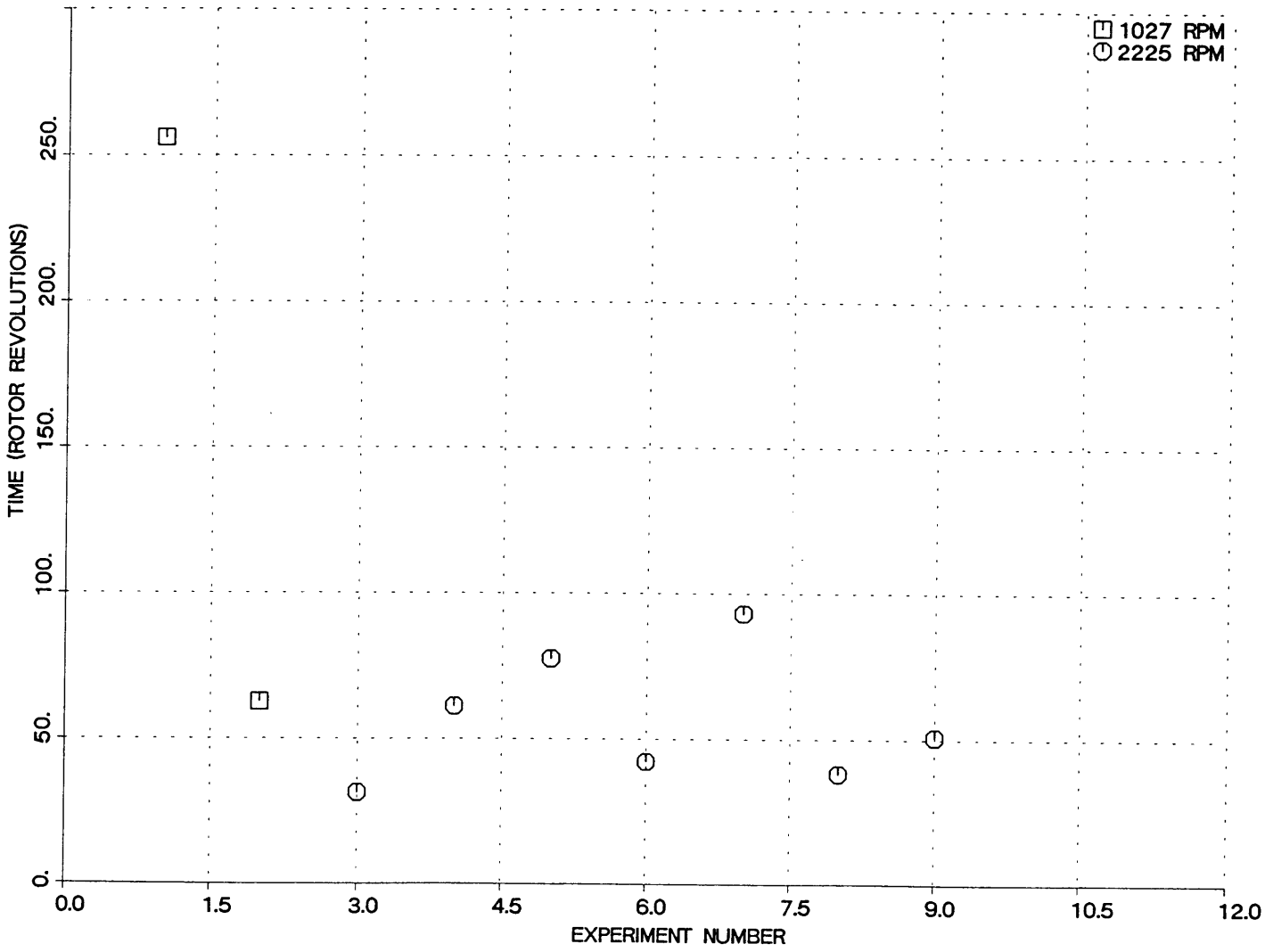

Figure (4-7) Three Stage Compressor: Small Amplitude Wave Time Extent at Quasi Zero Throttle Closing Rate

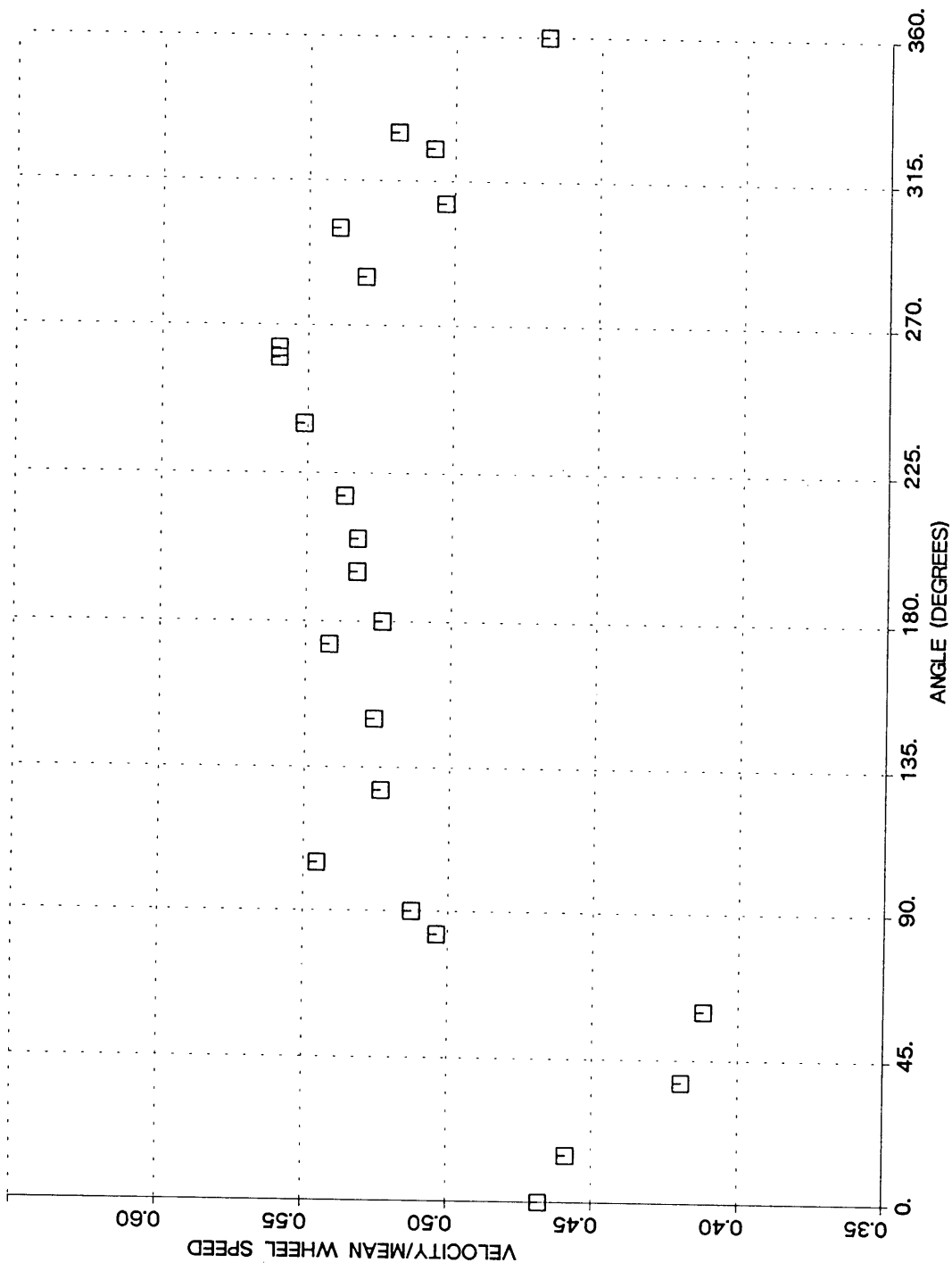

Figure (4-8) Three Stage Compressor: Inlet Distortion Characteristic

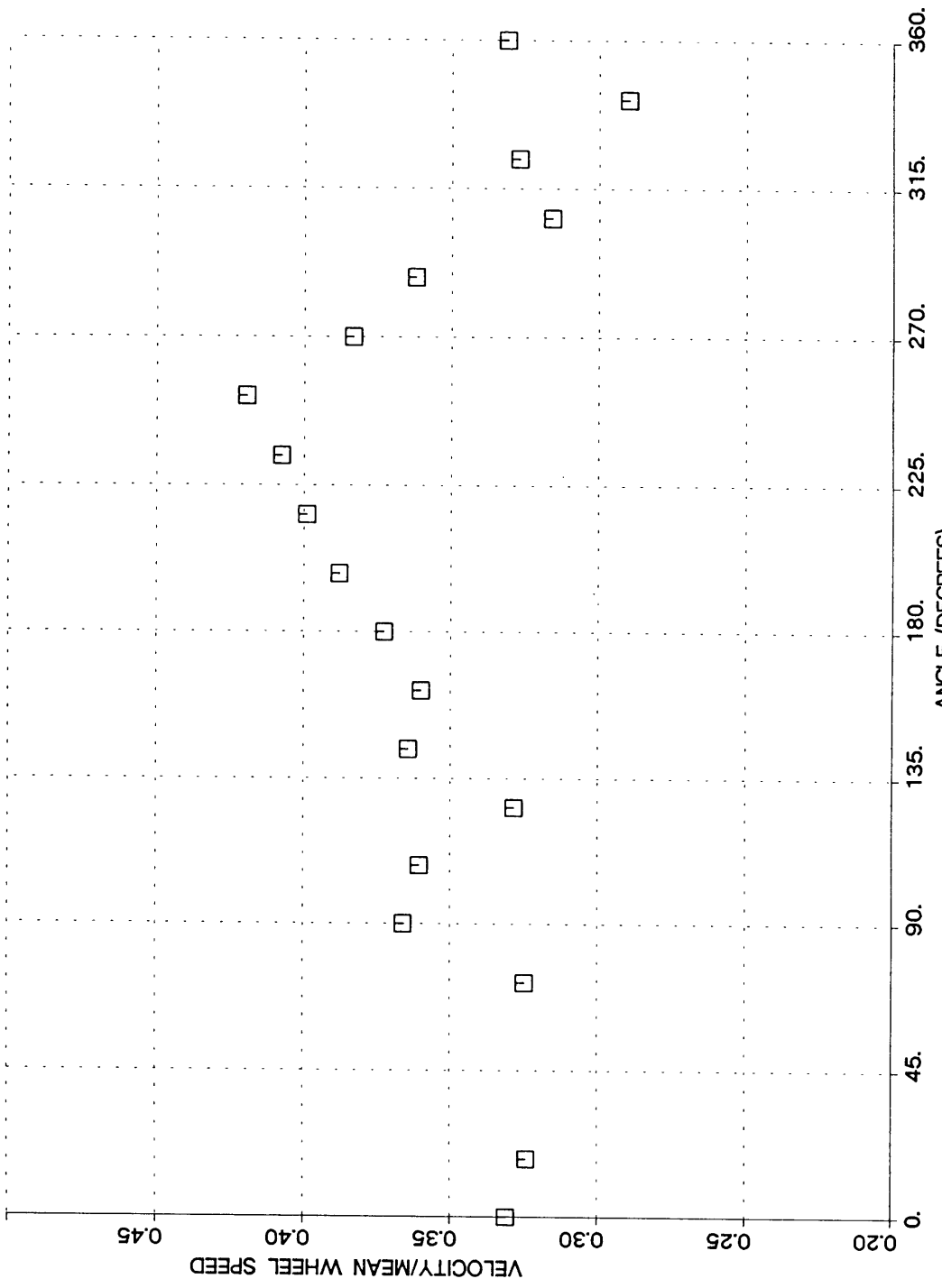

Figure (4-9) Single Stage Compressor: Inlet Distortion Characteristic

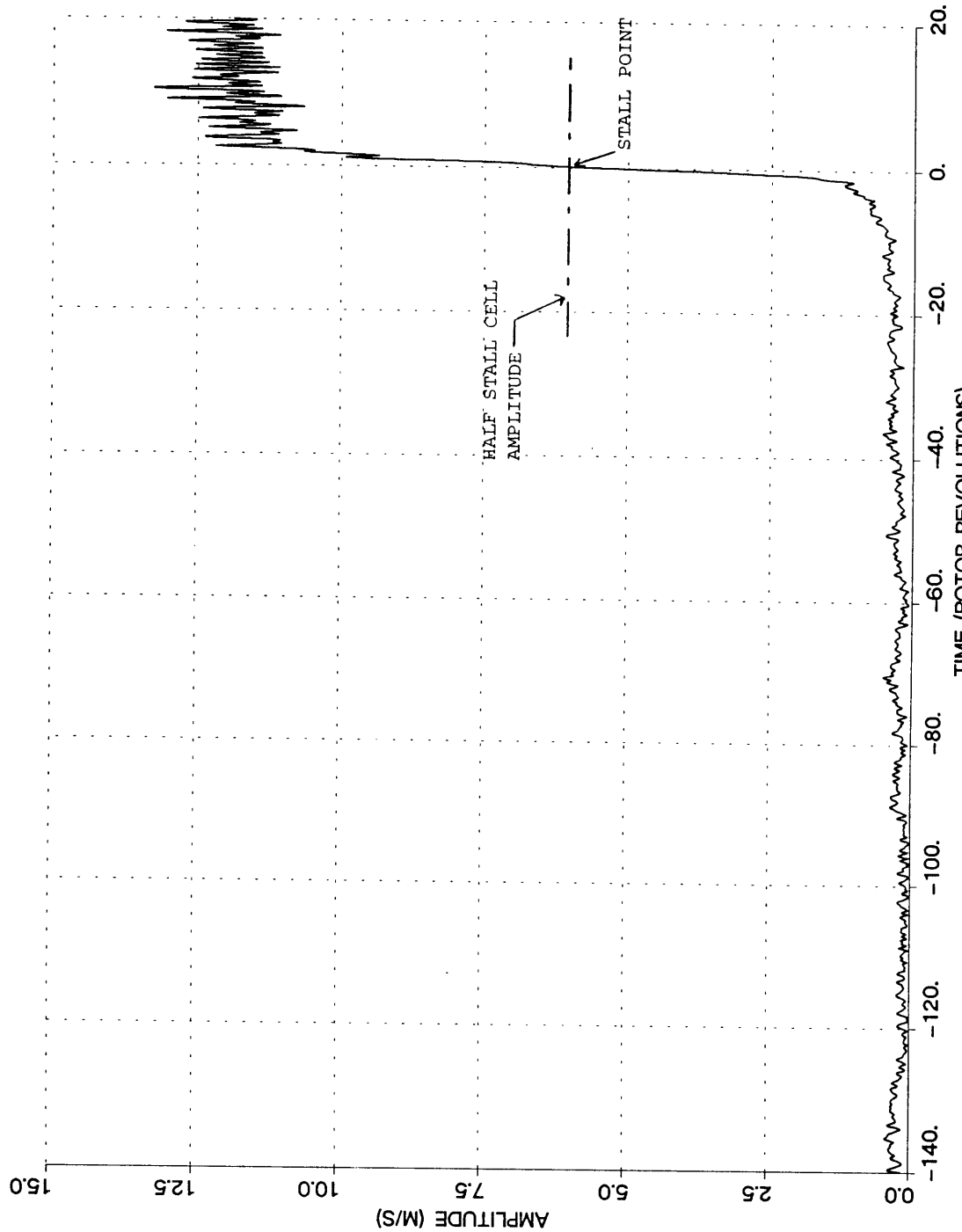

Figure (4-10a) Definition of Stall Point

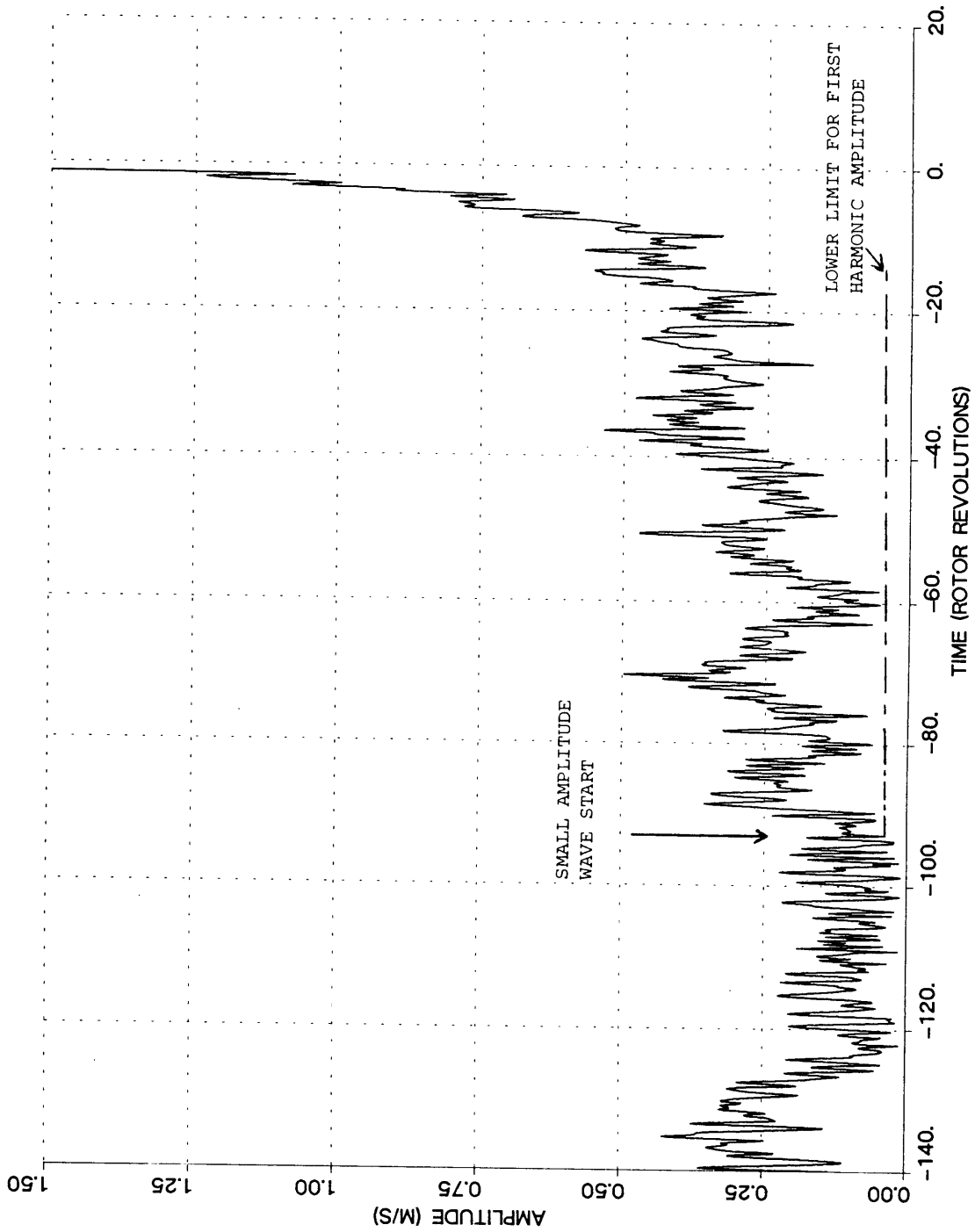

Figure (4-10b) Definition of Small Amplitude Start from First Harmonic Amplitude

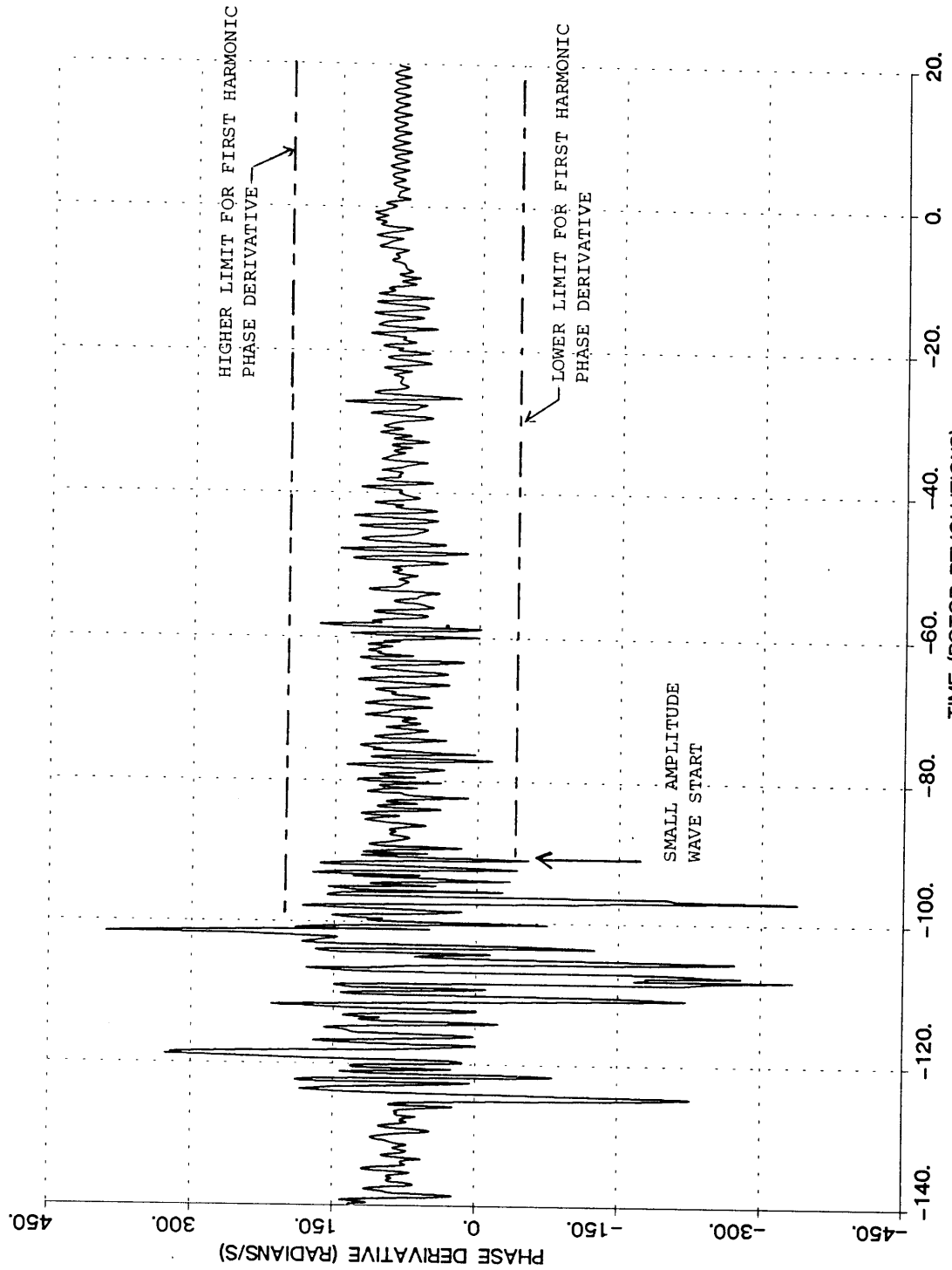

Figure (4-10c) Definition of Small Amplitude Wave Start from First Harmonic Phase Derivative

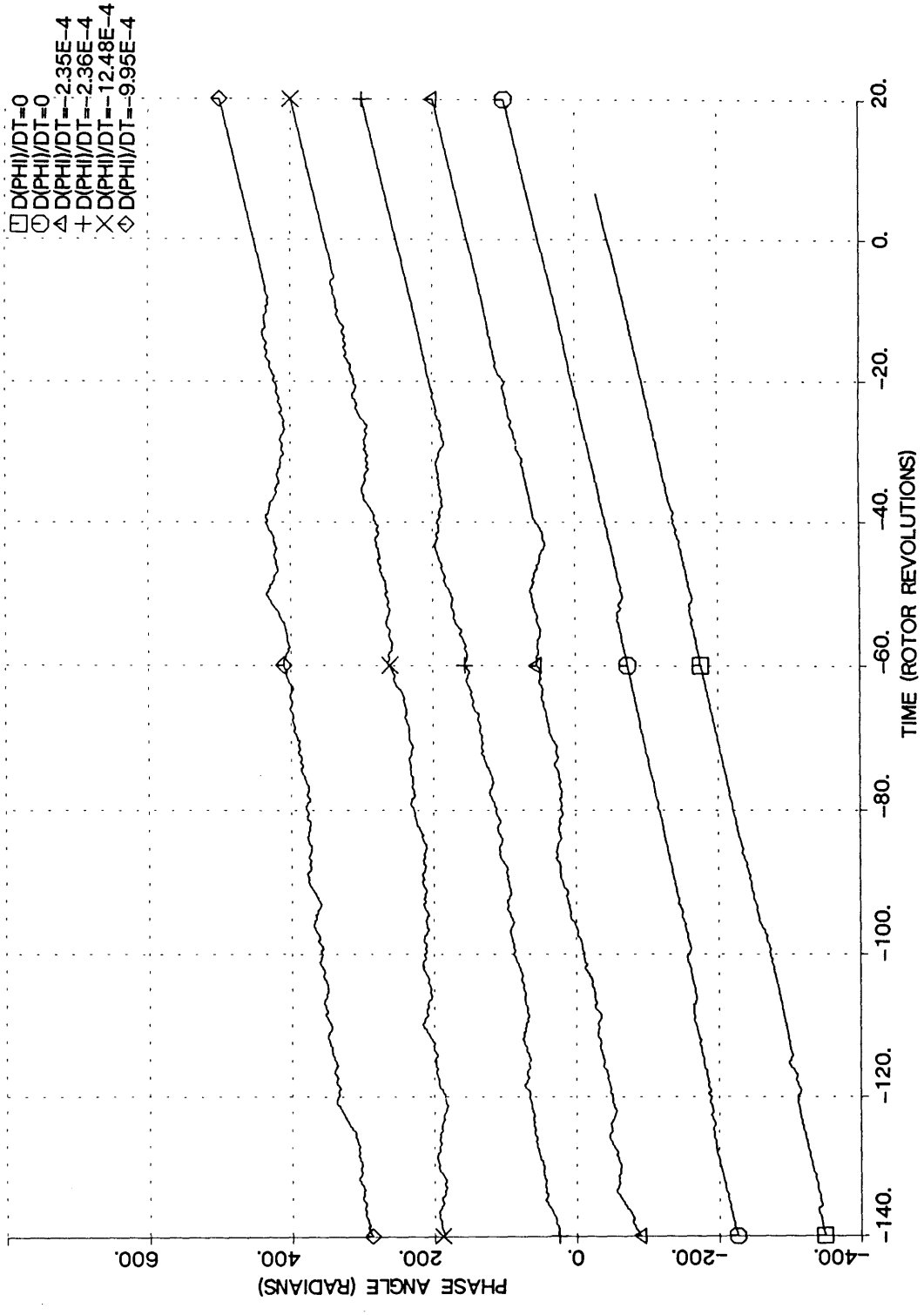

Figure (4-11) Three Stage Compressor: First Harmonic Phase During Transients with Uniform Inlet Flow

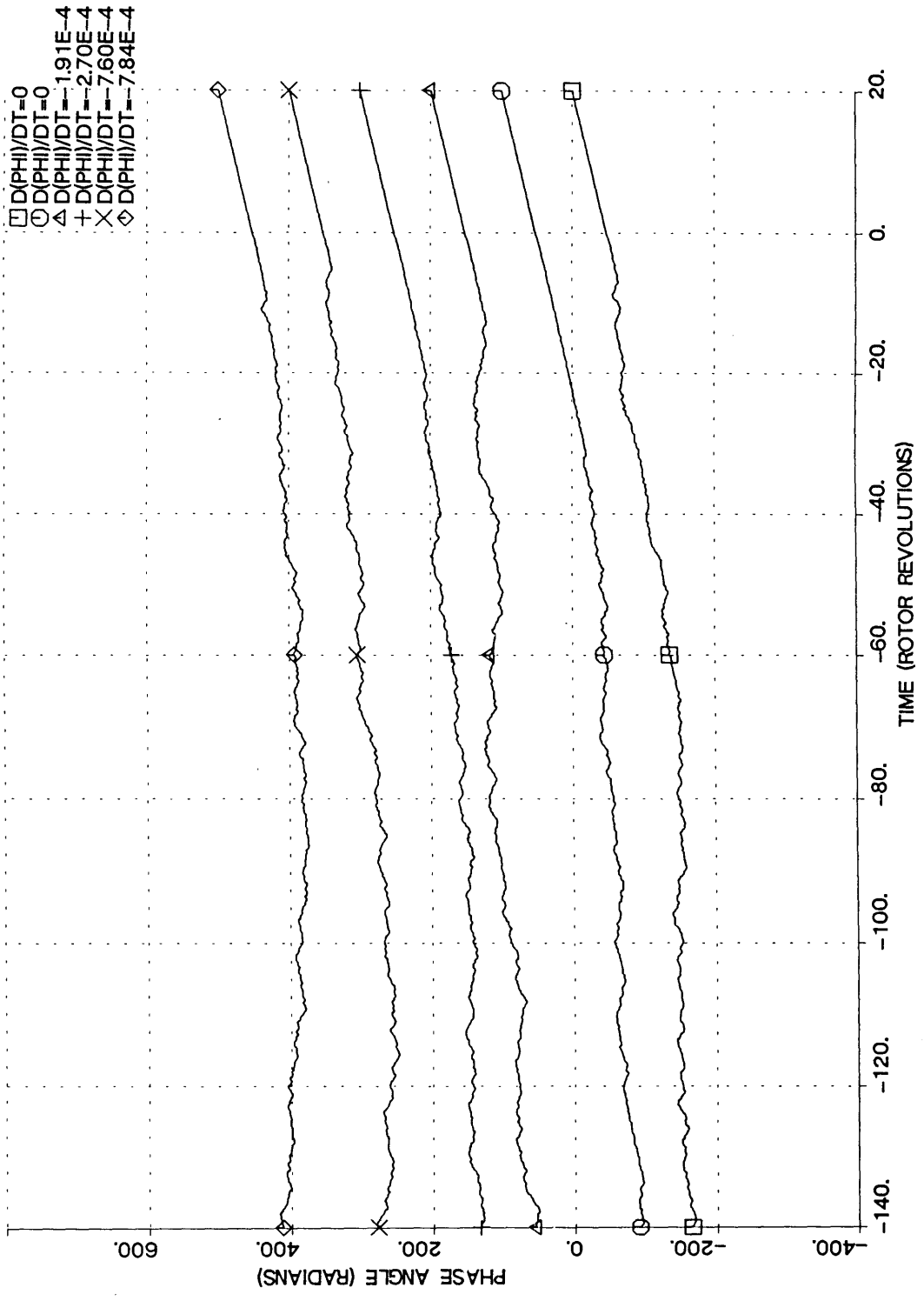

Figure (4-12) Three Stage Compressor: First Harmonic Phase During Transients with Distorted Inlet Flow

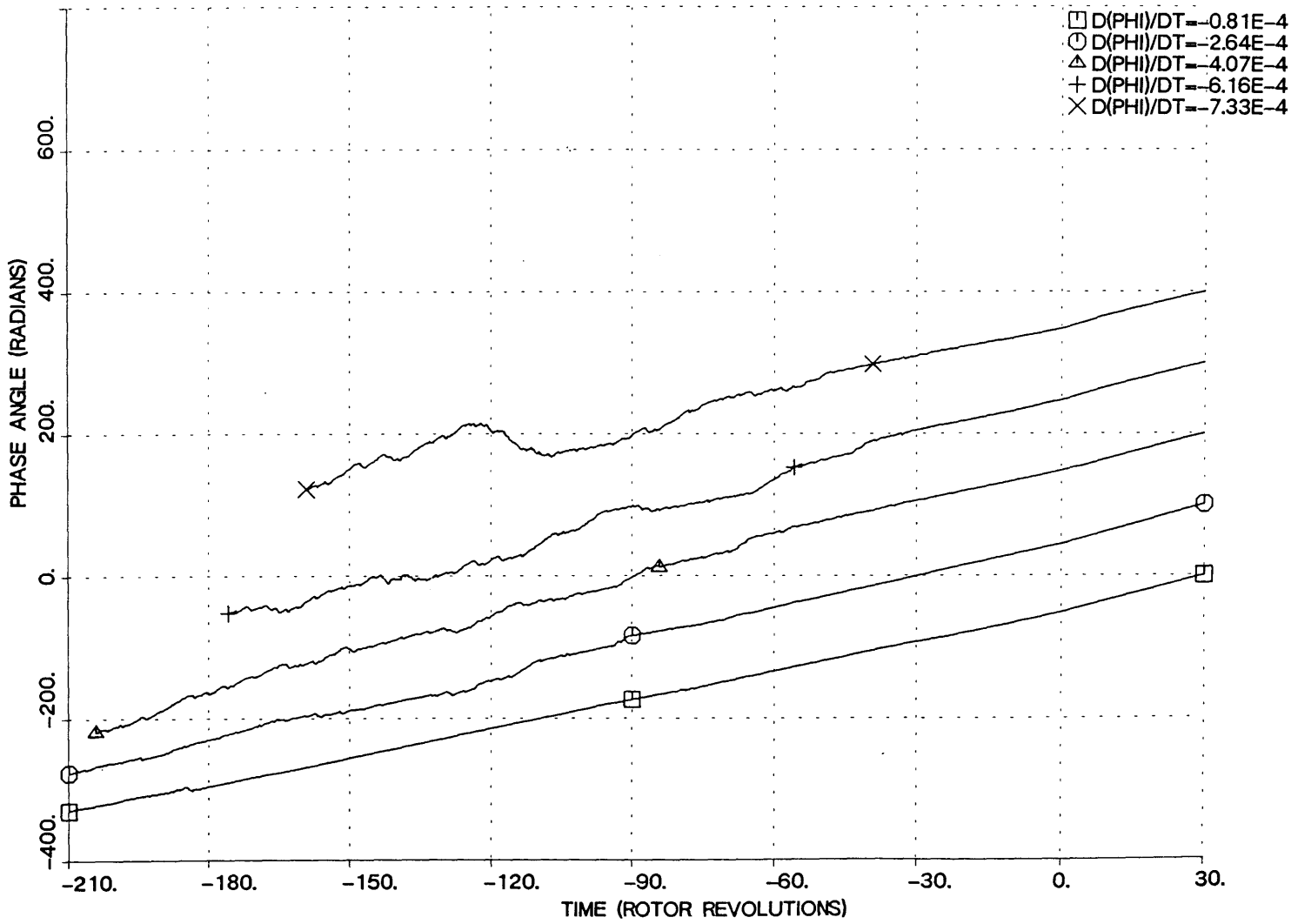

Figure (4-13) Single Stage Compressor: First Harmonic Phase During Transients with Uniform Inlet Flow

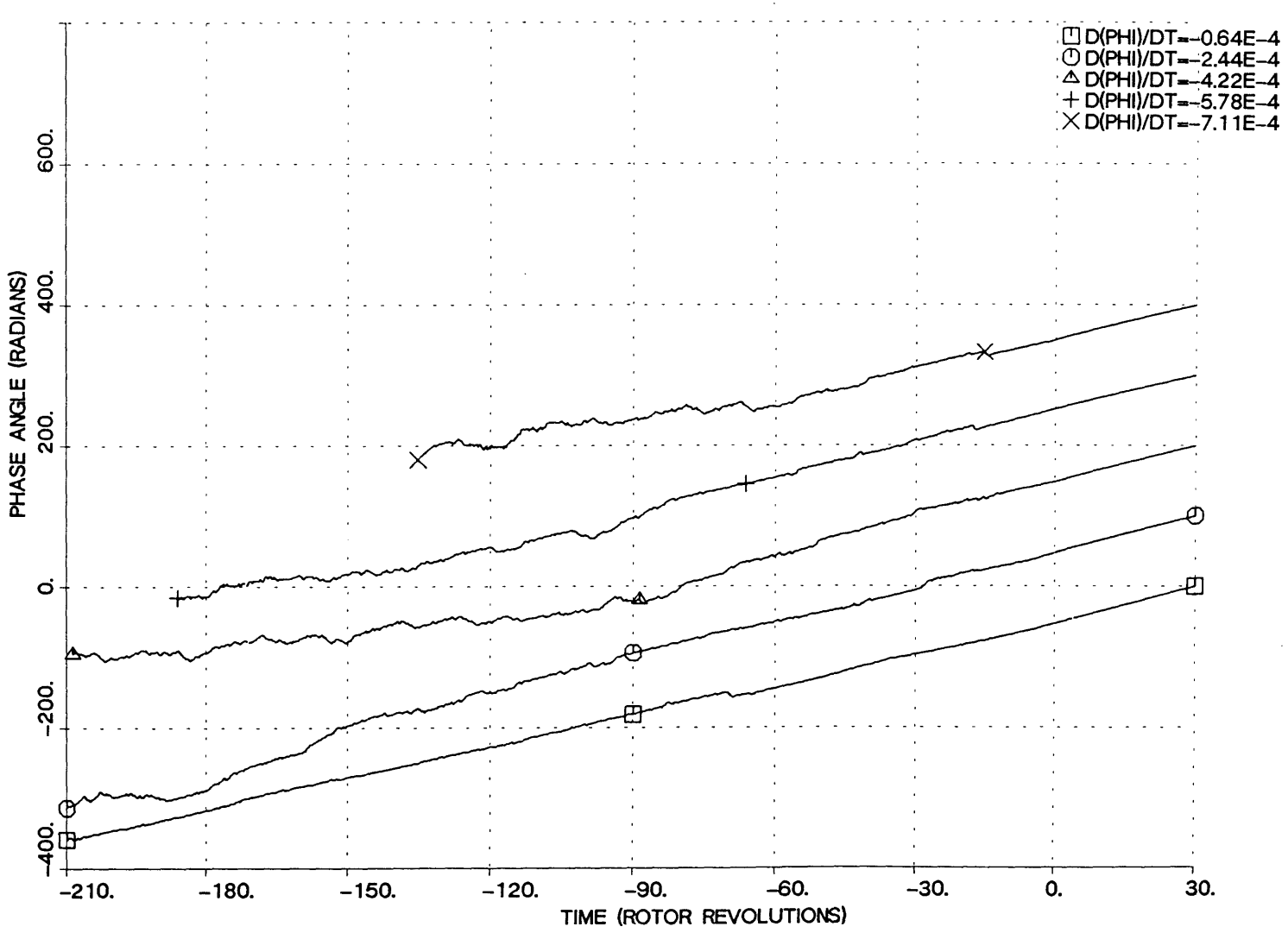

Figure (4-14) Single Stage Compressor: First Harmonic Phase During Transients with Distorted Inlet Flow

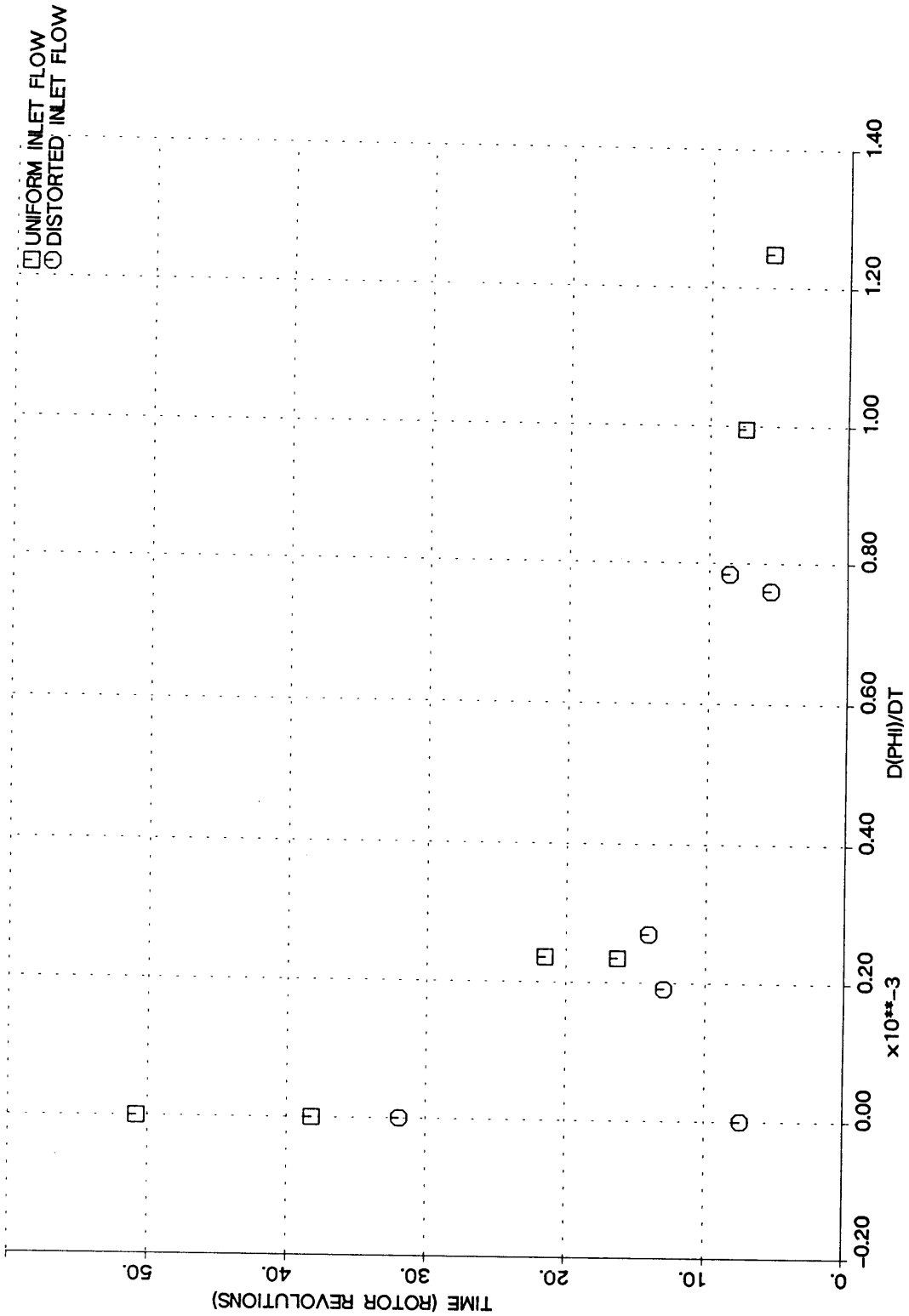

Figure (4-15) Three Stage Compressor: Small Amplitude Wave Time Extent During Transients

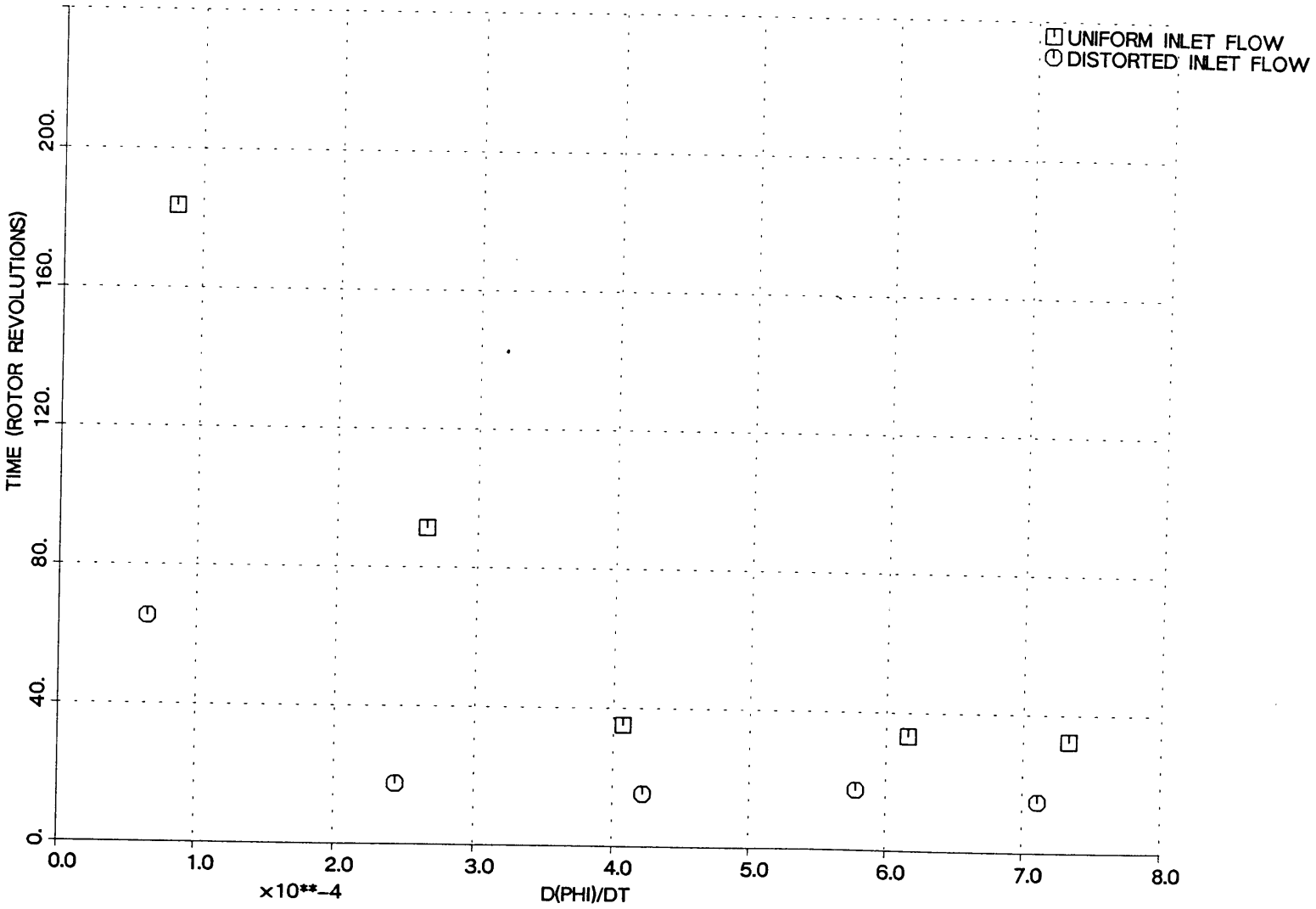

Figure (4-16) Single Stage Compressor: Small Amplitude Wave Time Extent During Transients

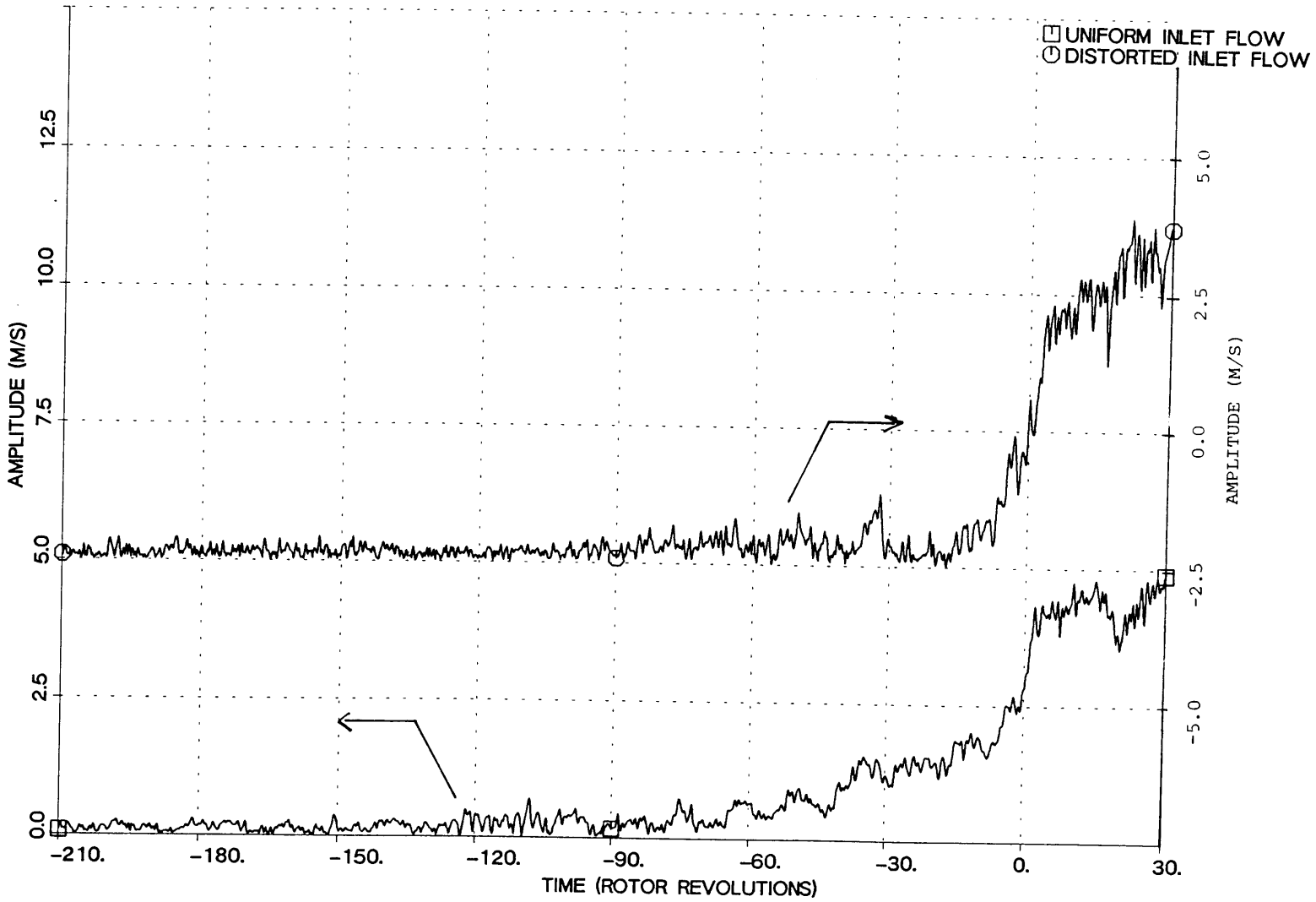

Figure (4-17) Single Stage Compressor: Comparison of First Harmonic Amplitude During Transient with Uniform and Distorted Inlet Flow

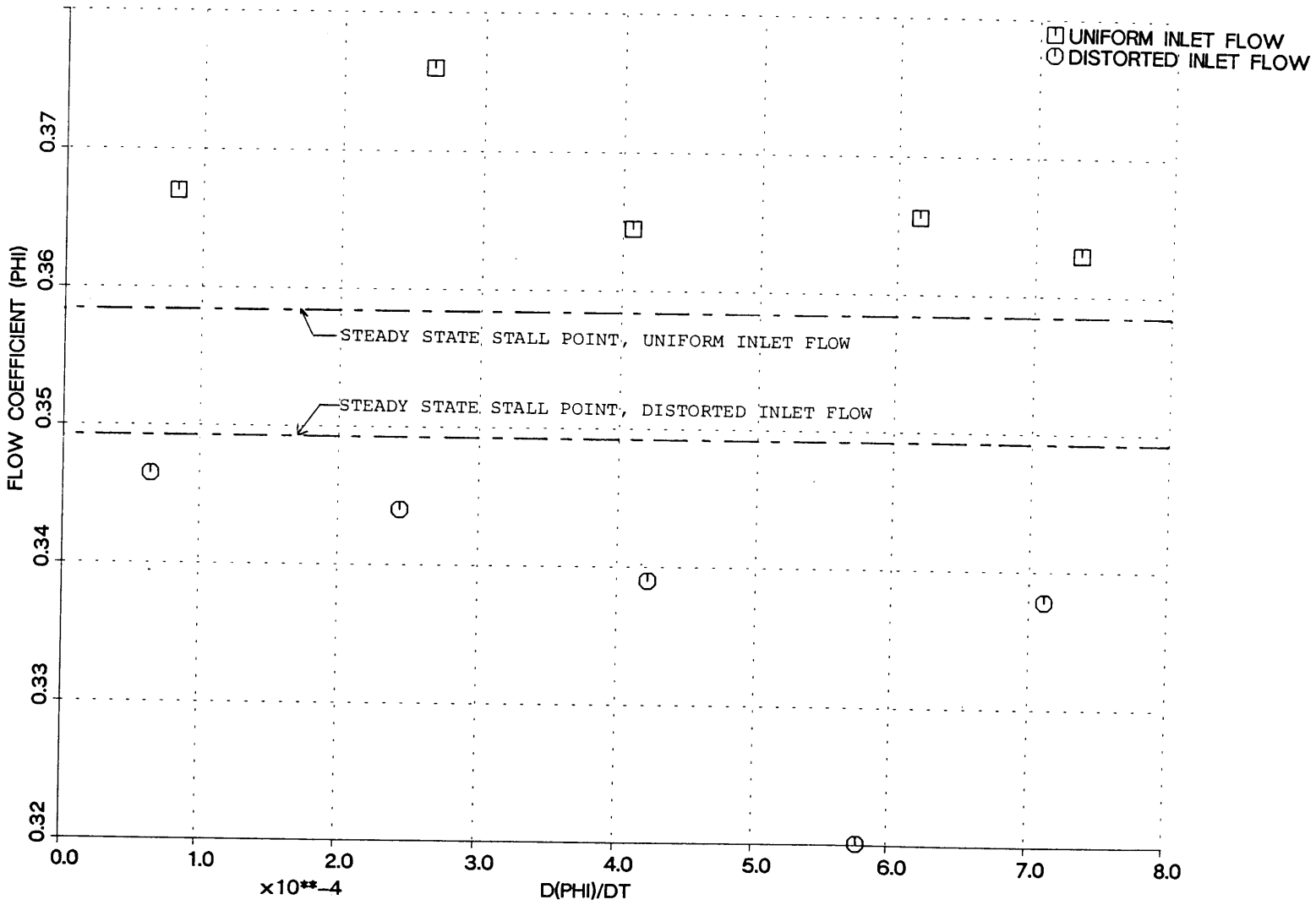

Figure (4-18) Single Stage Compressor: Flow Coefficient at Start of Small Amplitude Wave Propagation

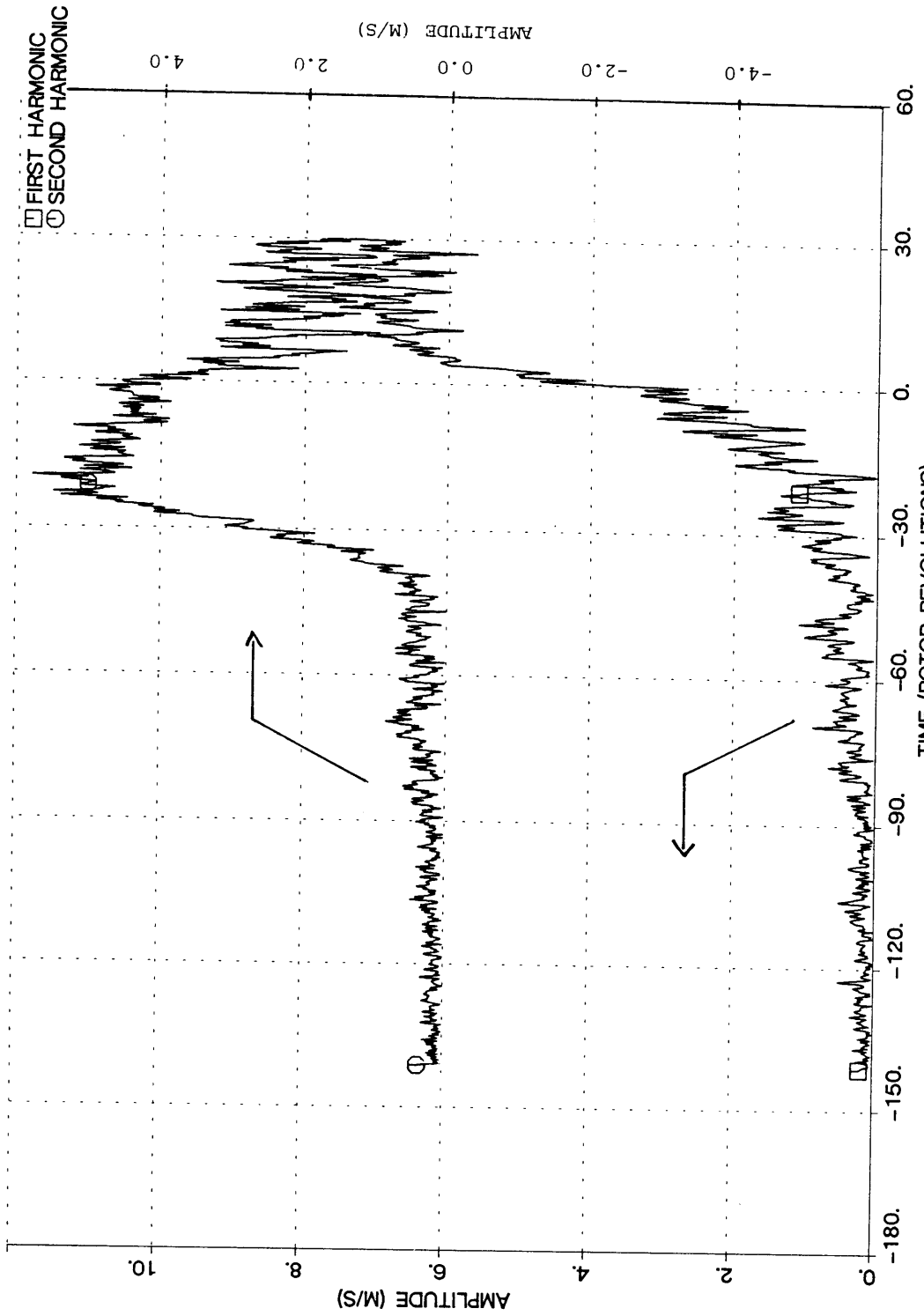

Figure (4-19) Single Stage Compressor: First and Second Harmonic Amplitude During Transient with Inlet Distortion, $d(\phi)/dt=-5.78e-4$

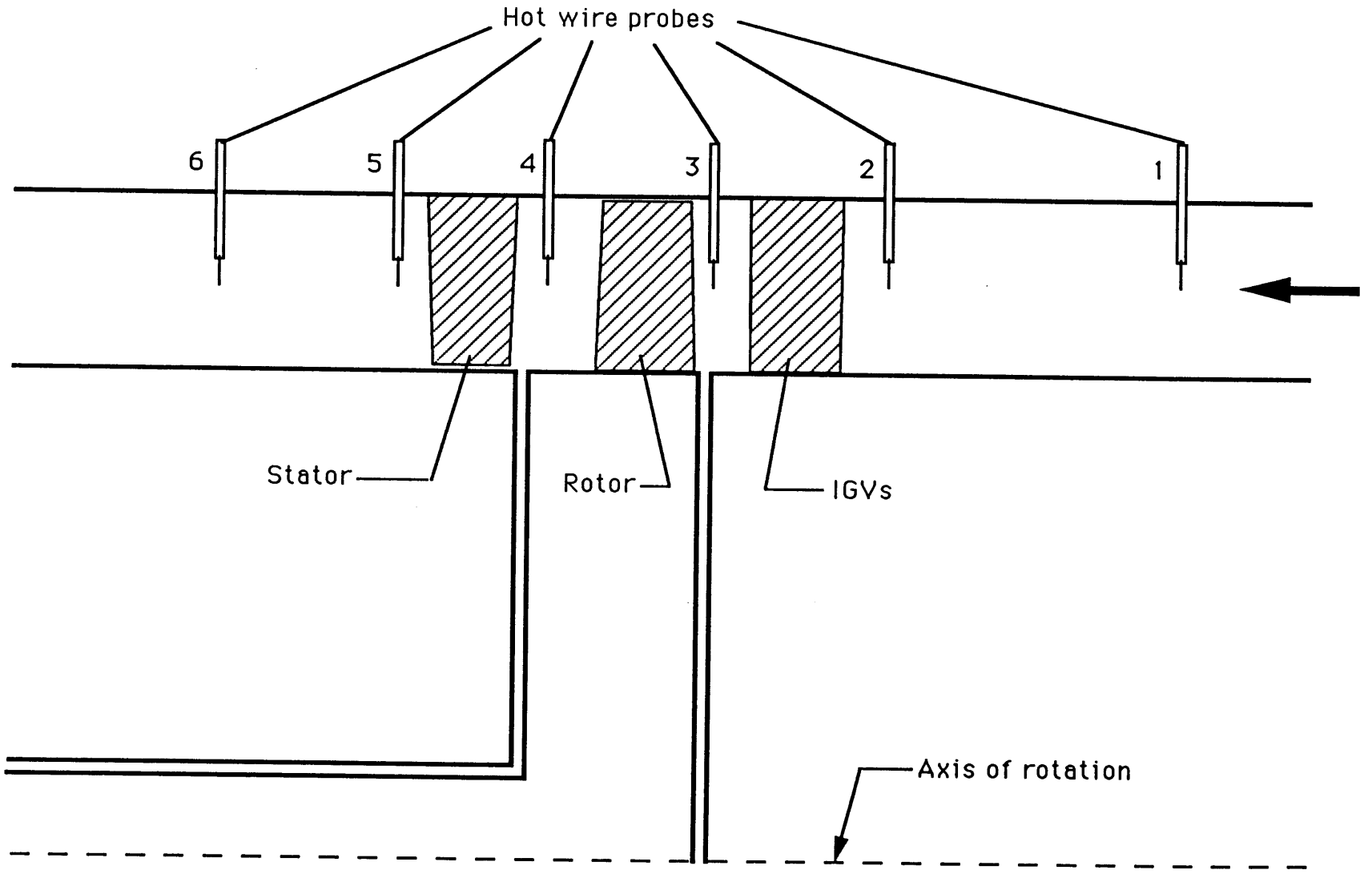

Figure (4-20) Single Stage Compressor: Schematic of Blading and Hot Wire Instrumentation Location

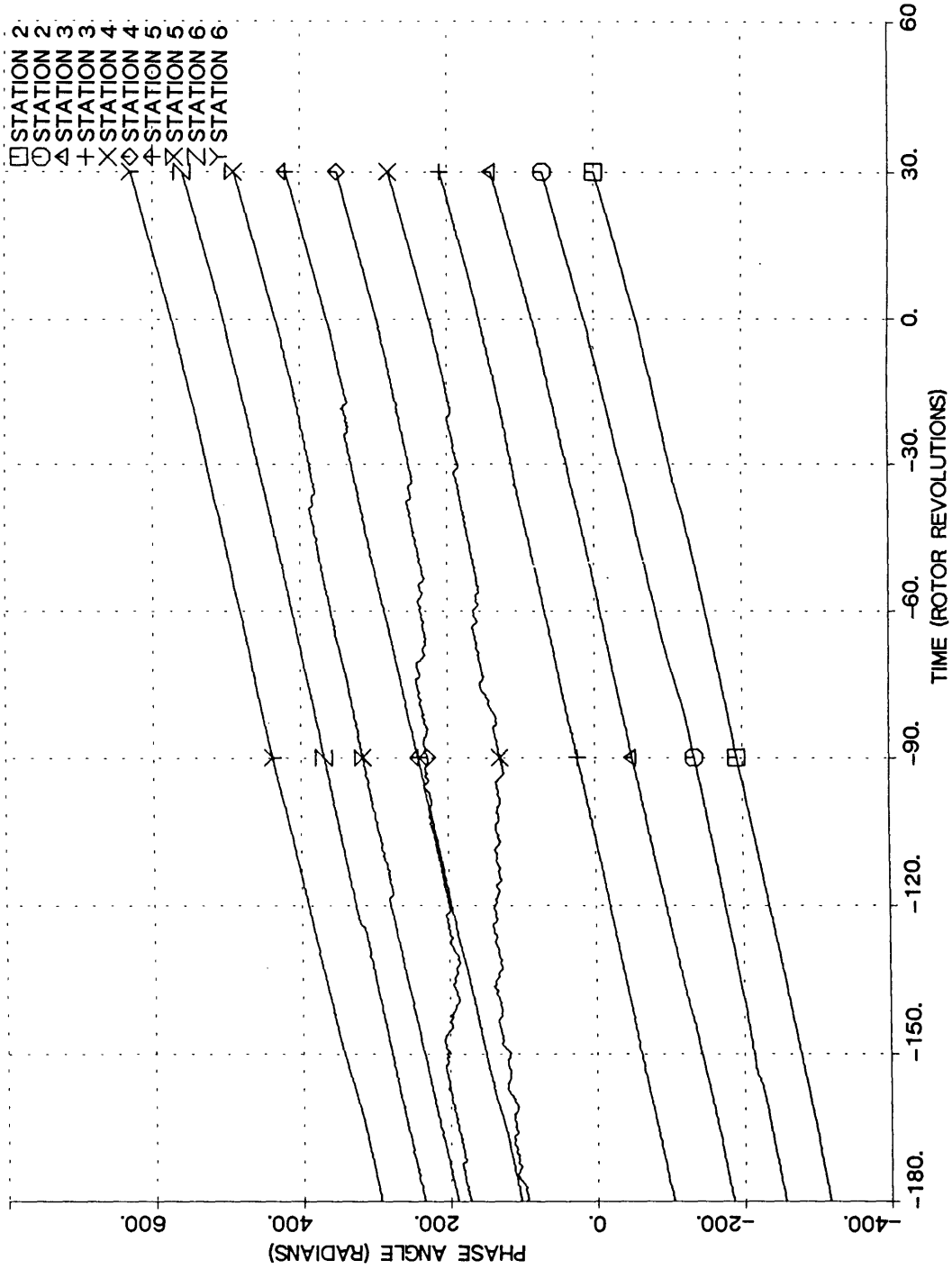

Figure (4-21) Single Stage Compressor: First Harmonic Phase During Very Slow Transients at Five Different Axial Locations

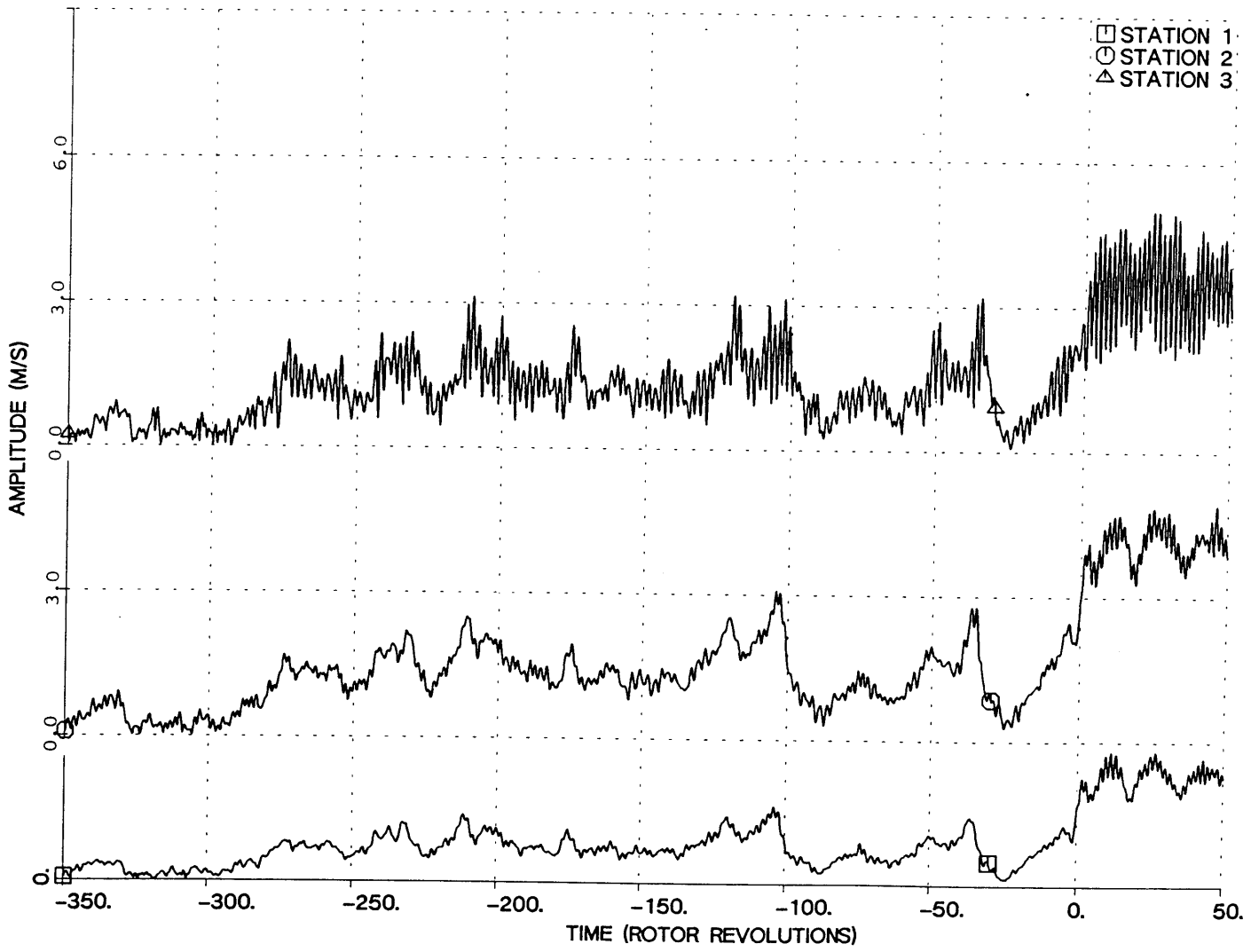

Figure (4-22) Single Stage Compressor: First Harmonic Amplitude at Stations 1,2 & 3 During Very Slow Transients

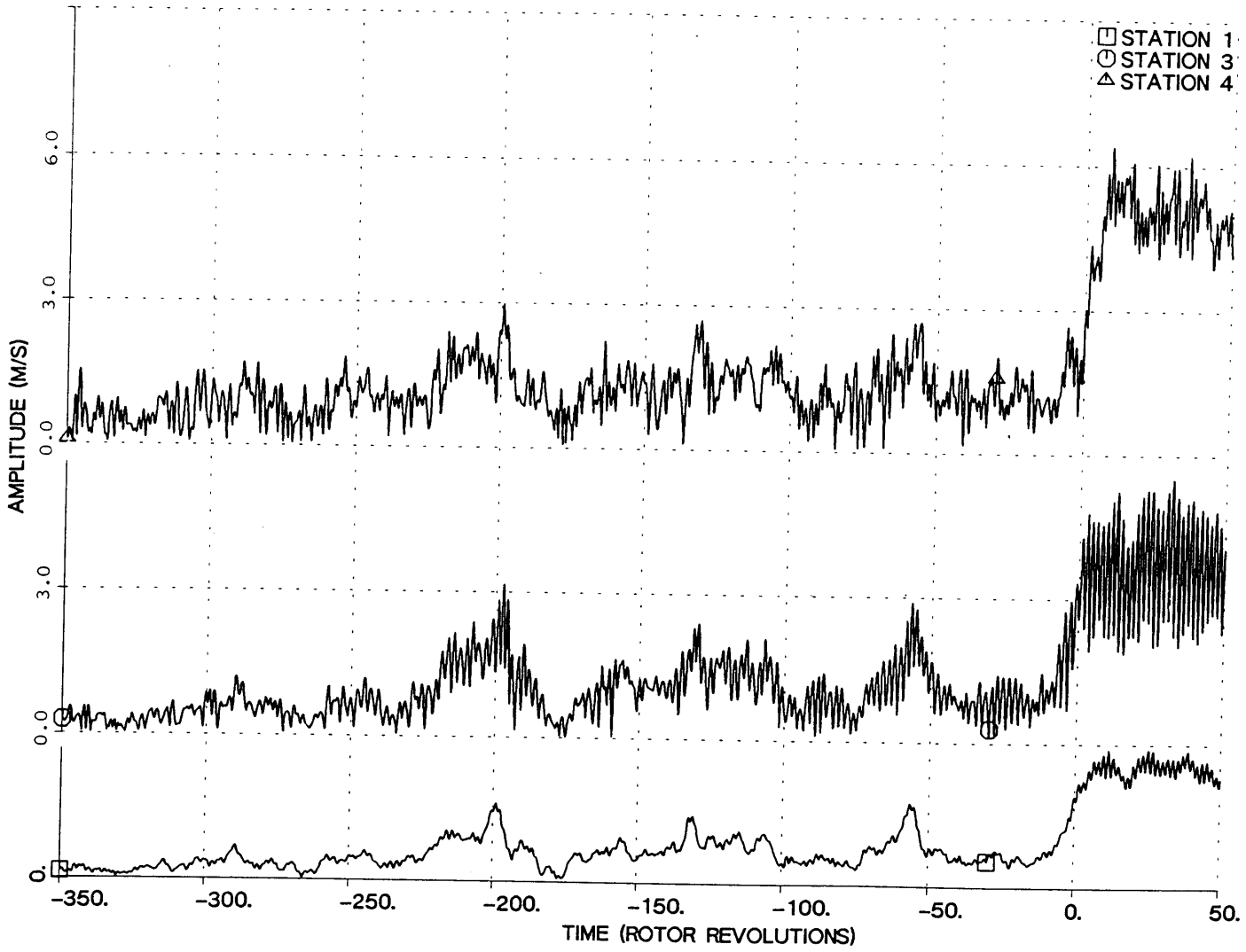

Figure (4-23) Single Stage Compressor: First Harmonic Amplitude at Stations 1,3 & 4 During Very Slow Transients

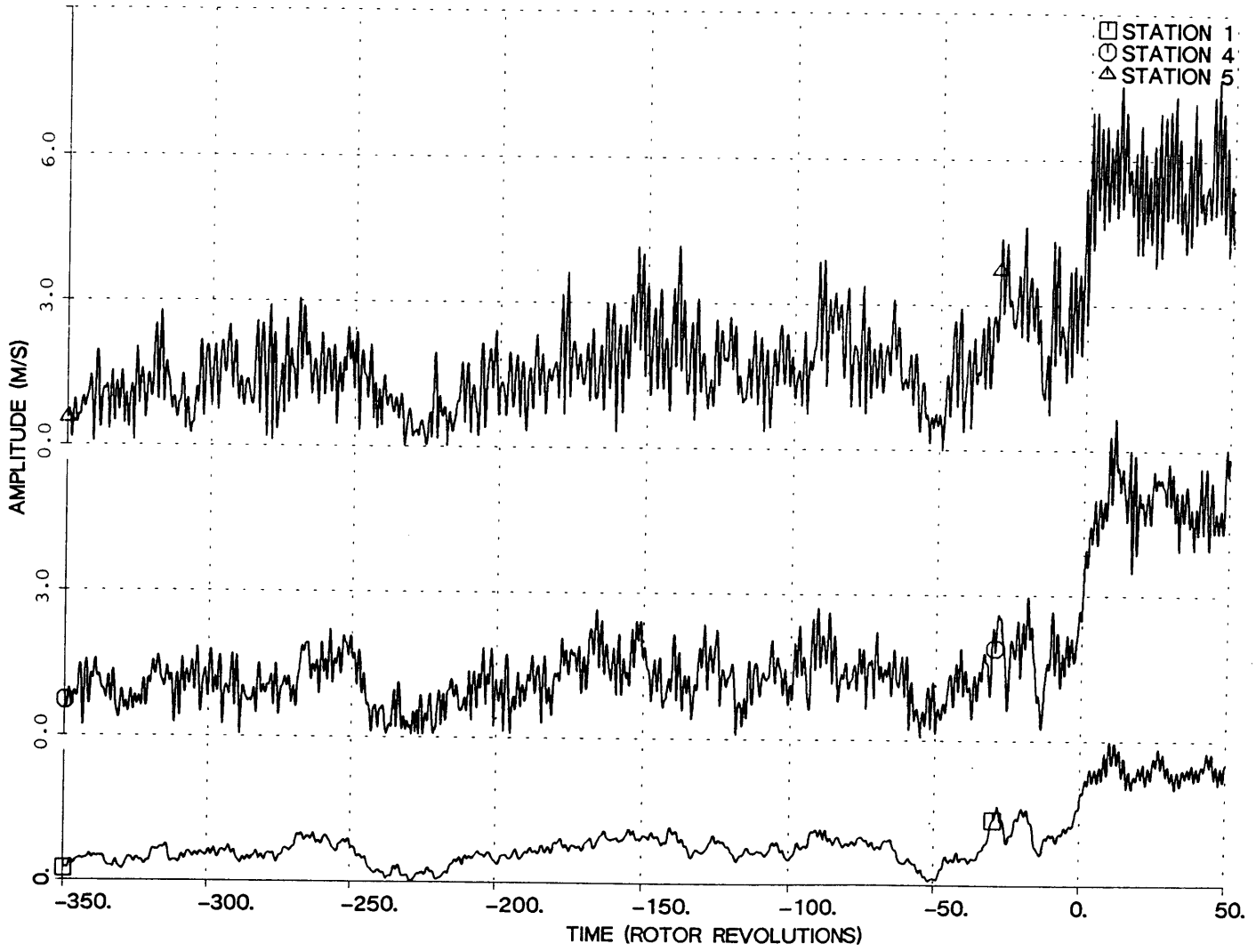

Figure (4-24) Single Stage Compressor: First Harmonic Amplitude at Stations 1,4 & 5 During Very Slow Transients

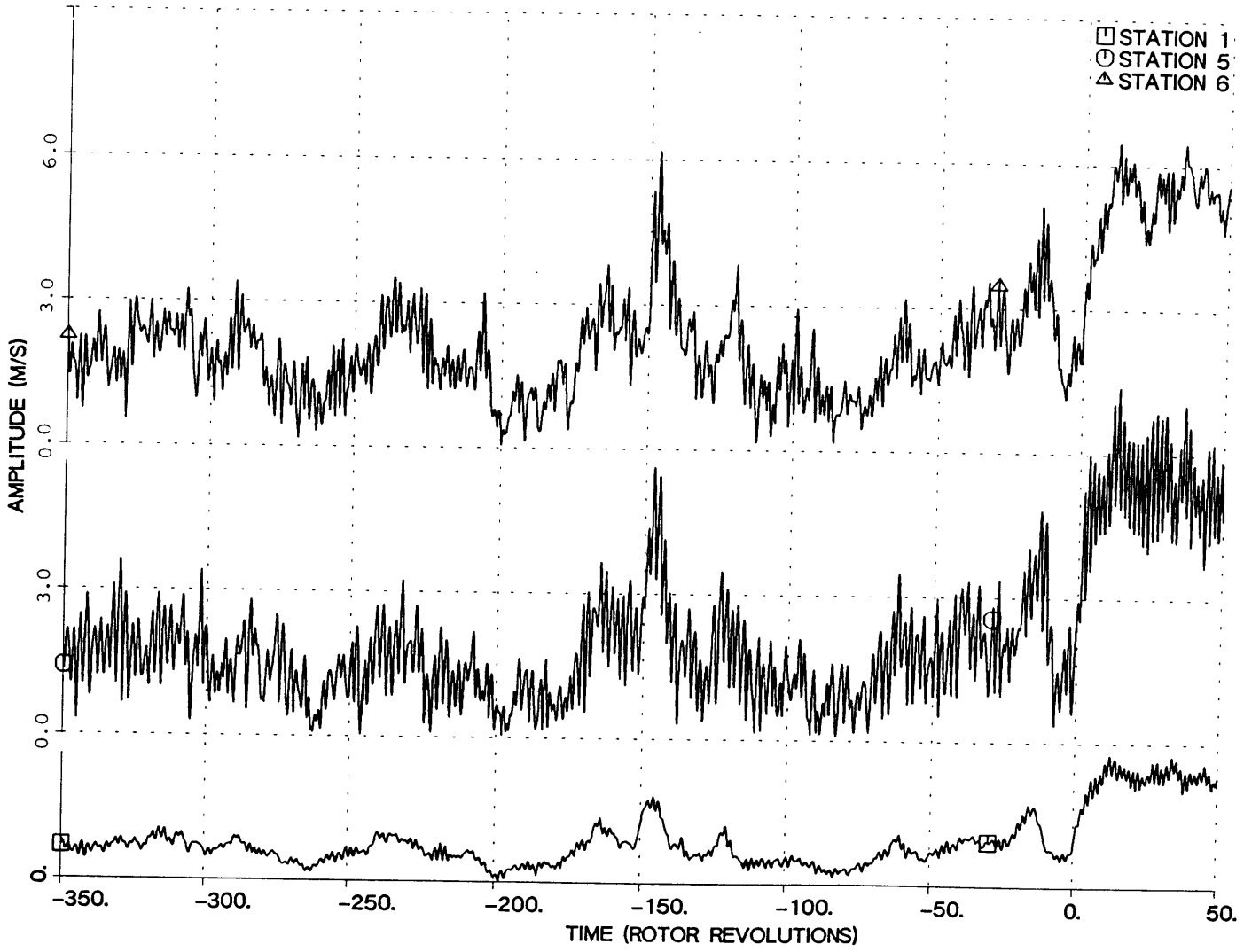

Figure (4-25) Single Stage Compressor: First Harmonic Amplitude at Stations 1,5 & 6 During Very Slow Transients

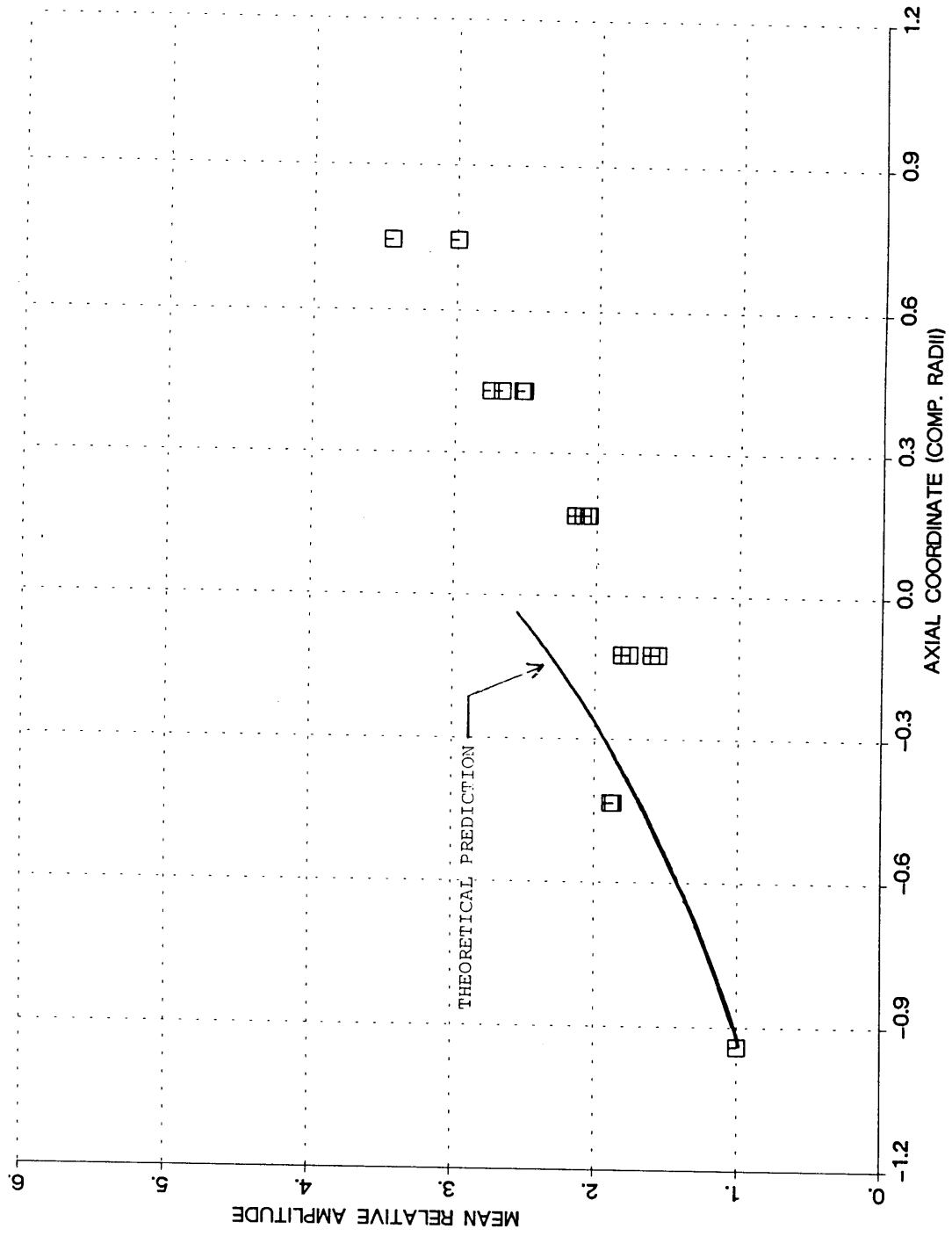

Figure (4-26) Single Stage Compressor: Mean Amplitude of First Harmonic Relative to Amplitude at Station 1

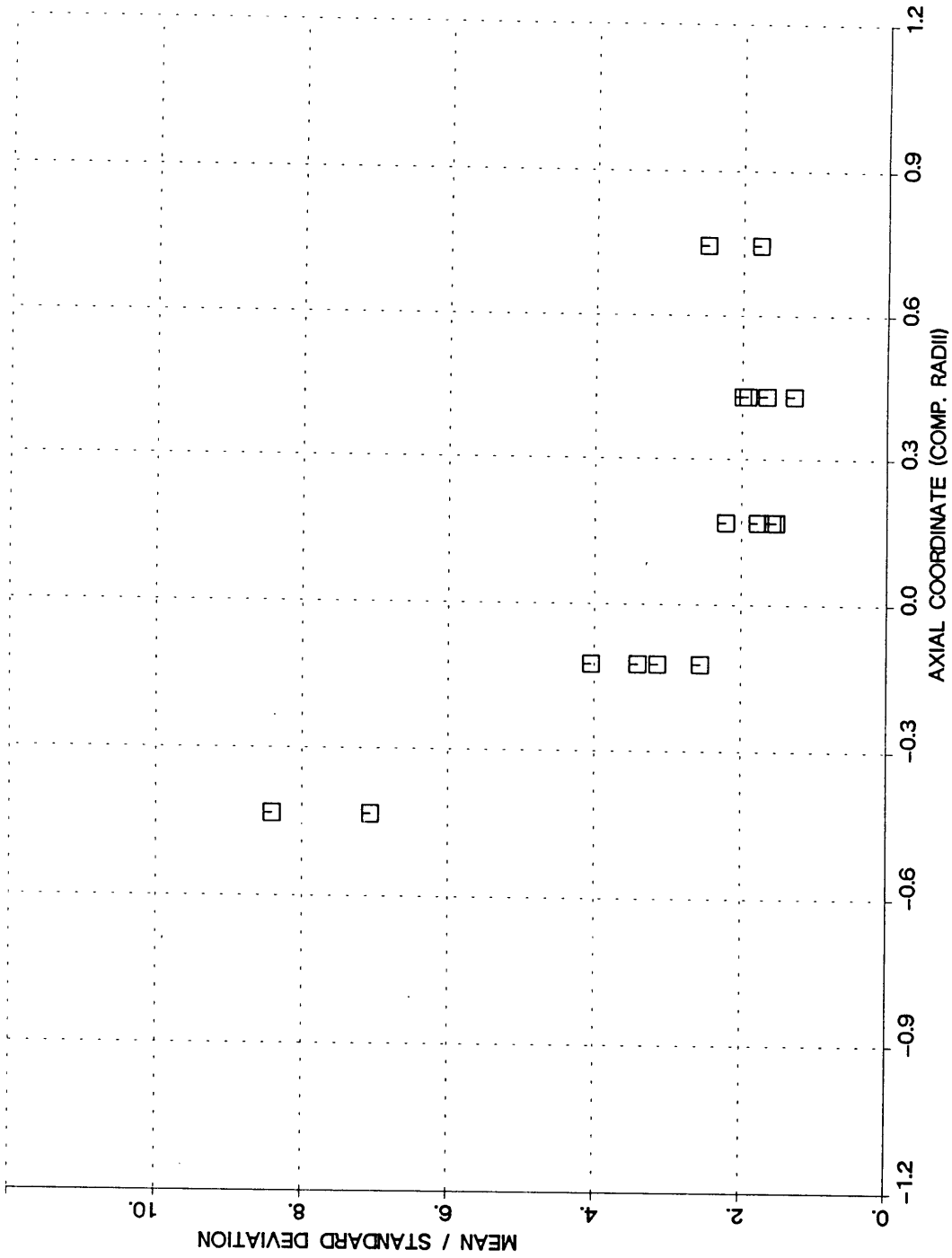

Figure (4-27) Single Stage Compressor. Relative Amplitude of First Harmonic: Mean/Standard Deviation

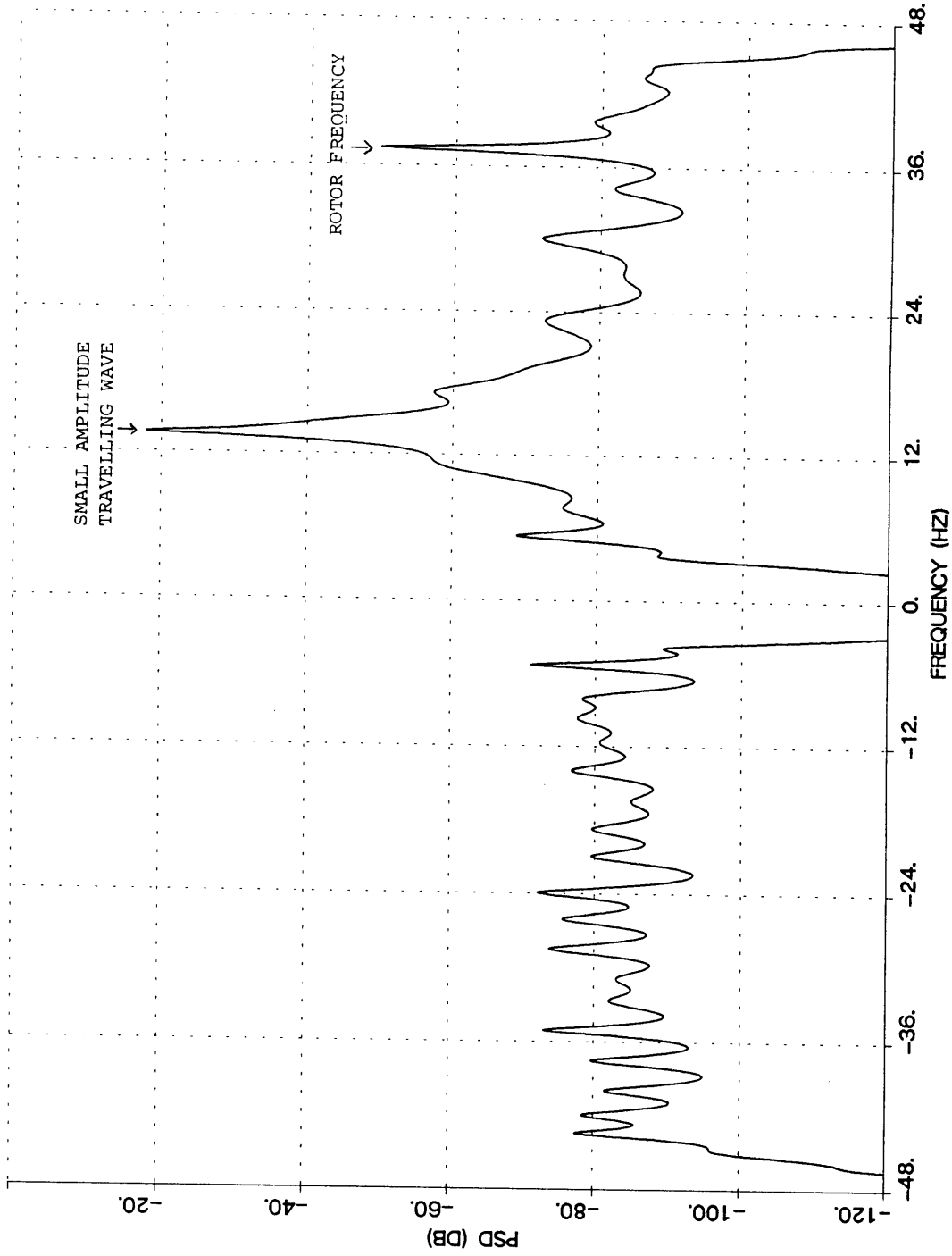

Figure (5-1a) Example of Frequency Resolution of Power Spectral Density: PSD of First Harmonic

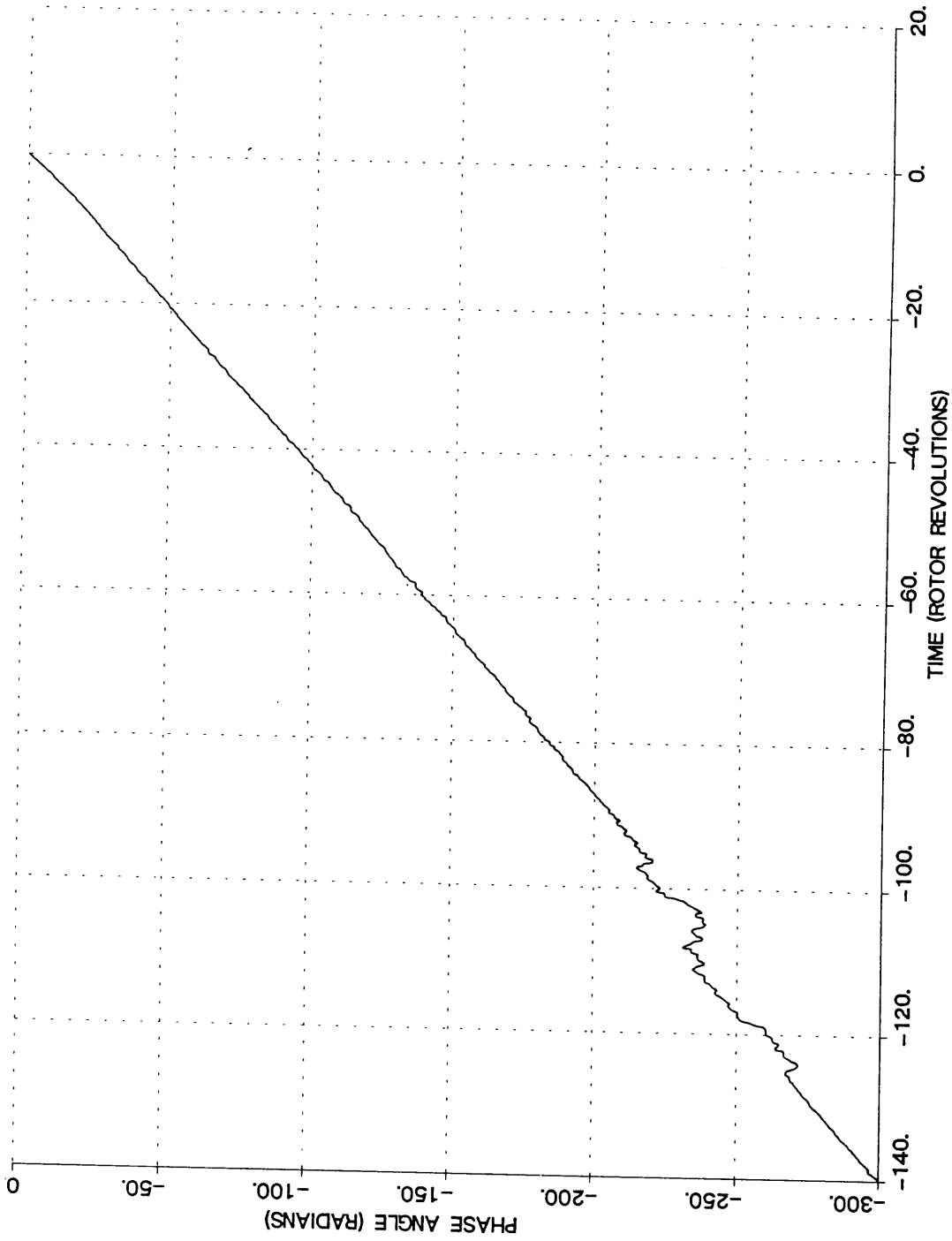

Figure (5-1b) First Harmonic Phase, Same Data as Figure (5-1a)

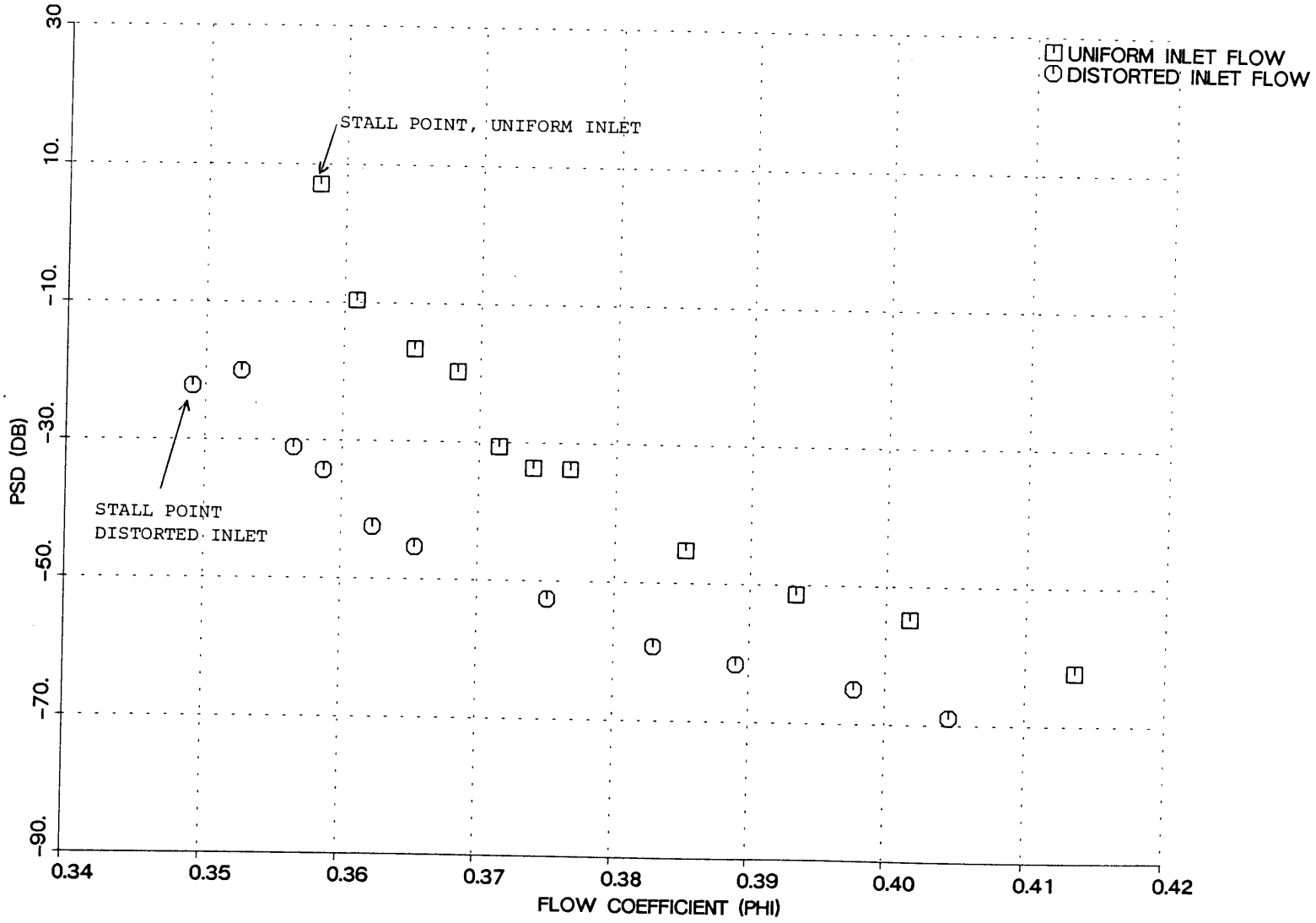

Figure (5-2) Power Density of Small Amplitude Travelling Wave (First Harmonic) vs Flow Coefficient

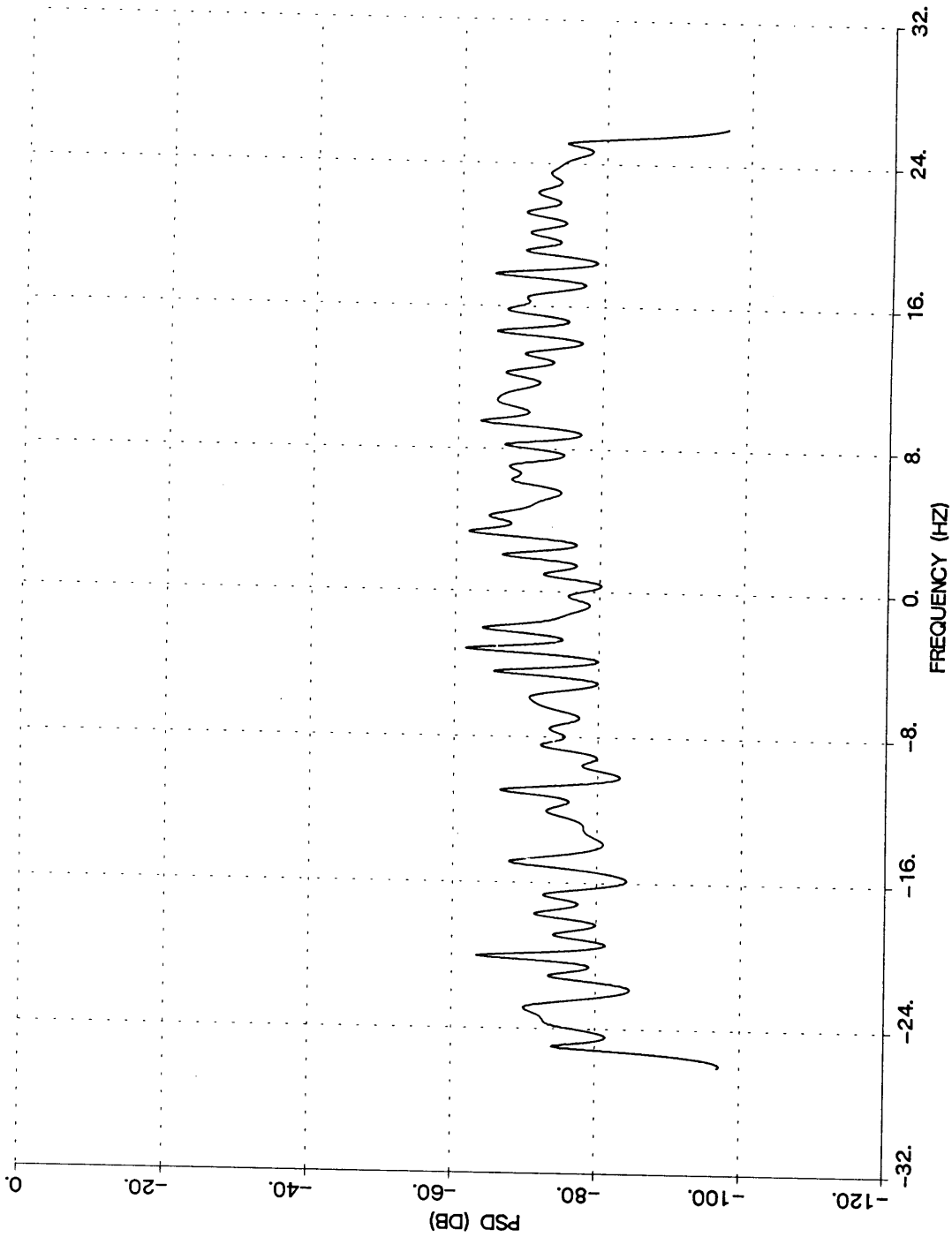

Figure (5-3) PSD of First Harmonic, Inlet Distortion, ϕ=0.405

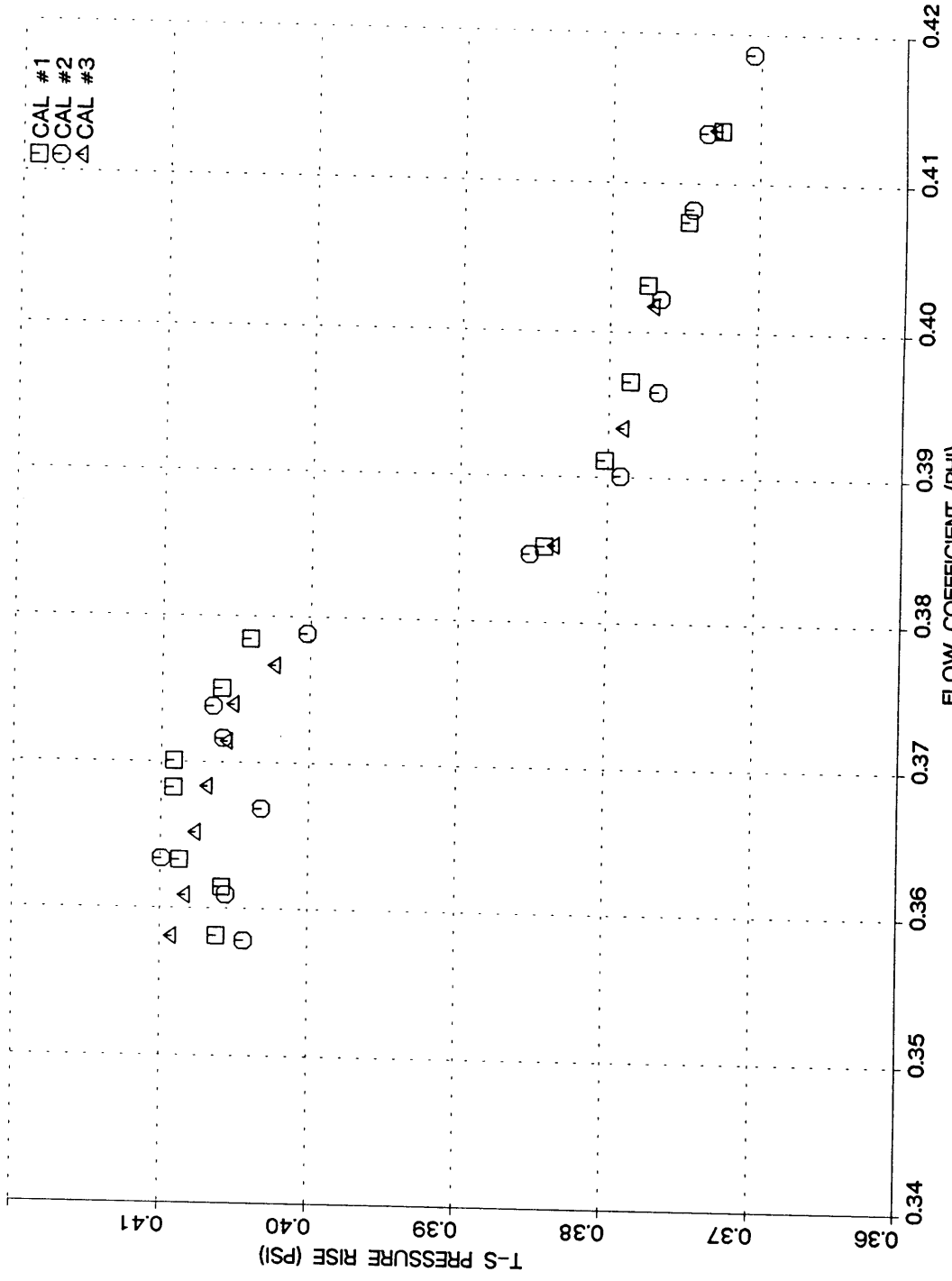

Figure (5-4a) Single Stage Compressor: Speedline at 2700 RPM, Uniform Inlet Flow

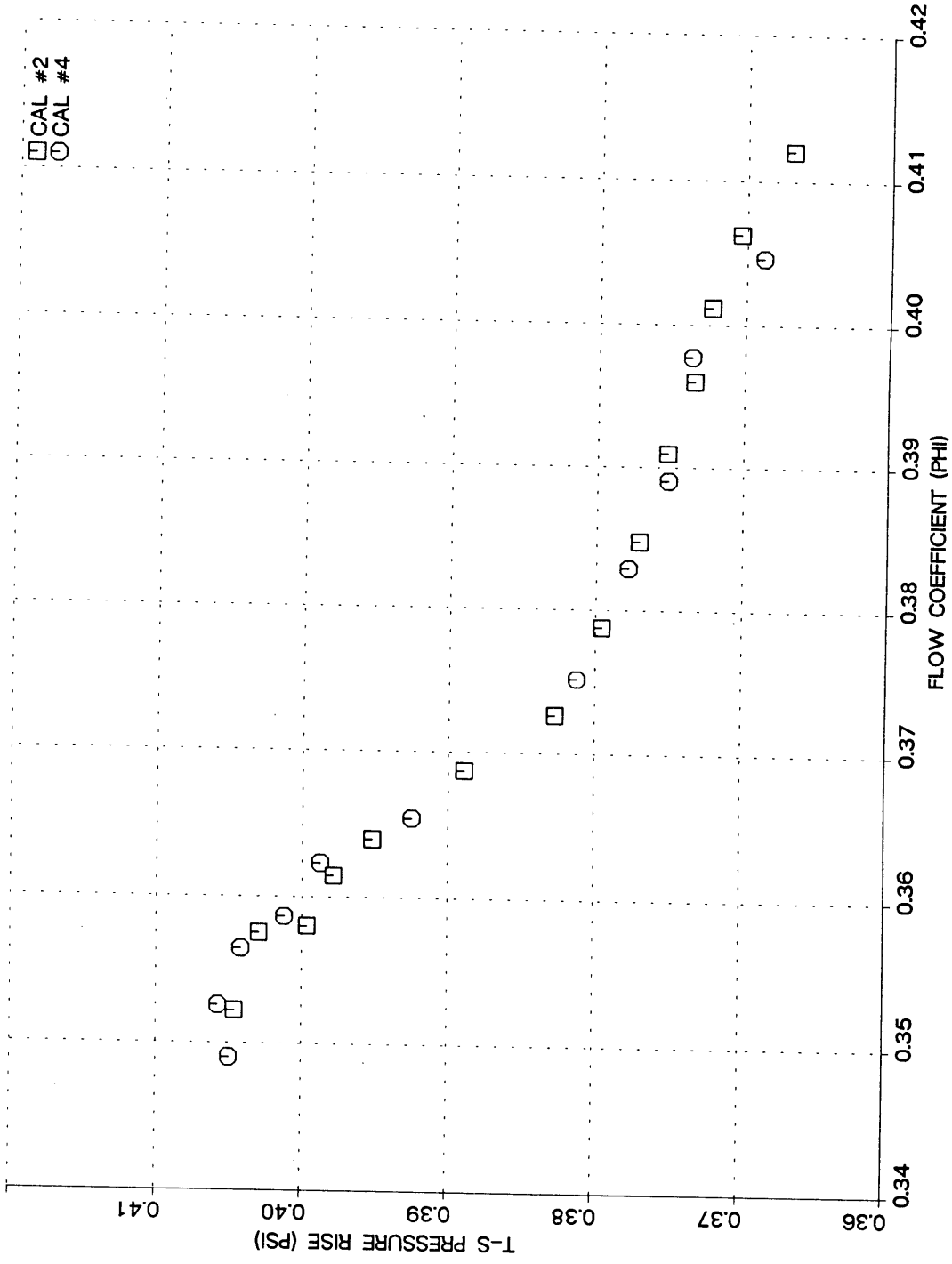

Figure (5-4b) Single Stage Compressor: Speedline at 2700 RPM, Distorted Inlet Flow

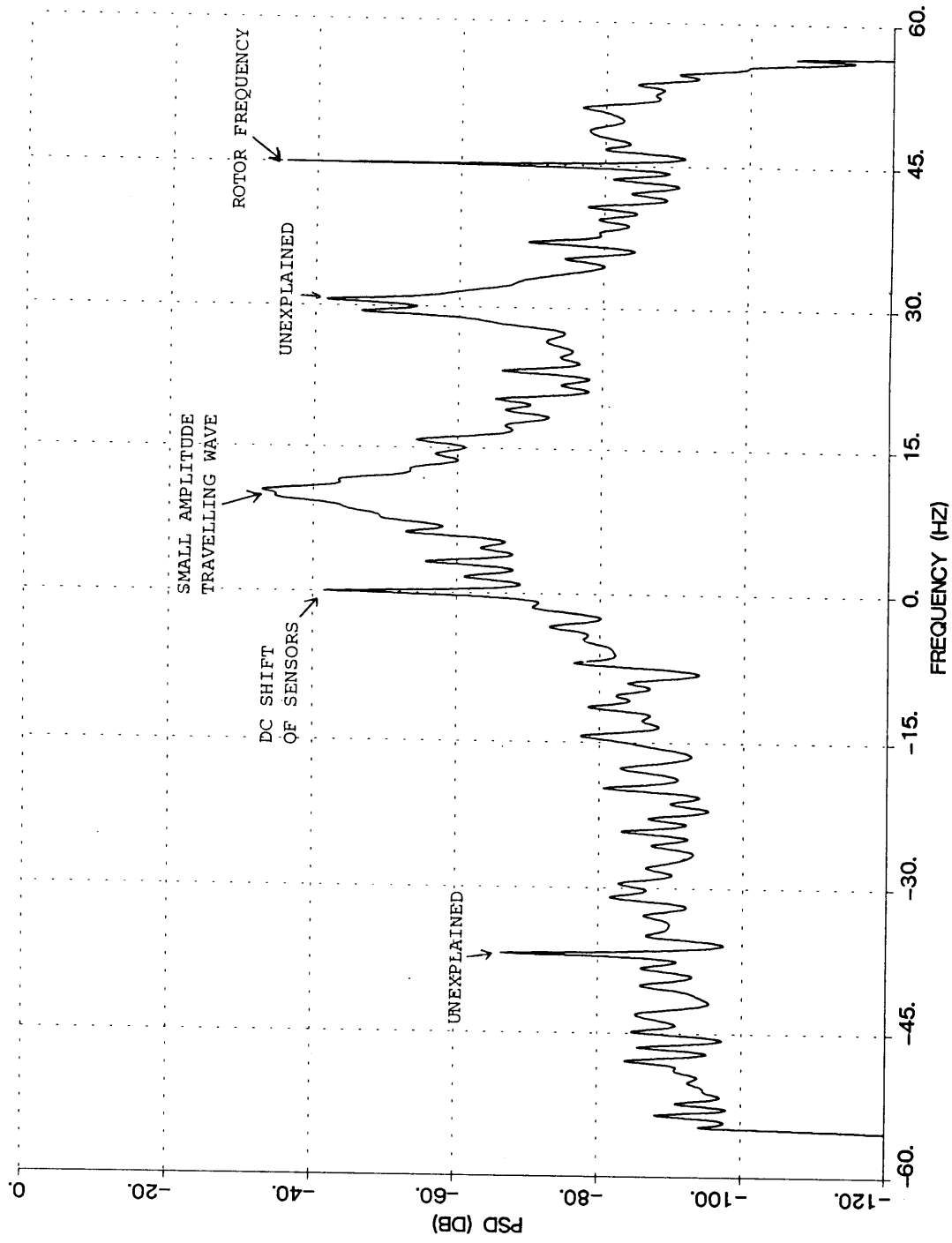

Figure (5-5) Typical Power Spectral Density of First Harmonic

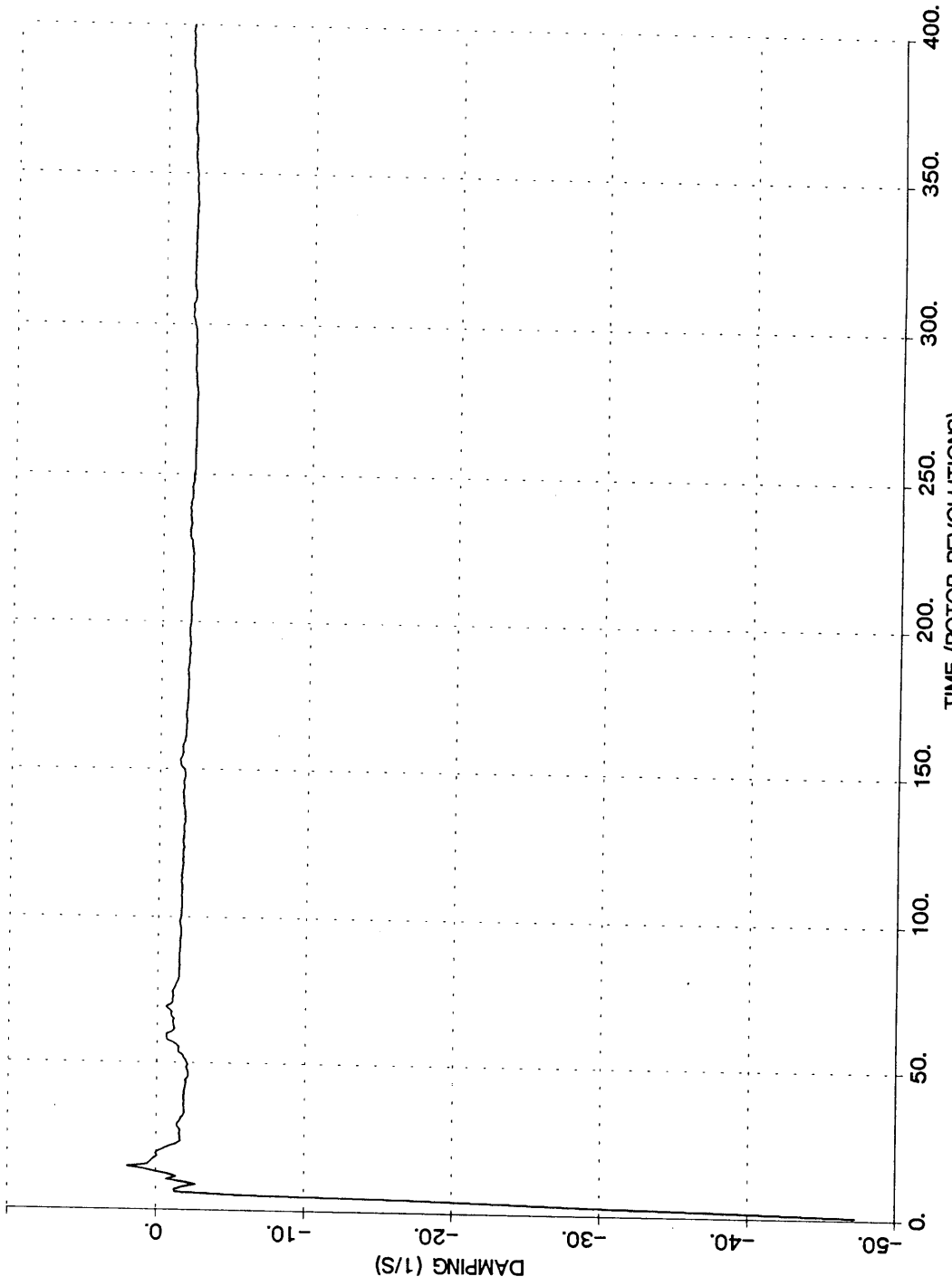

Figure (5-6) Convergence of Recursive Least Squares Algorithm, Uniform Inlet Flow, ϕ=0.361

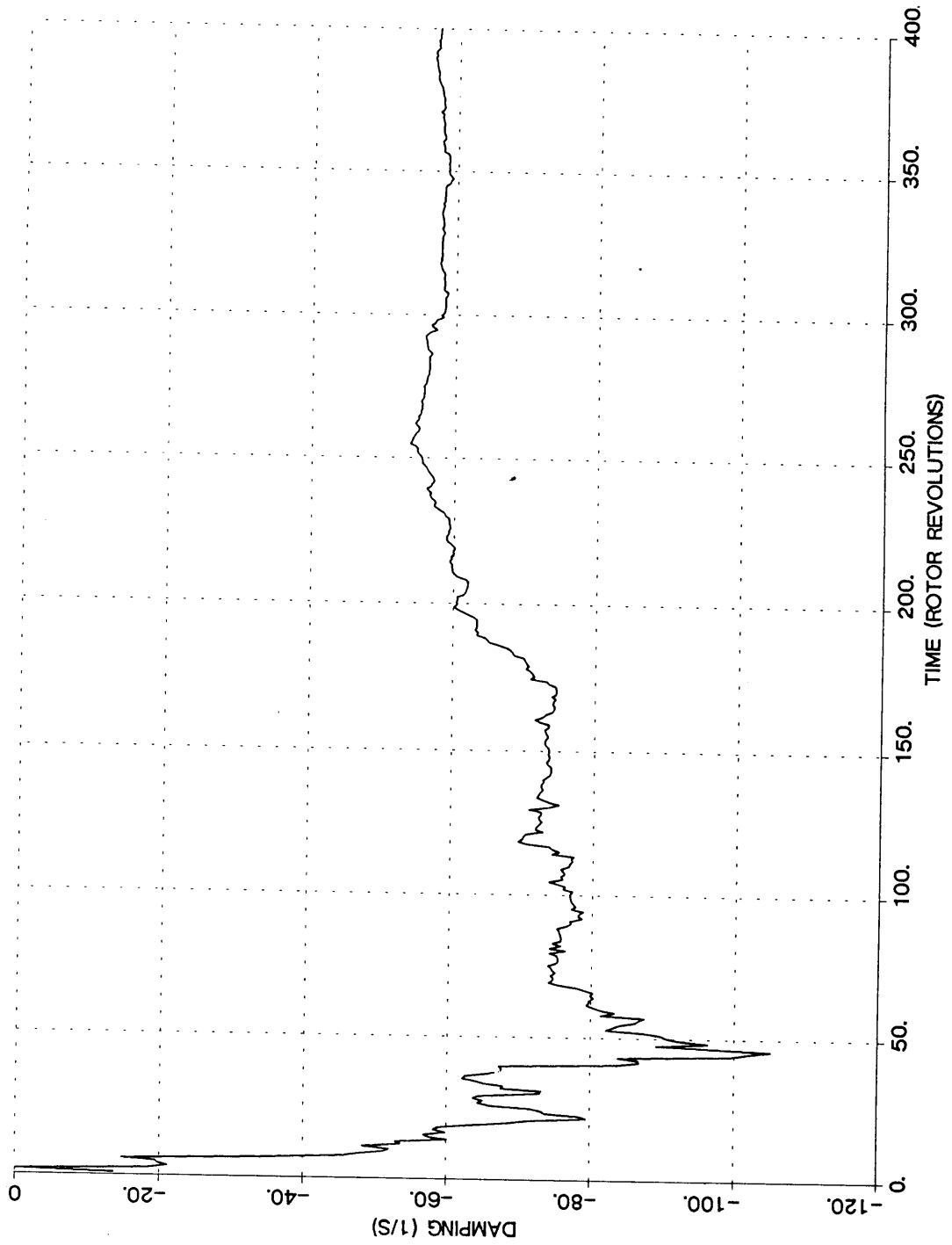

Figure (5-7) Convergence of Recursive Least Squares Algorithm, Distorted Inlet Flow, ϕ=0.398

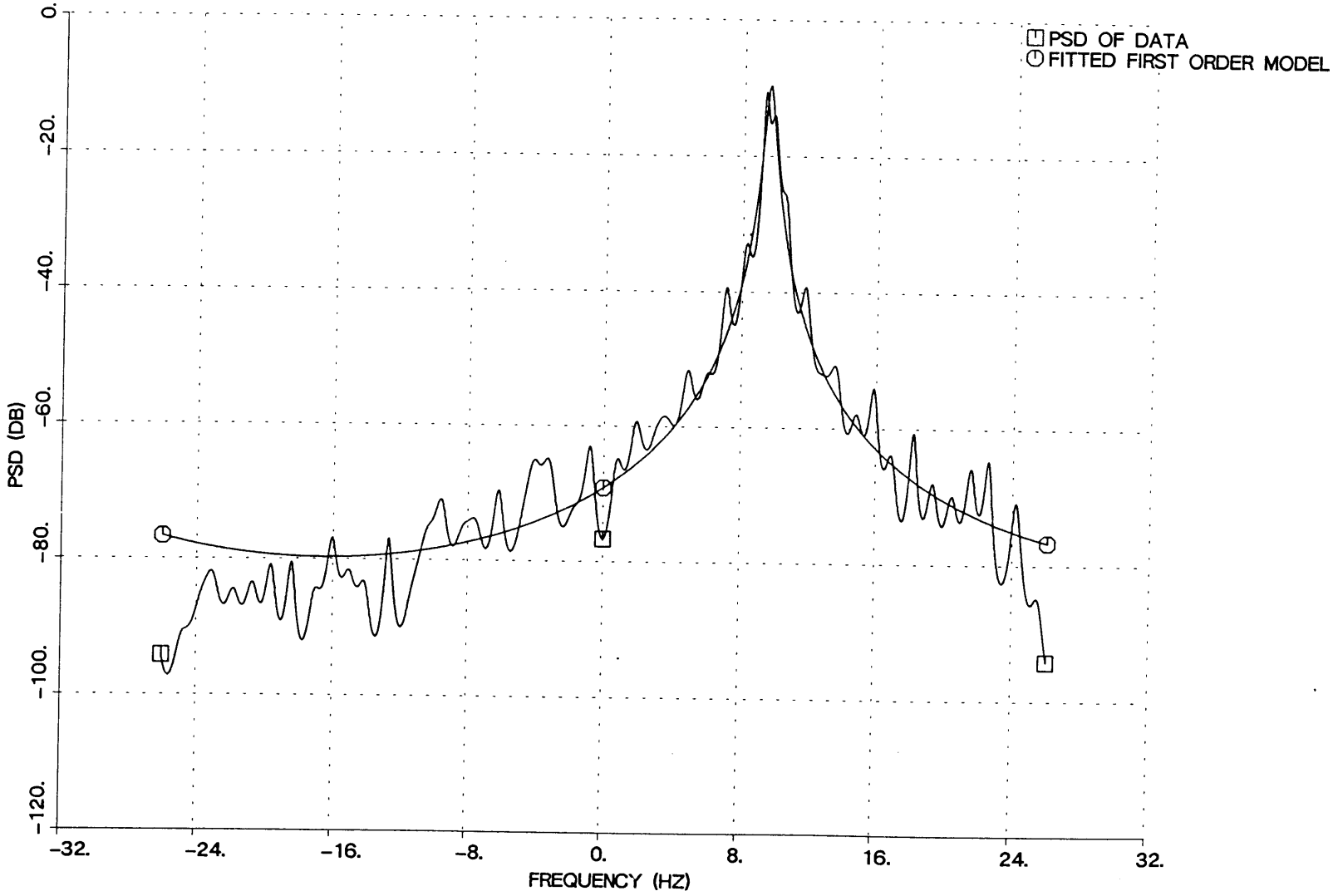

Figure (5-8) Comparison of Fitted Linear Model with PSD of First Harmonic, Uniform Inlet Flow, ϕ=0.361

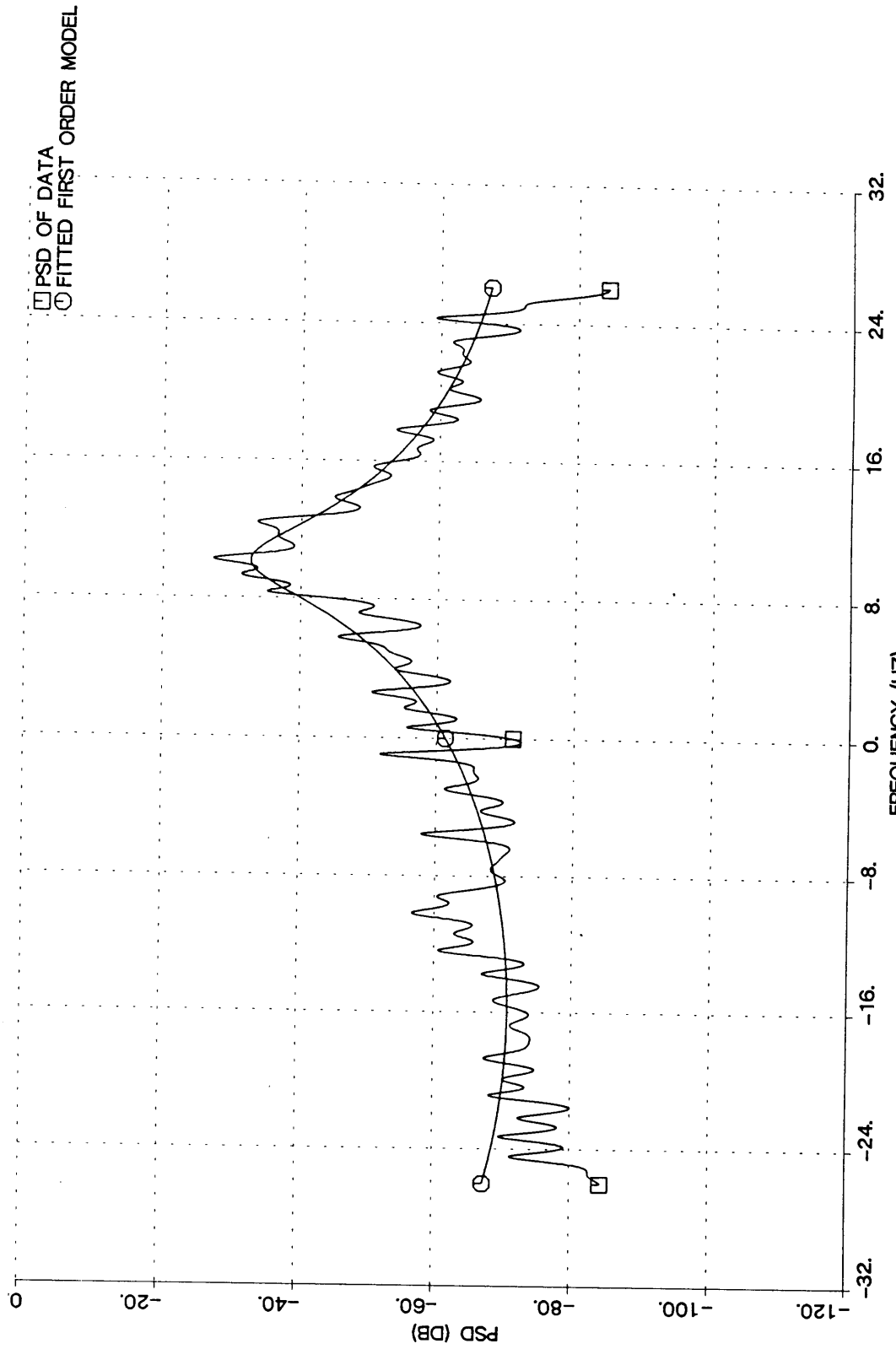

Figure (5-9) Comparison of Fitted Linear Model with PSD of First Harmonic, Distorted Inlet Flow, ϕ=0.356

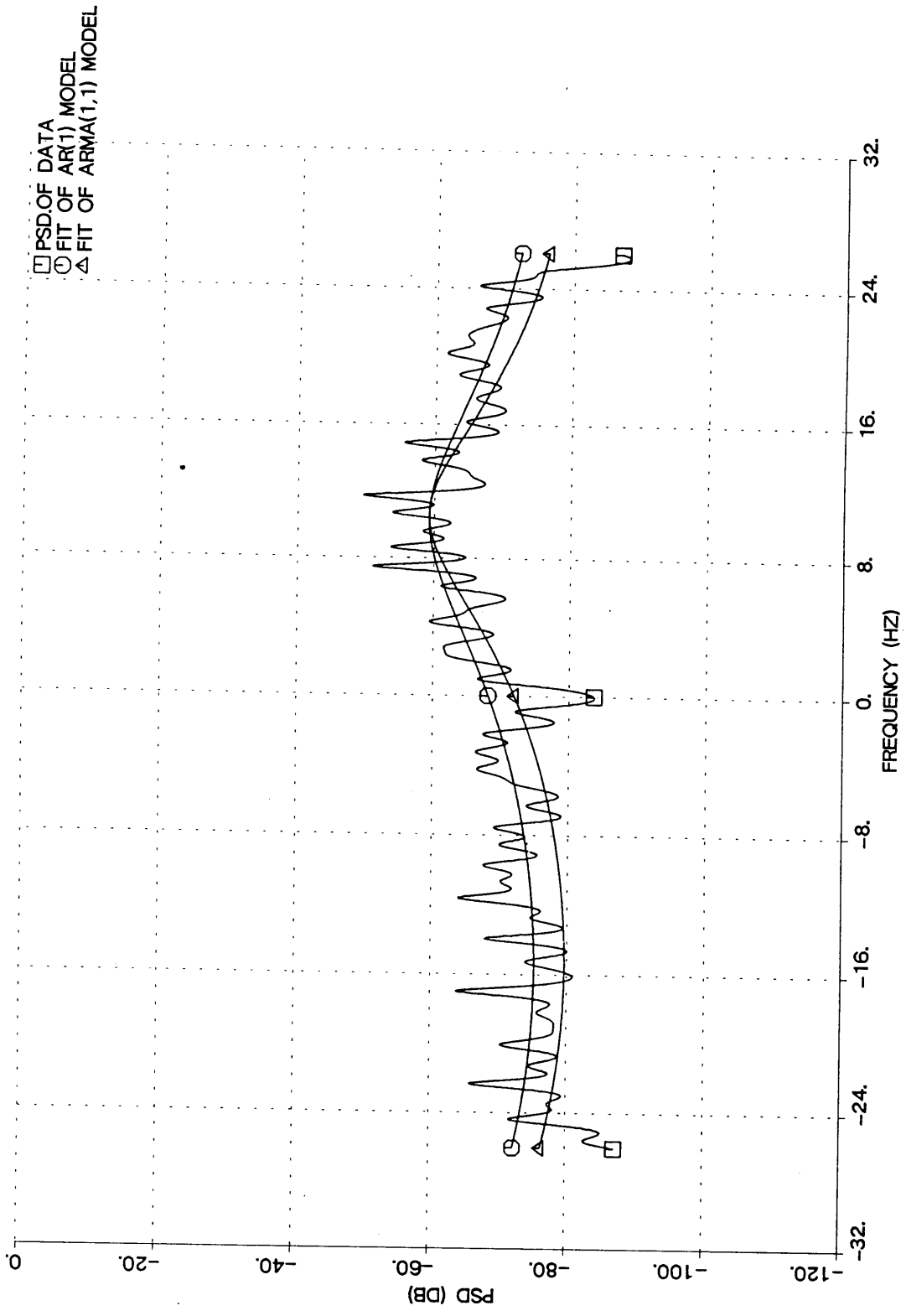

Figure (5-10) Comparison of AR(1) and ARMA(1,1) Models, Distorted Inlet Flow, ϕ=0.383

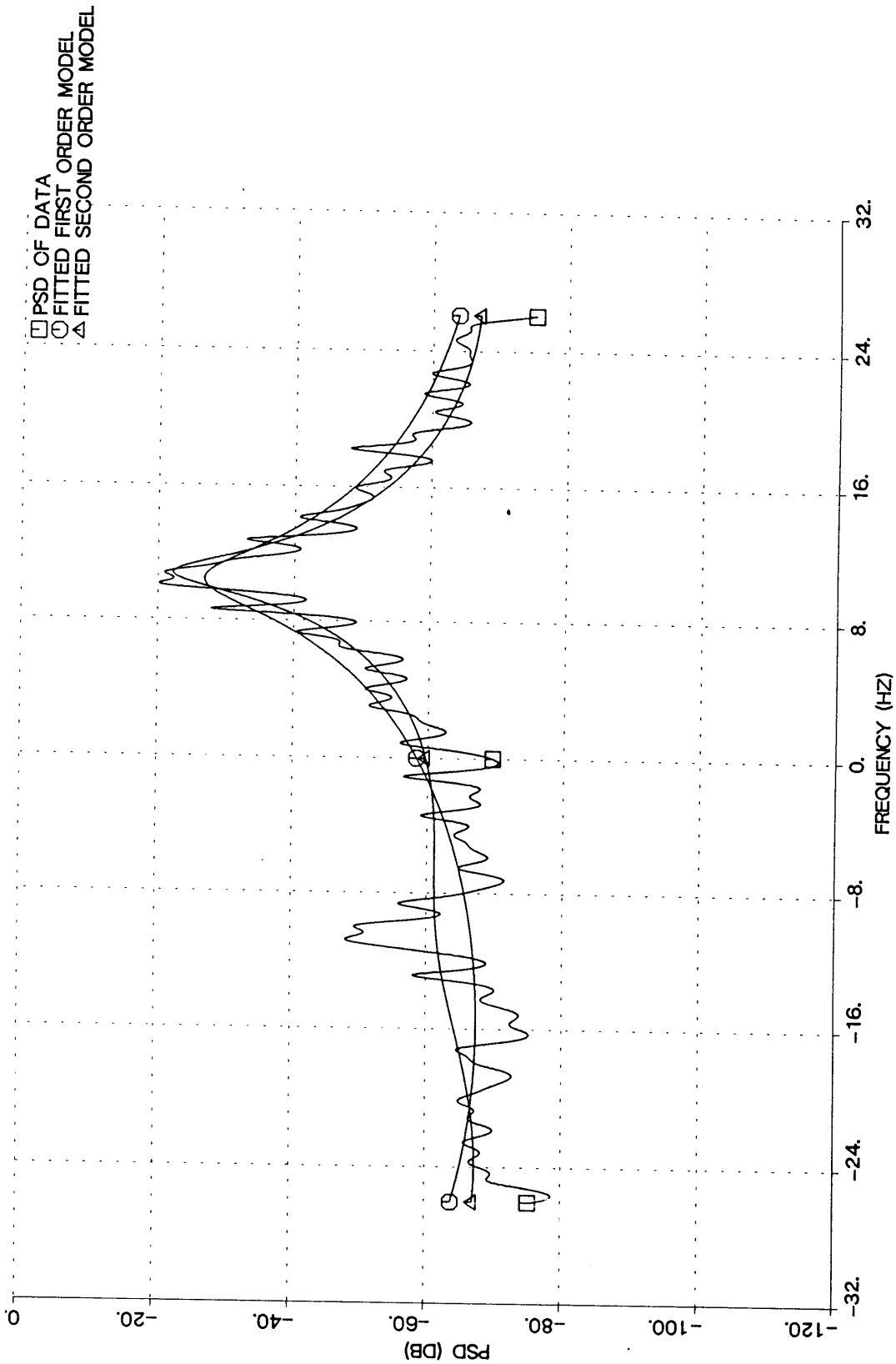

Figure (5-11) Comparison of AR(1) and AR(2) Models, Distorted Inlet Flow, ϕ=0.349

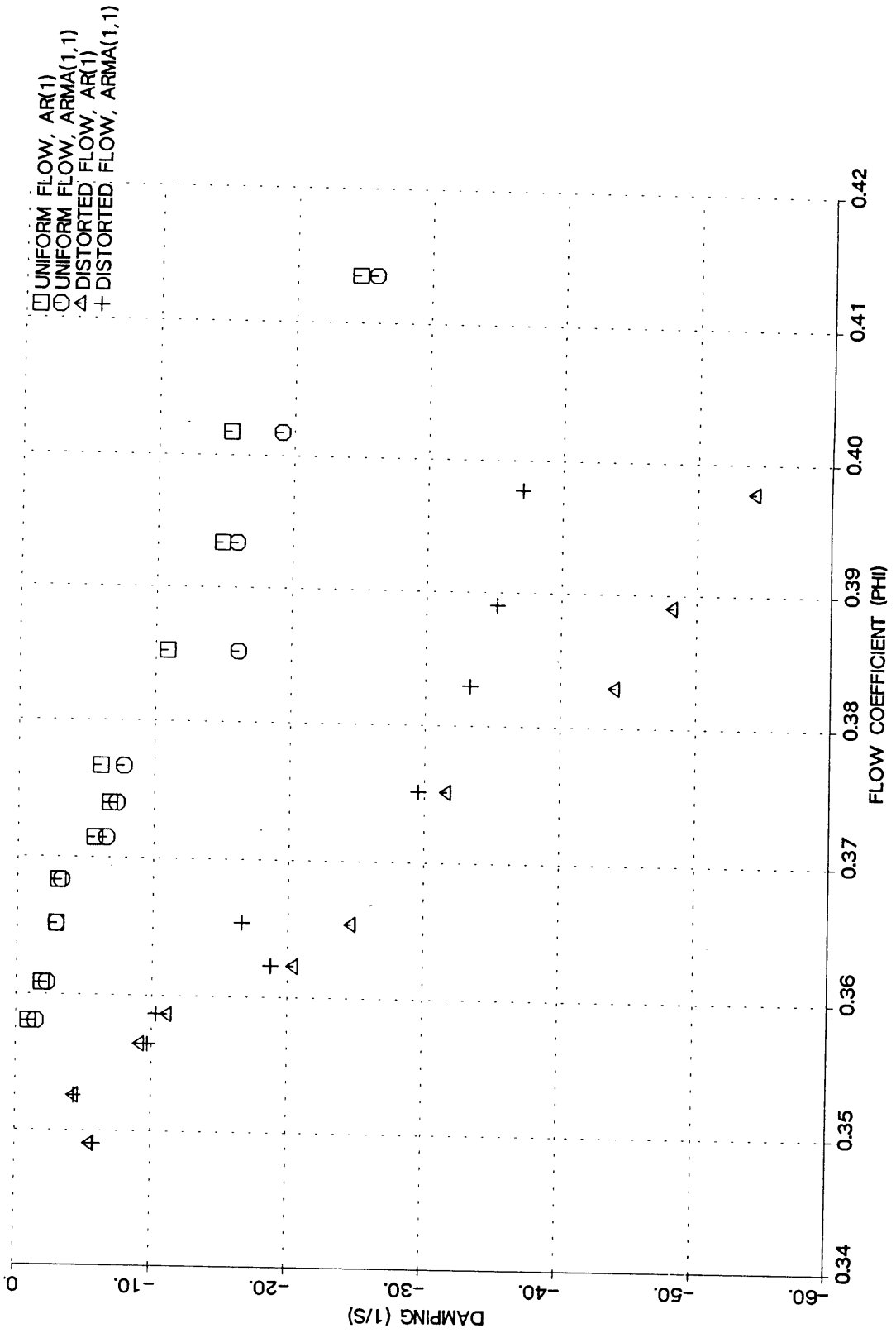

Figure (5-12) Damping of Small Amplitude Travelling Wave (First Harmonic) vs Flow Coefficient

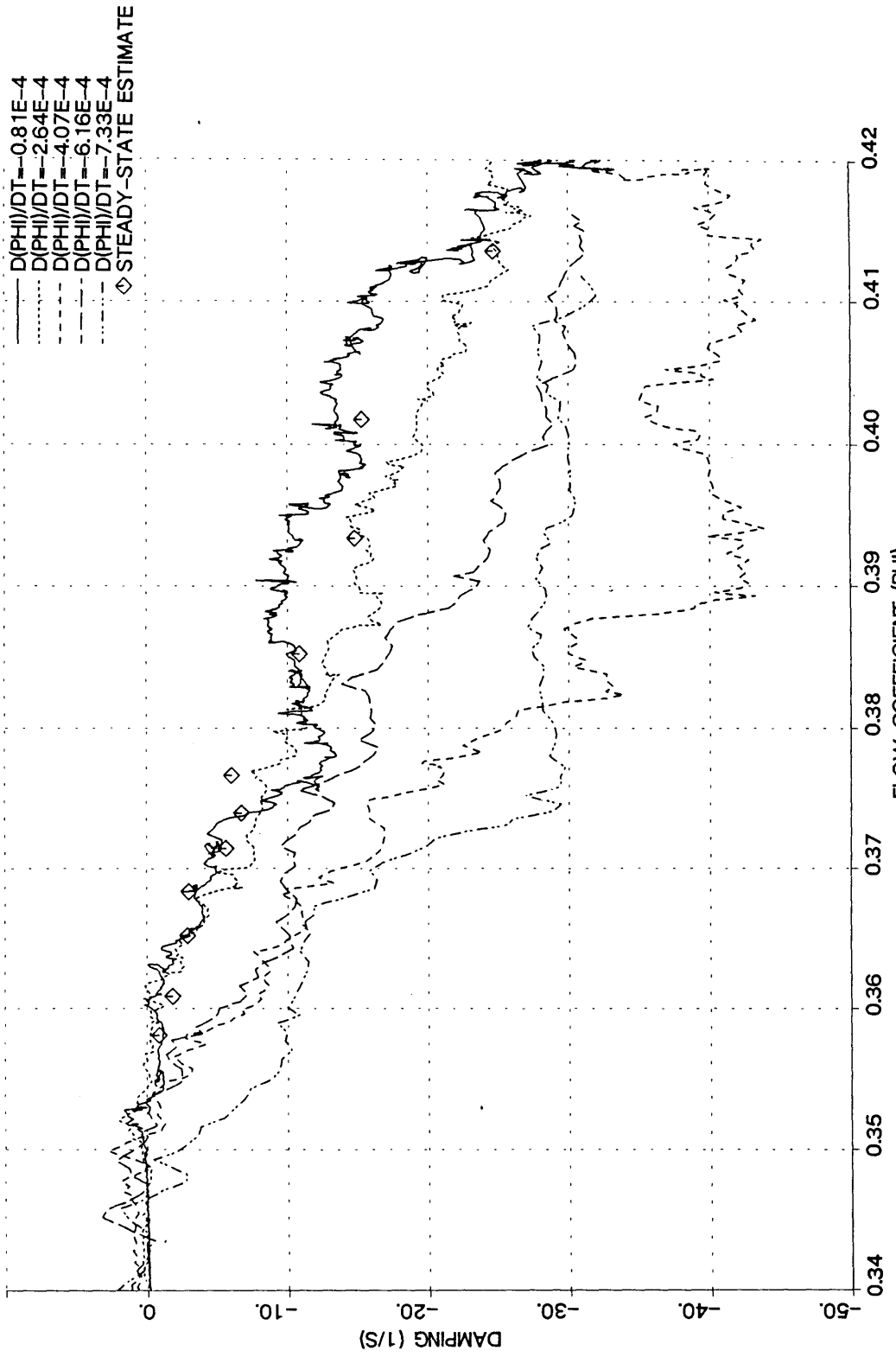

Figure (5-13) On-Line Estimation of Wave Damping During Transients, Uniform Inlet Flow, q=0.99

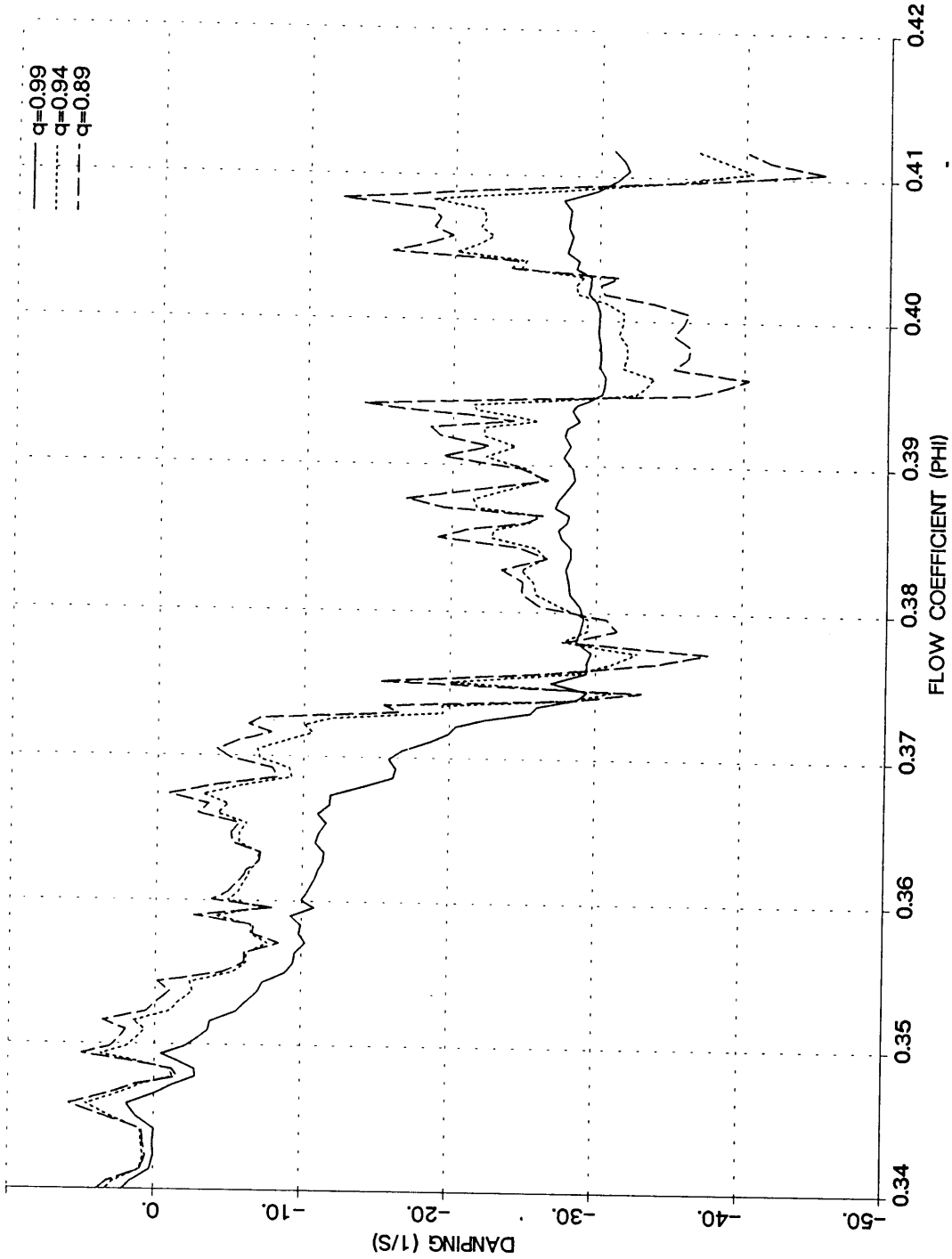

Figure (5-14) On-Line Estimation of Wave Damping During Transient at $d(\phi)/dt=-7.33e-4$ Uniform Inlet Flow, q=0.99, 0.96, 0.89

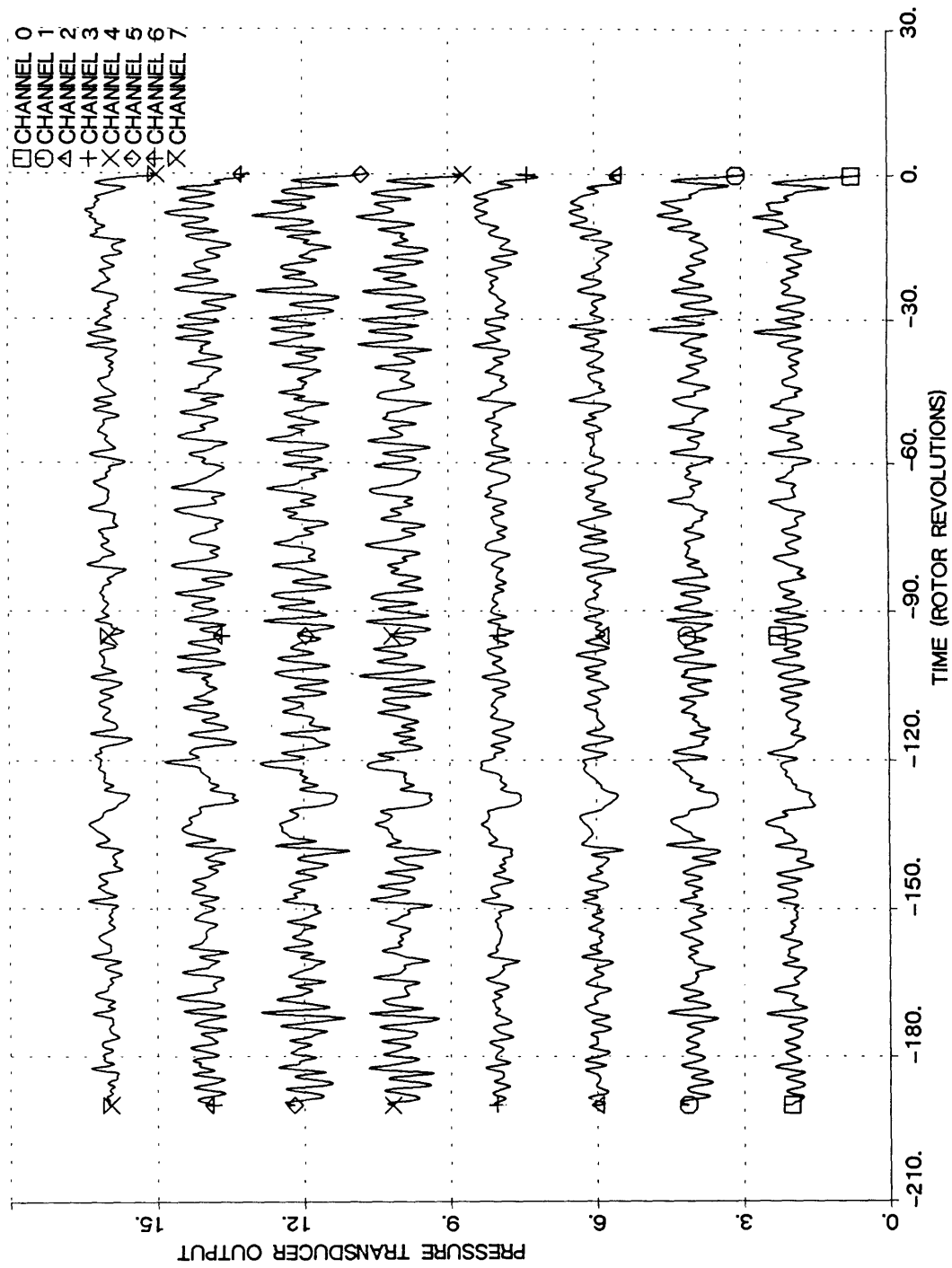

Figure (6-1) High-Speed Compressor: Eight Static Pressure Traces at Station 4
Very Slow Transient, Uniform Inlet Flow

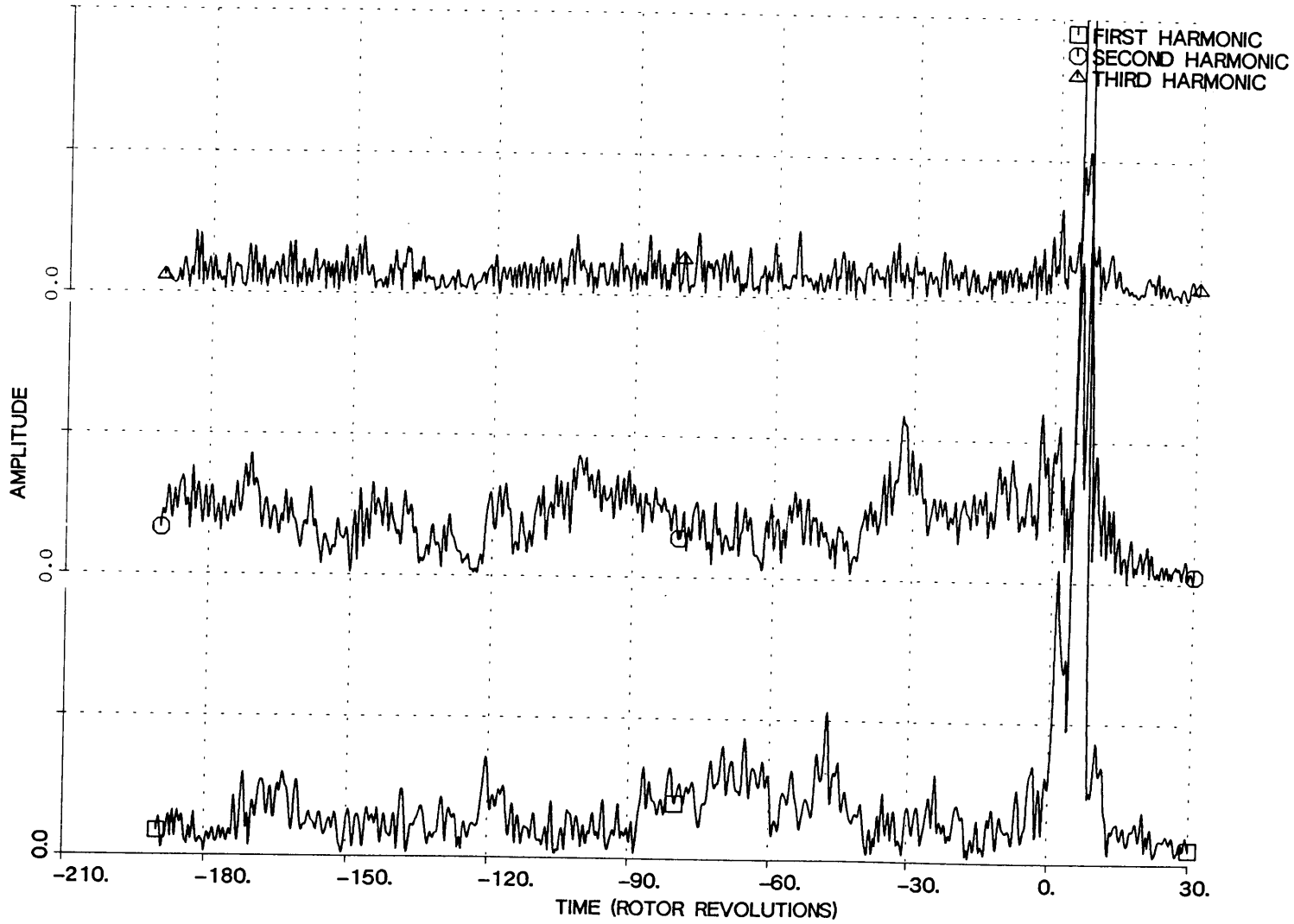

Figure (6-2) High-Speed Compressor: Amplitude of First, Second and Third Harmonic at Station 4 Very Slow Transient, Uniform Inlet Flow

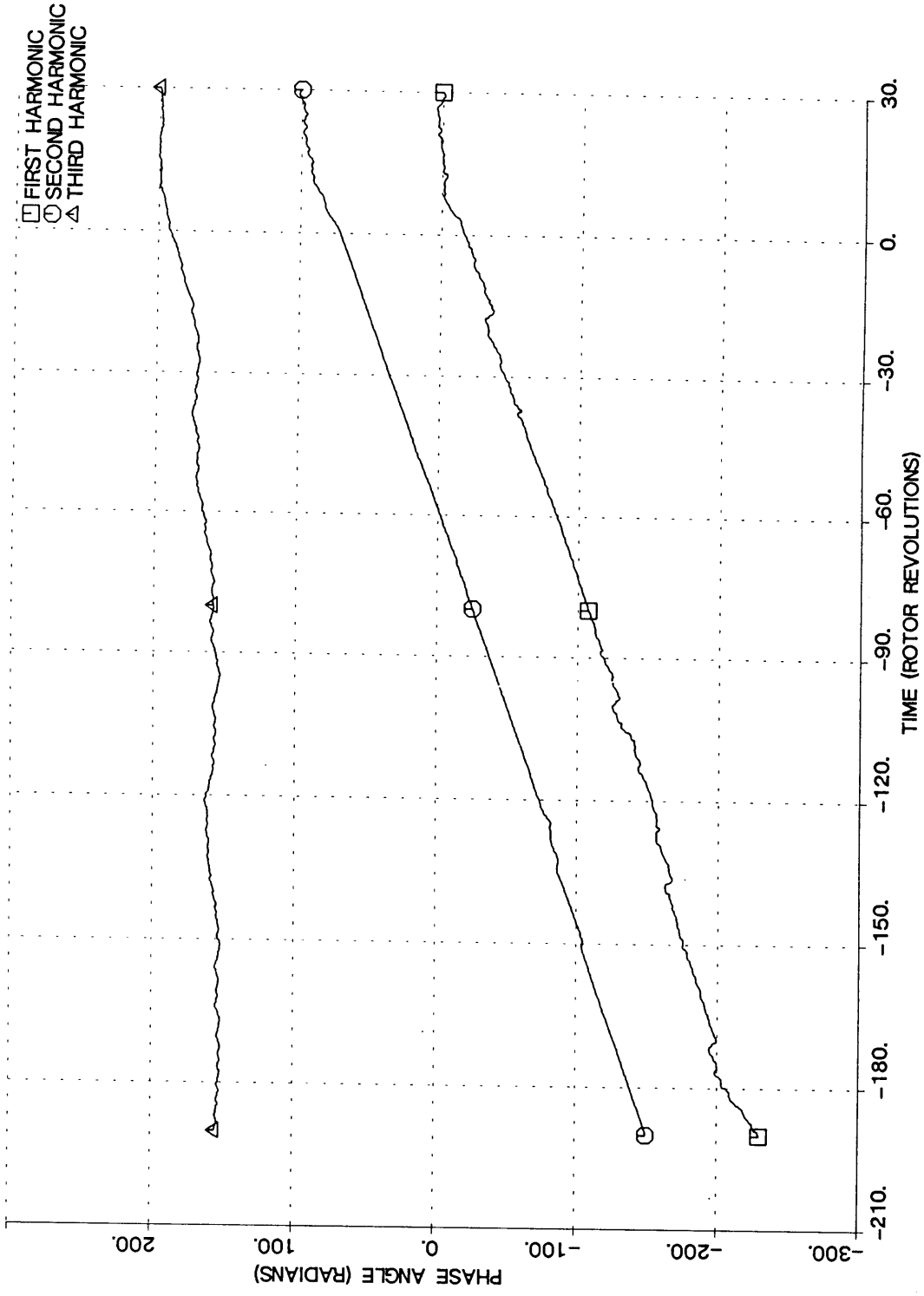

Figure (6-3) High-Speed Compressor: Phases of First and Second and Third Harmonic at Station 4
Very Slow Transient, Uniform Inlet Flow

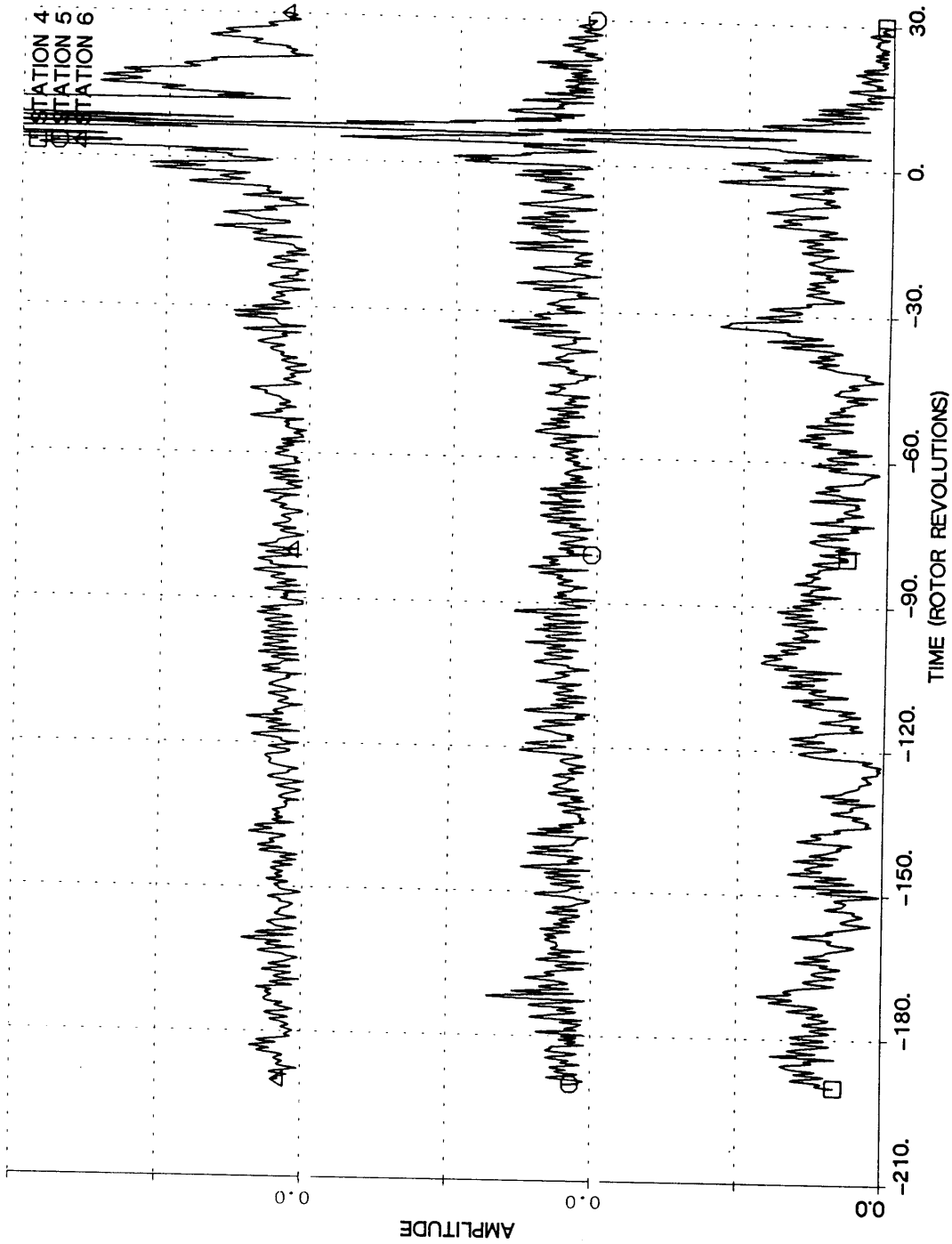

Figure (6-4) High-Speed Compressor: Ampliude of Second Harmonic at Stations 4, 5, and 6 Very Slow Transient, Uniform Inlet Flow

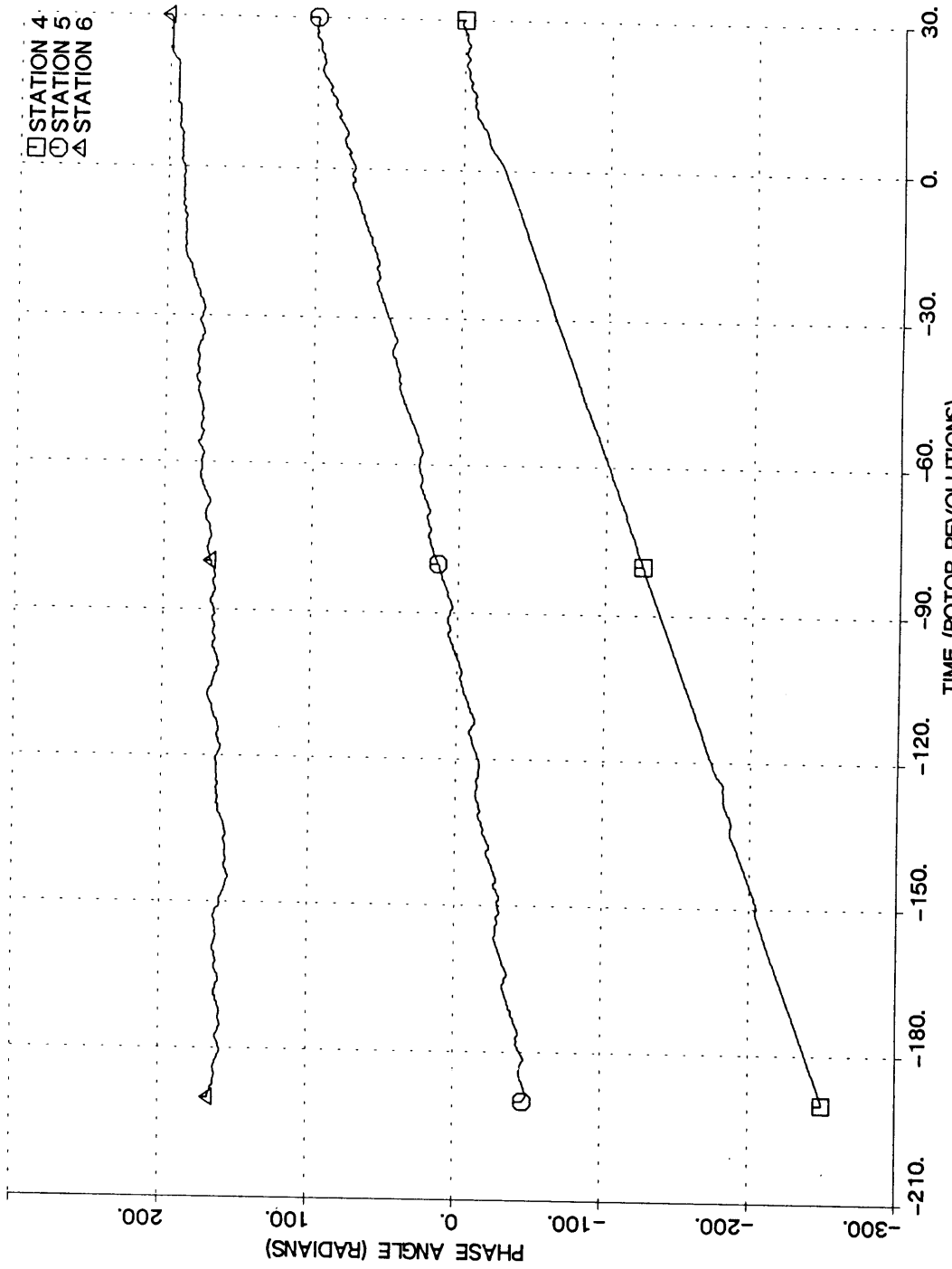

Figure (6-5) High-Speed Compressor: Phase of Second Harmonic At Station 4, 5, and 6
Very Slow Transient, Uniform Inlet Flow

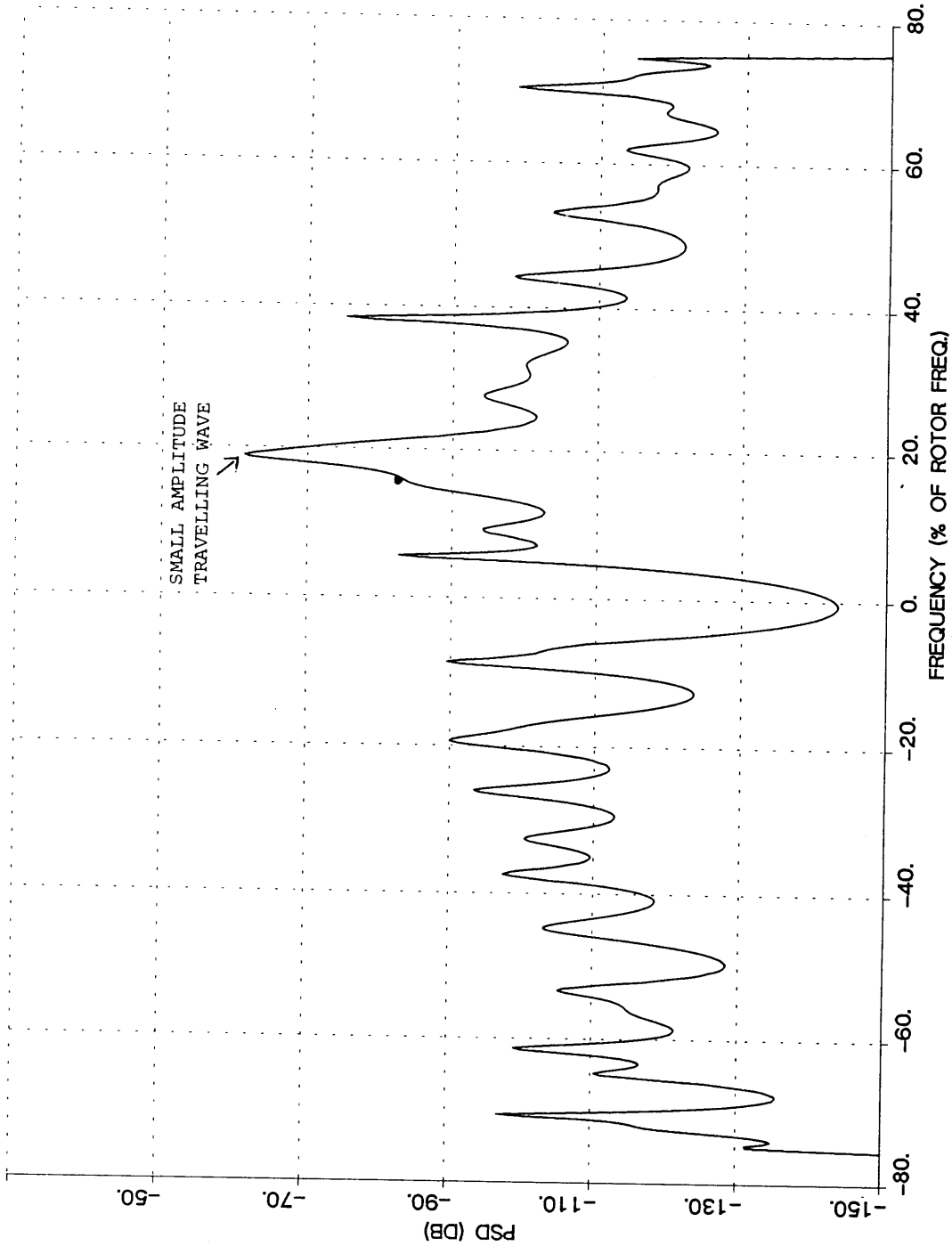

Figure (6-6a) High-Speed Compressor: PSD of First Harmonic at Station 4
Very Slow Transient, Uniform Inlet Flow

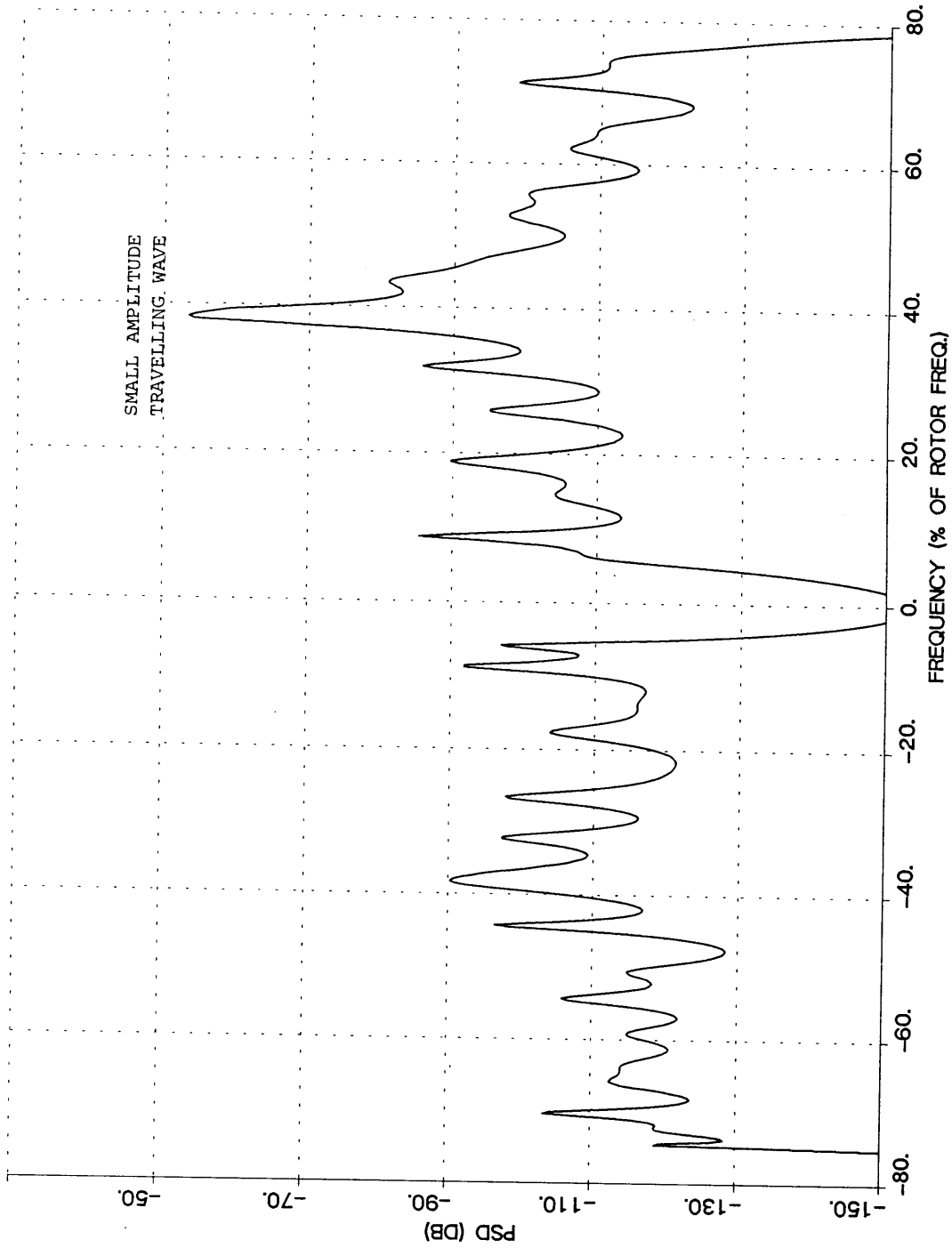

Figure (6-6b) High-Speed Compressor: PSD of Second Harmonic at Station 4
Very Slow Transient, Uniform Inlet Flow

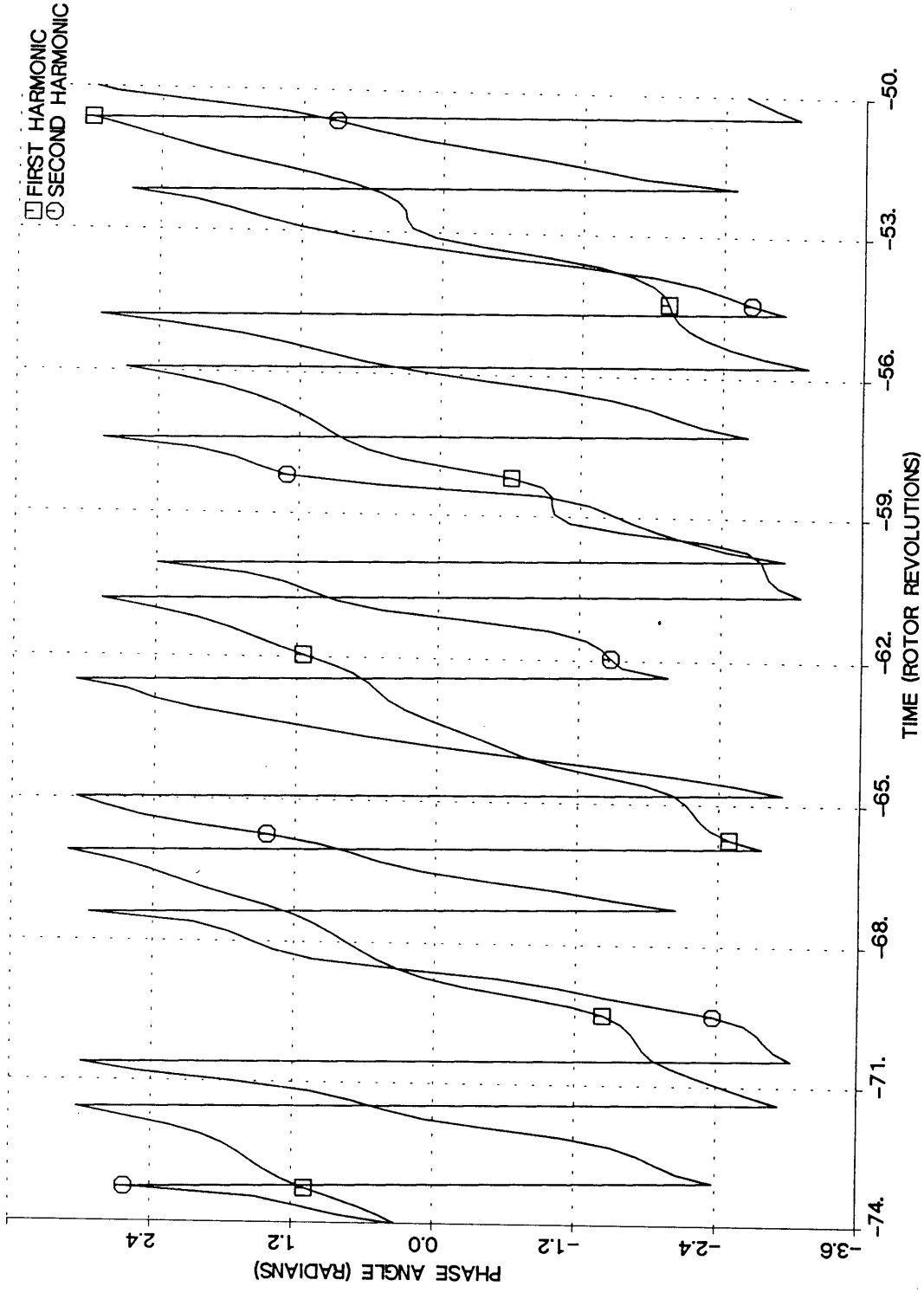

Figure (6-7) High-Speed Compressor: Phases of First and Second Harmonic at Station 4
Very Slow Transient, Uniform Inlet Flow

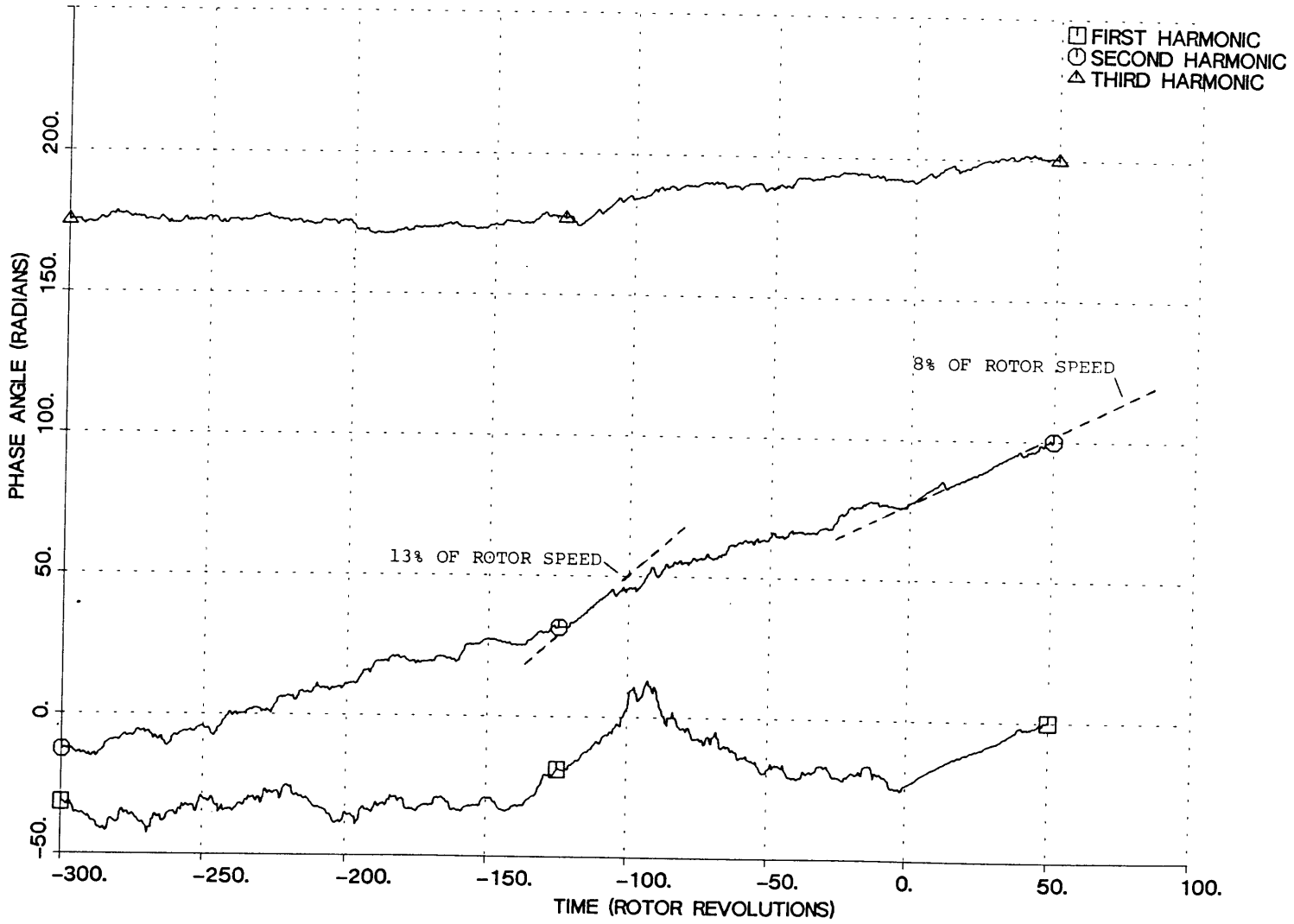

Figure (6-8) High-Speed Compressor: Phases of First, Second and Third Harmonic at Station 4 Very Slow Transient, Distorted Inlet Flow

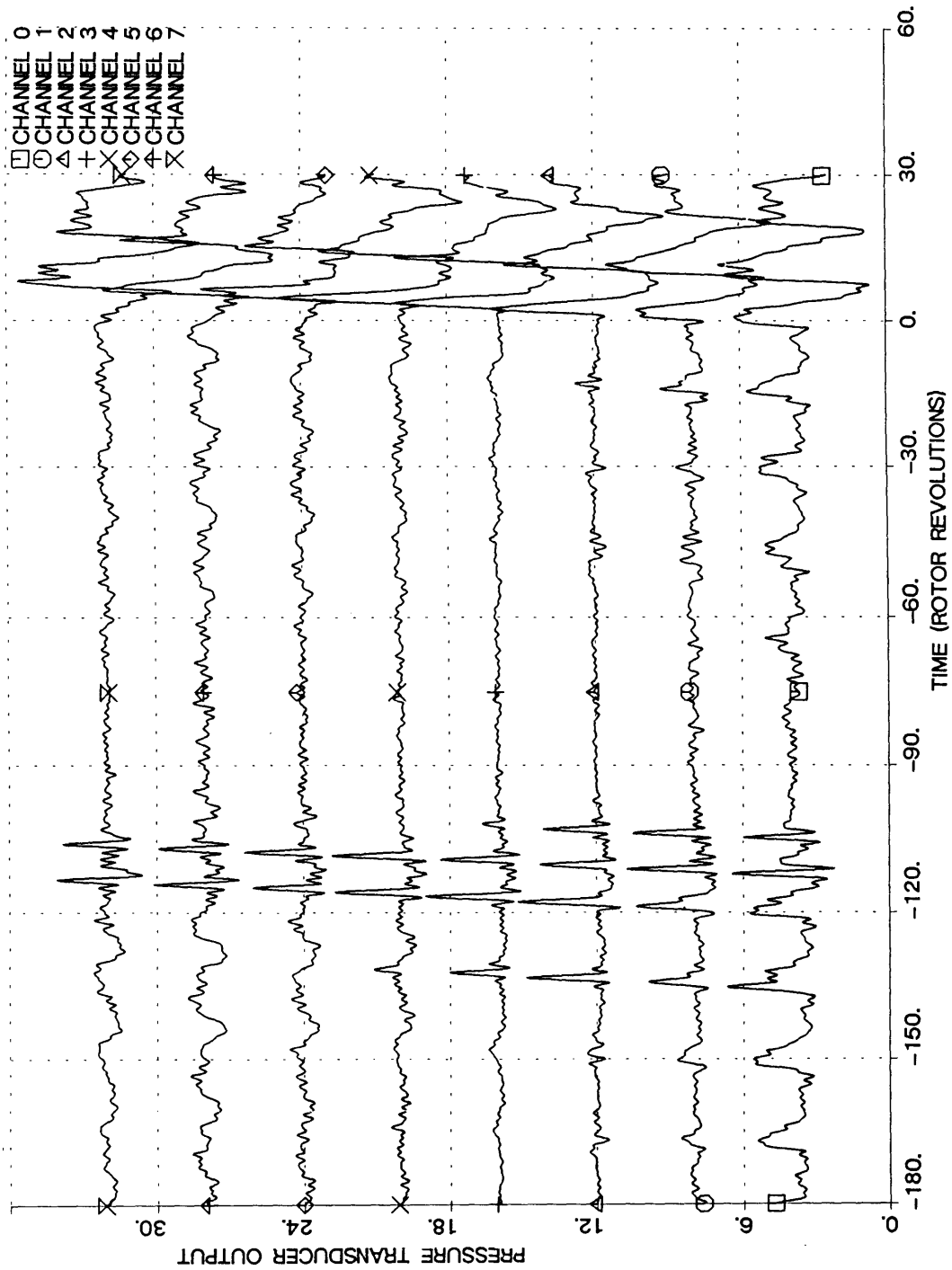

Figure (6-9) High-Speed Compressor: Eight Static Pressure Traces at Station 4
Very Slow Transient, Distorted Inlet Flow

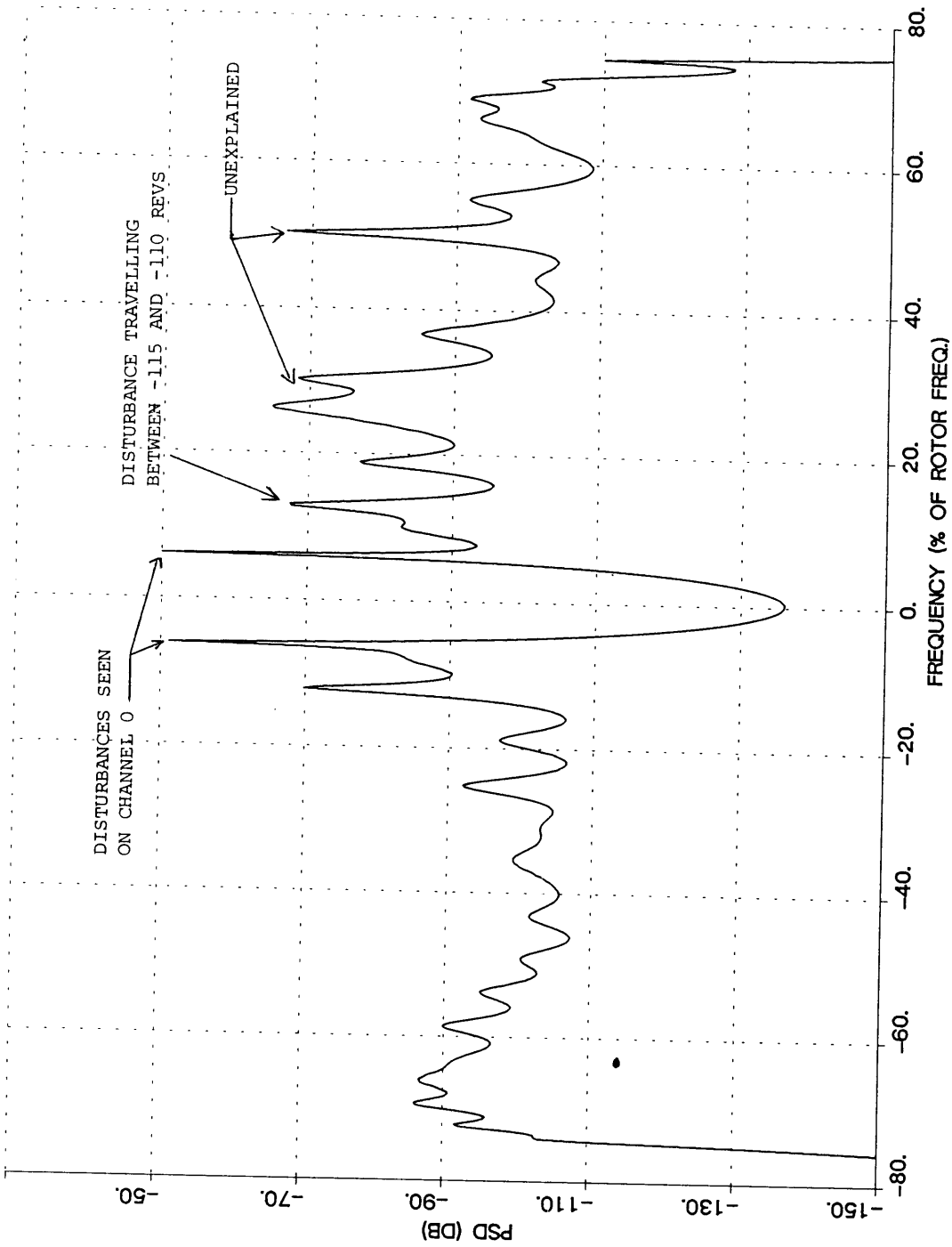

Figure (6-10) High-Speed Compressor: PSD of Second Harmonic at Station 4
Very Slow Transient, Distorted Inlet Flow

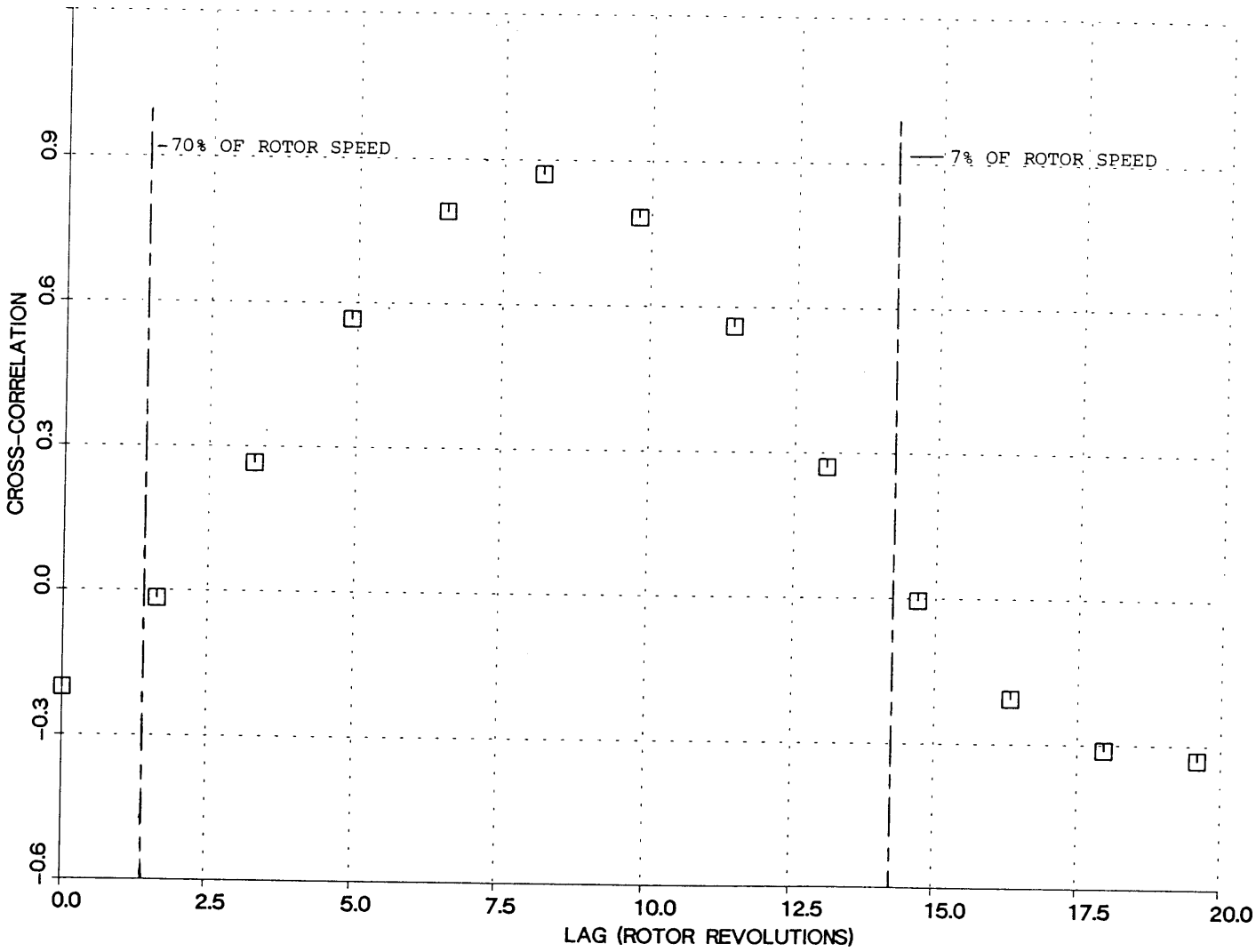

Figure (6-11) High-Speed Compressor: Example of Cross-Correlation Between Channels 0 and 1, T=-115 Revs Very Slow Transient, Distorted Inlet Flow

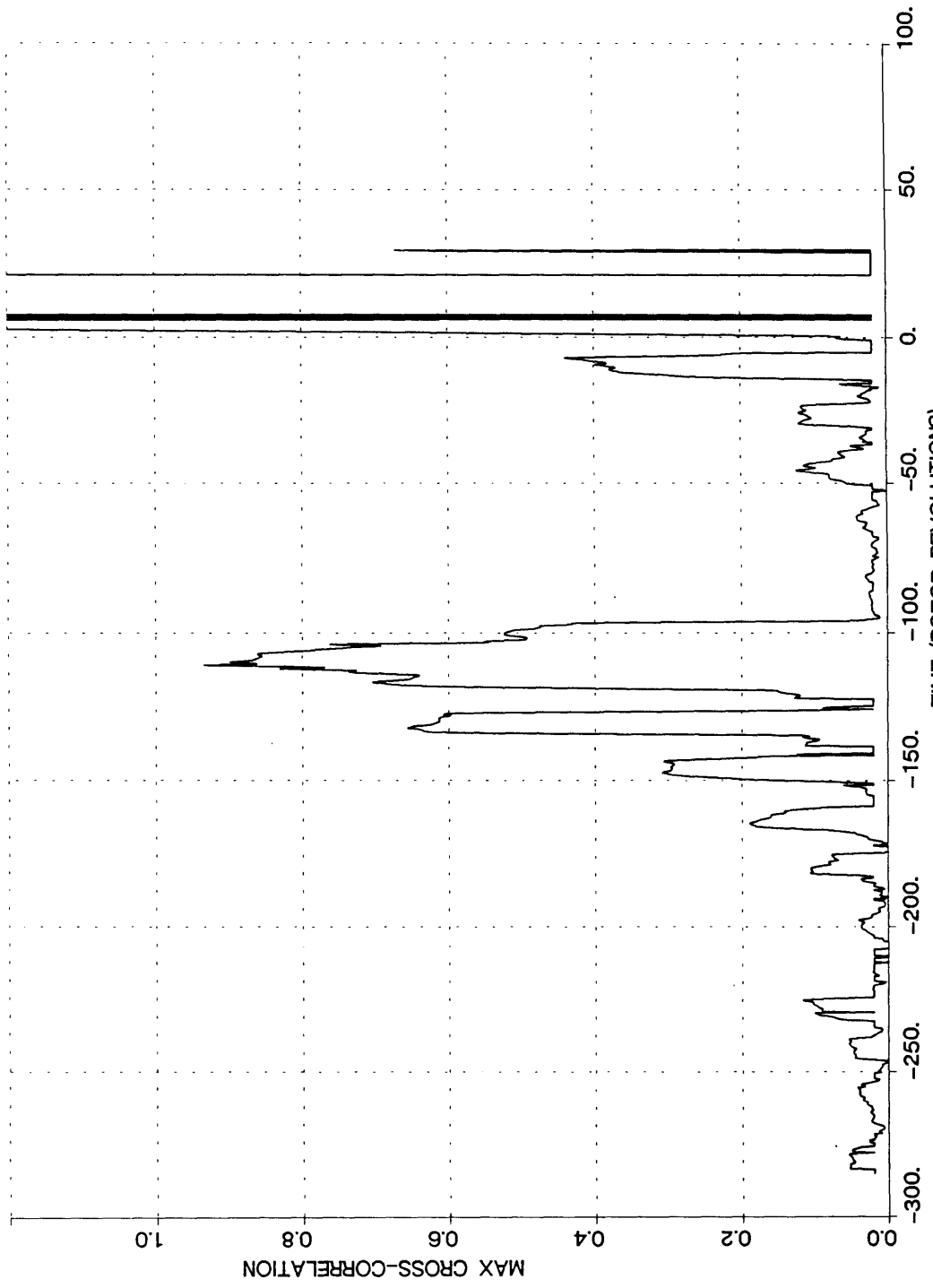

Figure (6-12) High-Speed Compressor: Maximum Cross-Correlation of Channels 0 and 1 vs Time
Very Slow Transient, Distorted Inlet Flow

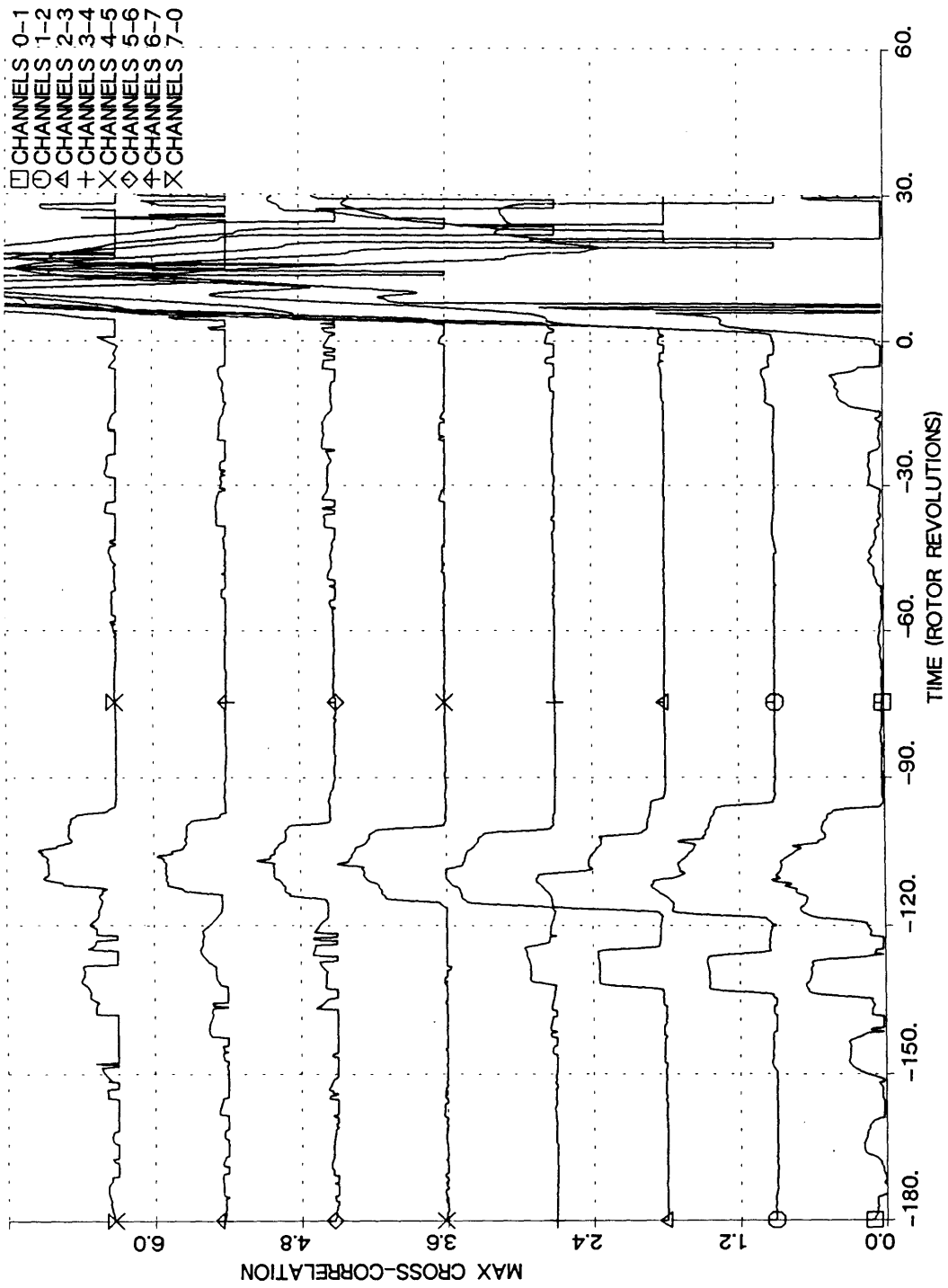

Figure (6-13) High-Speed Compressor: Maximum Cross-Correlation of Eight Pairs of Neighboring Transducers
Very Slow transient, Distorted Inlet Flow

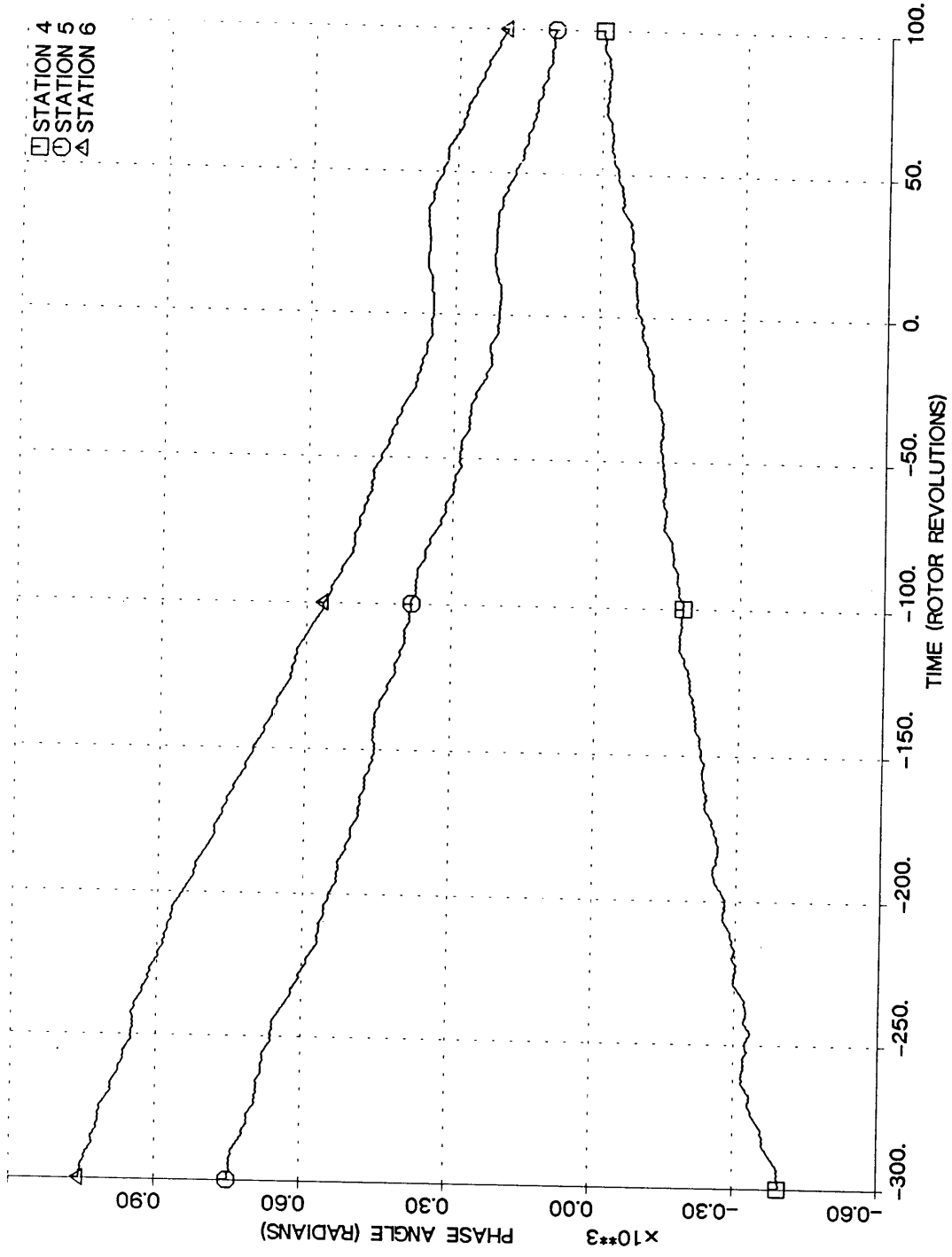

Figure (6-14) High-Speed Compressor: Phase of First Harmonic at Stations 4, 5 and 6, Fast Throttle Transient

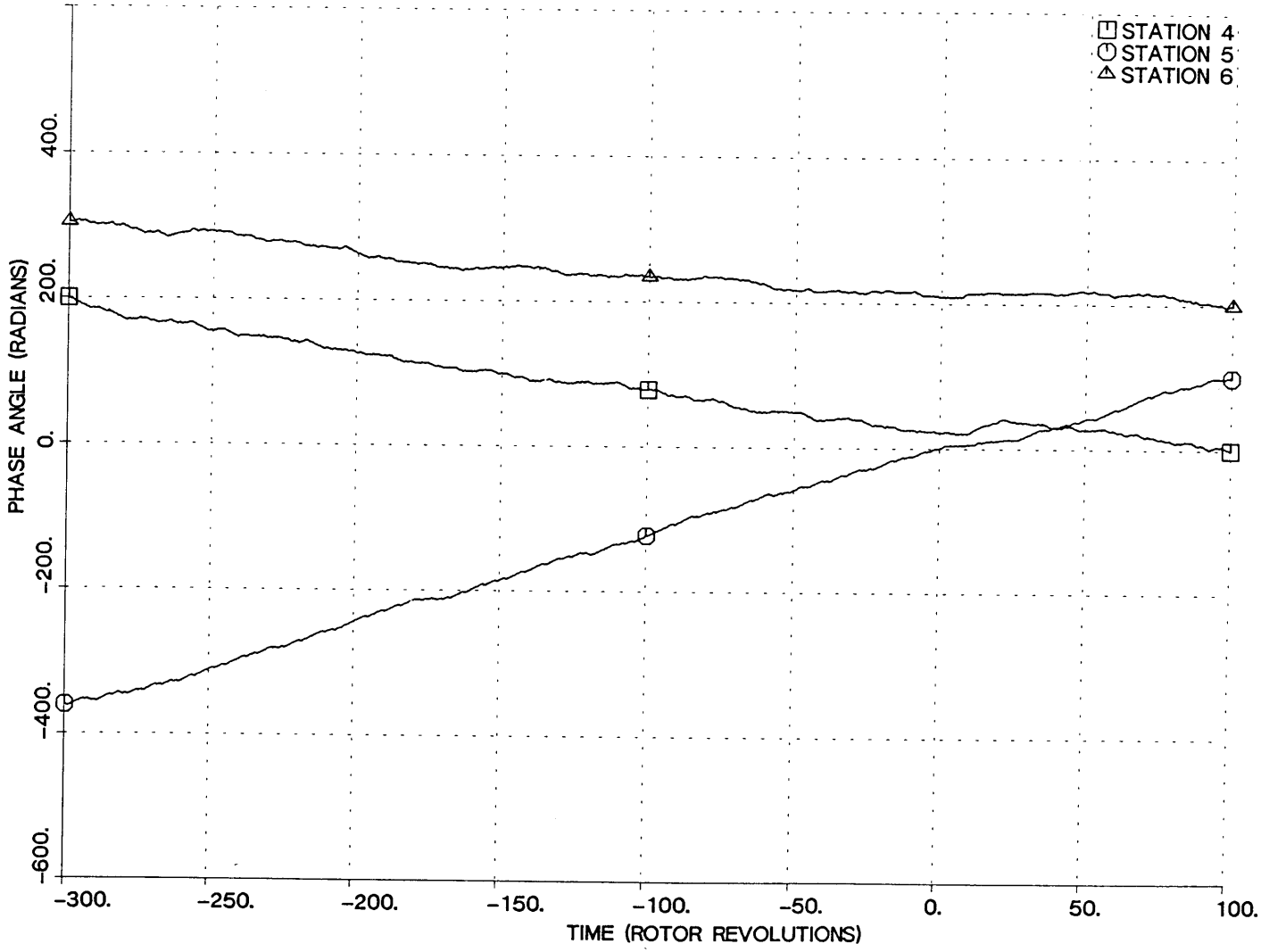

Figure (6-15) High-Speed Compressor: Phase of Second Harmonic at Stations 4, 5, and 6, Fast Throttle Transient

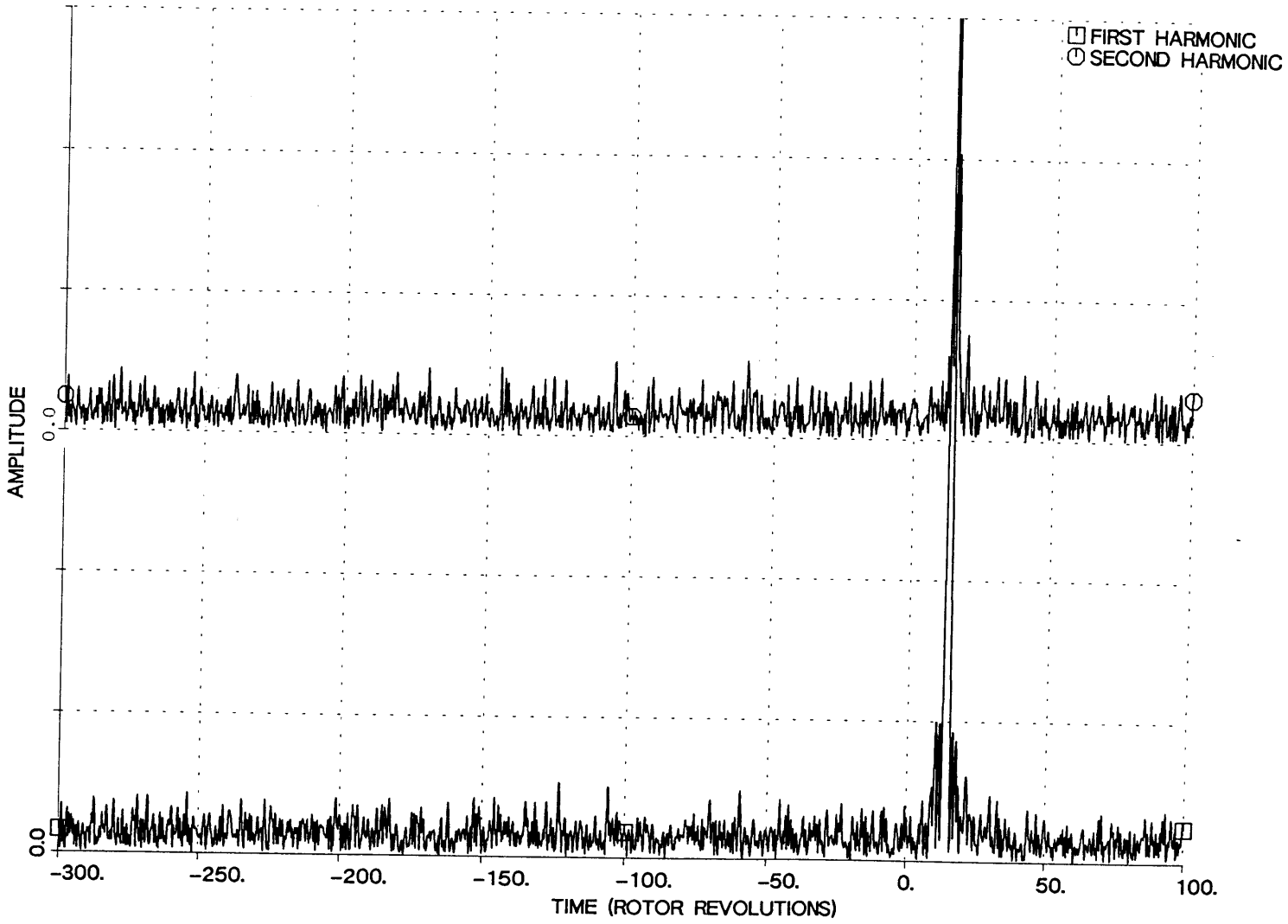

Figure (6-16) High-Speed Compressor: Amplitude of First and Second Harmonic at Station 4, Fast Throttle Transient

APPENDIX A

DERIVATION OF THE FOURIER TRANSFORM IN THE CASE OF UNEQUALLY SPACED MEASUREMENTS

Let us consider a discrete signal of period N, for example N measurements $x_0,..., x_{N-1}$, obtained at angular positions $\theta_0,..., \theta_{N-1}$. In this analysis we assume that N is even, because it corresponds to the case used in chapter six; the odd case if straightforward to derive. We can decompose the discrete periodic function x_l on the base of N complex exponentials:

$$\forall\, l \in \{0,..,N-1\}, \quad x_l = x(\theta_l) = \sum_{\frac{-N}{2}+1}^{\frac{N}{2}} C_k e^{ik\theta_l} \tag{A-1}$$

Let us define the base vectors:

$$W_k = \begin{bmatrix} e^{ik\theta_0} \\ \cdot \\ \cdot \\ e^{ik\theta_{N-1}} \end{bmatrix}, \quad k = \frac{-N}{2} + 1, \frac{N}{2} \tag{A-2}$$

Equation (A-1) can then be put in the following matrix form:

$$X = A\,C \tag{A-3}$$

$$X = \begin{bmatrix} x_0 \\ \cdot \\ \cdot \\ x_{N-1} \end{bmatrix}, \quad C = \begin{bmatrix} C_{-\frac{N}{2}+1} \\ \cdot \\ \cdot \\ C_{\frac{N}{2}} \end{bmatrix}$$

$$A = \begin{bmatrix} W_{-\frac{N}{2}+1} & \cdot & \cdot & W_{\frac{N}{2}} \end{bmatrix}$$

X and C are vectors of dimension N. A is an N by N matrix. Solving system (A-3) gives the N complex Fourier coefficients (C) from the N measurements (X).

Let us now emphasize the differences between the equally spaced and the non-equally spaced case.

- In the case of equal spacing, $\theta_l = \frac{2il\pi}{N}$, and the W_k's are orthogonal to one another. Consequently, $AA^* = N$, and $A^{-1} = 1/N\ A^*$: system (A-3) is easily solved! (This is also the basis for the computational efficiency of the Fast Fourier Transform). Another indirect consequence of this orthogonality is that the W_k's are periodic: $W_k = W_{k+N}$, and base $\{W_{+1},..., W\}$ is the same as base $\{W_0,..., W_{N-1}\}$. In practice, in fact, this latter base is often chosen, for ease of formulation.

In the case of unequal spacing, the W_k's are not orthogonal, and are not periodic any more. $\{W_{+1},..., W\}$ is not the same base as $\{W_0,...,W_{N-1}\}$, and we have to be careful which one we use to decompose our signal on, because they are not equivalent. In this calculation, we chose $\{W_{+1},...,W\}$ because it is (almost) symmetric with respect to zero, and can be directly transferred to a base of sines and cosines, according to the relations:

$$C_k e^{ik\theta} + C_{-k} e^{-ik\theta} = a_k \cos(k\theta) + b_k \sin(k\theta) \qquad (A\text{-}4)$$

$$C_k = \frac{1}{2}(a_k - i\, b_k)$$
$$C_{-k} = \frac{1}{2}(a_k + i\, b_k) \qquad (A\text{-}5)$$

$$a_k = C_k + C_{-k} \qquad \text{(A-6)}$$

$$b_k = i\,(C_k - C_{-k})$$

From these relations, we see that C_{-k} has the phase and half the amplitude of the sinusoid of mode k present in the measurements.

A side aspect of A not being orthogonal is that its conditioning number is greater than unity. In other words, any error in the measurements is amplified when solving the system (A-3) to obtain the C_k's. The more unequally spaced the measurements are, the greater the error amplification. It is easily understood that measurements concentrated in 1/4 of the circumference (for example) will yield less accurate Fourier coefficients than if they were equally spaced.

Another consequence of unequal spacing is the following: since the base vectors on which we decompose our signal are not orthogonal, aliasing will affect all coefficients, and in asymmetric ways: C_k and C_{-k} will not be complex conjugates any more, and the difference between the two is a measure of the aliasing present. For practical purposes, $(C_{-k}+C_k^*)/2$ can be taken instead of simply C_{-k}.